

Lecture notes Santiago de Chile

**Electromagnetic Methods in Geophysics**

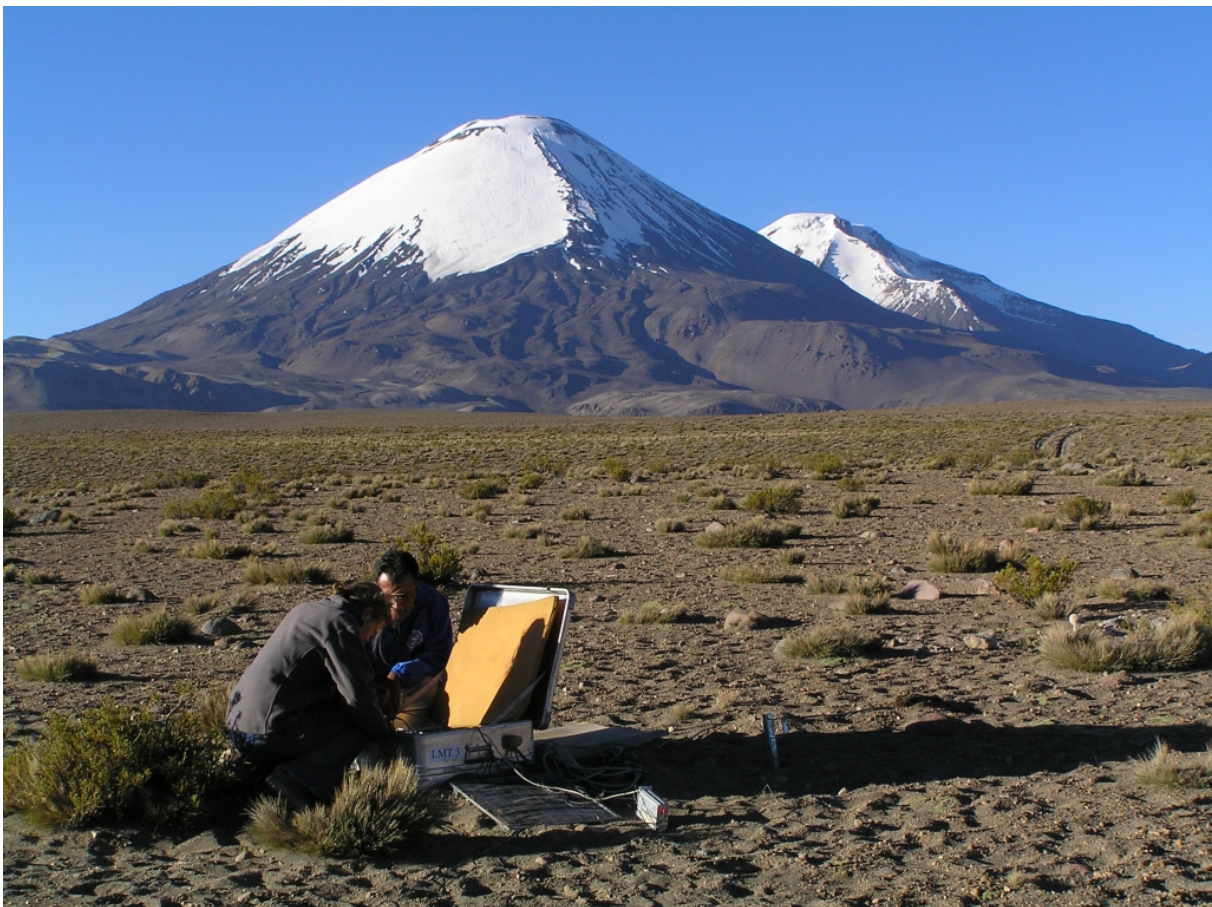
**Part I: Fundamentals of Magnetotellurics**

October 2011

Heinrich Brasse  
Fachrichtung Geophysik  
Freie Universität Berlin  
Malteserstr. 74-100  
D-12249 Berlin  
Germany

Email: [heinrich.brasse@fu-berlin.de](mailto:heinrich.brasse@fu-berlin.de)

Web: <http://userpage.fu-berlin.de/~hbrasse>



*Magnetotelluric field work in the Central Andes of Chile and Bolivia*

# **Content**

## **Part I: Magnetotellurics**

1. Introductory notes
2. Basics
3. EM-fields in homogeneous and isotropic good conductors
4. Geomagnetic variations – an overview
5. Measuring instruments and analysis of time series
6. Magnetotellurics on a layered half space
7. Two- and three dimensional conductivity distribution in MT
8. Some basic remarks on inversion of EM data

## **Part II: Other methods**

9. DC geoelectrics
  10. Self-Potential
  11. Induced Polarization
  12. FEM and TEM
- Case histories (separate files)
- Literature (separate file)

## 0 Introductory notes

The importance of geoelectric methods has increased in recent years, namely caused by new demands in environmental research (search for waste site locations, examination of leakages, etc.), geothermal resources and offshore exploration. They are divided into a great number of methods, which differ in, e.g., kind of source (synthetic or natural), inclusion of a magnetic field or not, DC- or AC-methods. An attempt of classification is given below; though, in practice, the distinction is often not easy to understand (e.g., a DC-geoelectric sounding is also possible with AC)<sup>1</sup>.

### A possible classification of the geoelectric methods

- **DC-methods**
  - DC geoelectrics (DCR, VES)
  - Method of induced polarization (IP)
  - Self or spontaneous potential method (SP)
- **electromagnetic methods with low frequencies**
  - Magnetotellurics (MT), geomagnetic deep sounding (GDS)  
Particularly: Audio Magnetotellurics (AMT),  
Controlled Source AMT (CSAMT),  
VLF, VLF-R,  
Radio Magnetotellurics (RMT)  
*Unimportant today: Tellurics, AFMAG*
  - „Real“ electromagnetic induction methods, classified in frequency domain and time domain methods (FD, TD)<sup>2</sup>  
Many FD-methods, e.g., Slingram, Turam  
TDEM- or TEM- („transient“-EM) methods
- **ground-penetrating-radar (EMR, GPR)**
- **borehole methods**
- **aero geophysical methods**

Magnetotelluric and geomagnetic deep sounding, respectively, differ particularly from most other methods in the way, that they use natural sources; nature – as sun and the atmosphere – perform the experiment and geophysicists are limited to the role of an observer. As we will

---

<sup>1</sup> New methods, which are not very popular yet, are, e.g., the MMR method (Magnetometric Resistivity), a variant of geoelectrics, in which measurement of voltage is substituted by measurement of the magnetic field. Another method is the SNMR (Surface Nuclear Magnetic Resonance) which is a combination of the TEM and proton magnetometers in some way. The protons in the subsurface (e.g. in the aquifer) are excited to a precession by a transmitter signal and after having stopped the signal the resulting magnetic field is measured.

<sup>2</sup> *Frequency domain*: the dependent variable (e.g., apparent resistivity) is a function of frequency  $f$  and period  $T = 1/f$ , generally by a Fourier transformation. *Time domain*: the dependent variable (e.g., the decrease of voltage at an instrument) is a function of time  $t$ .

see, this is one of their fundamental disadvantages, i.e., we cannot easily improve the signal-to-noise ratio by increasing the „transmitter power“.

Time-varying magnetic fields induce geoelectric (or telluric, from Latin *tellus*, concerning the earth) currents in the conductive earth, which themselves cause a secondary magnetic field. The primary fields can either arise from a natural (current systems in the ionosphere and the magnetosphere, radiation from lightnings) or a synthetic source (very long wavelength transmitter).

In *magnetotellurics* (*MT*), the field variations encompass a large period range of approximately  $10^{-4} - 10^5$  s. For the frequency range  $f > 1$  Hz the method is also called *audio magnetotellurics* (*AMT*). In a variant, called active AMT or *CSAMT* (controlled source AMT), the signals are generated by a transmitter. Here the horizontal components of the magnetic and the electric fields are measured and correlated conveniently. The application range of magnetotellurics is studying the conductivity of the middle and lower crust; AMT also serves for the exploration of near-surface structures.

The *VLF method* (very low frequency) has a great practical importance, especially in environmental research. Here one uses the secondary magnetic field, which is caused by lateral conductivity anomalies. The sources are electromagnetic waves generated by huge transmitters, which are installed for the communication with submarines, operating at frequencies between 15 - 25 kHz. While in the usual VLF method only the magnetic fields are measured and their components are taken into account, in the *VLF-R method* (R from resistivity) the electric fields are recorded, too, so it actually constitutes a variant of magnetotellurics. For higher frequencies up to some hundreds of kHz this method is called *radio magnetotellurics* (*RMT*).

These different types of electromagnetic deep sounding are based on the same electromagnetic theory of induction in good electrical conductors. This is the reason why this manuscript deals with both of them together.

The different methods of geoelectrics and geoelectromagnetics are applied to similar multifaceted problems. The most important application areas are:

- environmental geophysics;
- hydrology and hydrogeology, permafrost, geothermal resources;
- archaeology;
- exploration of minerals and munitions or similar (UXO);
- exploration of sedimentary basins, sub-salt structures;
- exploration of mineral deposits;
- tectonic questions, shear zones and
- study of the deeper crust and the upper mantle.

It has to be mentioned already here, that due to the inherent multitude of interpretation of geophysical deep exploration often only a combination of different methods, as gravity, seismics and electromagnetics will lead to success.



In this script the SI system is used throughout. The cgs system, which is attractive for theoretical physics, plays only a historic role in geophysics (here especially geomagnetics excelled in a certain chaos). Some conversions are shown beneath. The coordinate system is (nearly always) right-handed, with x-axis positive to the north, y-axis to the east and z-axis positive downwards.

### Units (SI vs. cgs-System)

electrical („telluric“) field strength:  $[E] = \text{mV/km} = 10^{-6} \text{ V/m}$

magnetic induction flux density, magnetic induction:  $[B] = \text{nT} = 10^{-9} \text{ Vs/m}^2$

components of  $\underline{B}$ :  $\underline{B} = (B_x, B_y, B_z) = (H, D, Z) = (X, Y, Z)$  <sup>3</sup>

magnetic field strength:  $[H] = \text{A/m}$

induction constant ( $B = \mu_0 H$ ):  $[\mu_0] = 4\pi \times 10^{-7} \text{ Vs/Am}$

permittivity of free space ( $D = \epsilon_0 E$ ):  $[\epsilon_0] = 8.8542 \times 10^{-12} \text{ As/Vm}$

resistivity:  $[\rho] = \Omega\text{m}$

conductivity:  $[\sigma] = \text{S/m} = 1/\Omega\text{m} = \text{„mho/m“}$  (1 Siemens = 1mho =  $1/\Omega$ )<sup>4</sup>

In the cgs-system Gauss (G) is the unit of the induction with the equivalent  $1 \text{ T} = 10^4 \text{ G}$ , furthermore  $1 \text{ G} = 10^5 \gamma$  (Gamma) and  $1 \gamma = 1 \text{ nT}$ .

In cgs units, the field strength  $H$  (measured in Oersted = Oe) is equal to the magnetic induction:  $B = H$  and with it  $1 \text{ Oe} = 1 \text{ G}$  (and thus a distinction of both quantities is rather inconsistent), while in the SI system applies:  $B = \mu_0 H$  with  $\mu_0 = 4\pi \times 10^{-7} \text{ Vs/Am}$  and  $[H] = \text{A/m}$  with the translation:

$$1 \text{ Oe} = \frac{1000}{4\pi} \frac{\text{A}}{\text{m}} = 79.59 \frac{\text{A}}{\text{m}}.$$

In geomagnetism one often uses the Gauss as the unit for the magnetic field strength  $H$ !

### Earth's magnetic main field, magnetic elements

Geographical coordinates:

X: northern component      Y: eastern component      Z: vertical component

Cylindrical coordinates:

H: horizontal intensity      D: declination      Z: vertical component

Spherical coordinates:

F or T: total intensity      D: declination      I: inclination (dip angle)

<sup>3</sup> Here  $H$  is the horizontal component (in the direction of magnetic north) and  $D$  the declination in degrees,  $X$  and  $Y$  are the components in geographic northern and eastern directions while  $B_x$  and  $B_y$  denote magnetic North and East, respectively.  $Z$  or  $B_z$  are always positive with depth. In this script nearly always the depiction  $B_x, B_y, B_z$  is chosen.

<sup>4</sup> Instruments for measuring conductivity, e.g., of water samples often measure in  $\mu\text{S/cm} = 10^{-4} \text{ S/m}$  or  $\text{mS/cm} = 0.1 \text{ S/m}$ .

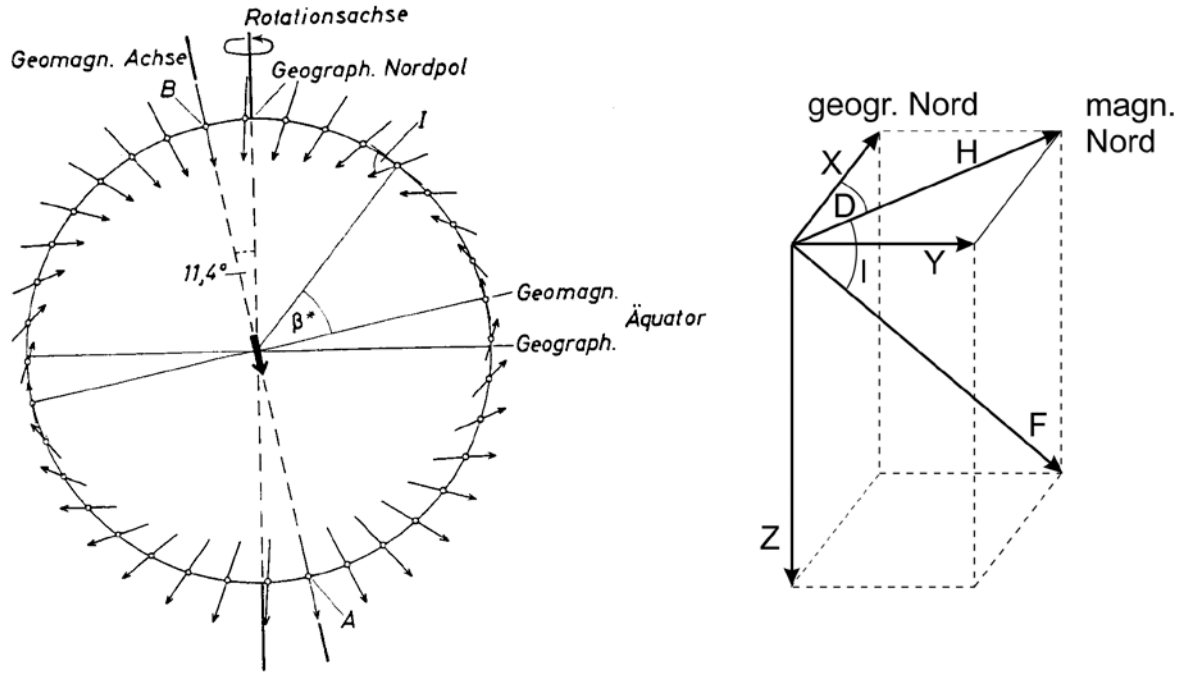


Fig. 0.1: The geomagnetic dipole field and the magnetic elements

$D = \text{const.}$ : isogone ( $D = 0^\circ$ : agone)

$I = \text{const.}$ : isocline ( $I = 0^\circ$ : magn. equator, dip equator)

$H = \text{const.}$ : isodyne

Geomagnetic coordinates are applied to the dipole part with  $\beta^*$  as the geomagnetic latitude and  $\lambda^*$  as the geomagnetic longitude.

Potential of the dipole field:

$$\Phi = -M \left[ \frac{\partial}{\partial z} \left( \frac{1}{r} \right) \right]_0 = M \frac{P_1(\cos \vartheta)}{r^2} = M \frac{\cos \vartheta}{r^2}$$

with the zonal spherical function  $P_1(\cos \vartheta)$

Height dependency:

$$F(r_E + h) = F_s \left( \frac{r_E}{r_E + h} \right)^3 \approx F_s \left( 1 - 3 \frac{h}{r_E} + \dots \right)$$

For Berlin one gets  $\partial F / \partial z = -0.025 \text{ nT/m}$ .

The actual geomagnetic field is a multipole field; for the mathematical description one uses a spherical function analysis (here only the inner part):

$$\Phi = r_E \sum_{\ell=1}^{\infty} \left( \frac{r_E}{r} \right)^{\ell+1} \sum_{m=0}^{\ell} \left[ g_{\ell}^m \cos m\lambda + h_{\ell}^m \sin m\lambda \right] P_{\ell}^m(\cos \vartheta) \text{ für } r \geq r_E$$

For measurements over a large area, the horizontal gradients of the main field have to be taken into account. This is either done by a trend subtraction of the field or spherical function synthesis. One gets  $g$  and  $h$  from tables (IGRF = International Geomagnetic Reference Field for special epochs, e.g. 2010.0 = 1 January 2010). They also contain the first temporal

derivative of the fields and therefore an estimation of secular variation. For information on the calculation of the main field see: <http://www.ngdc.noaa.gov/geomag/magfield.shtml>

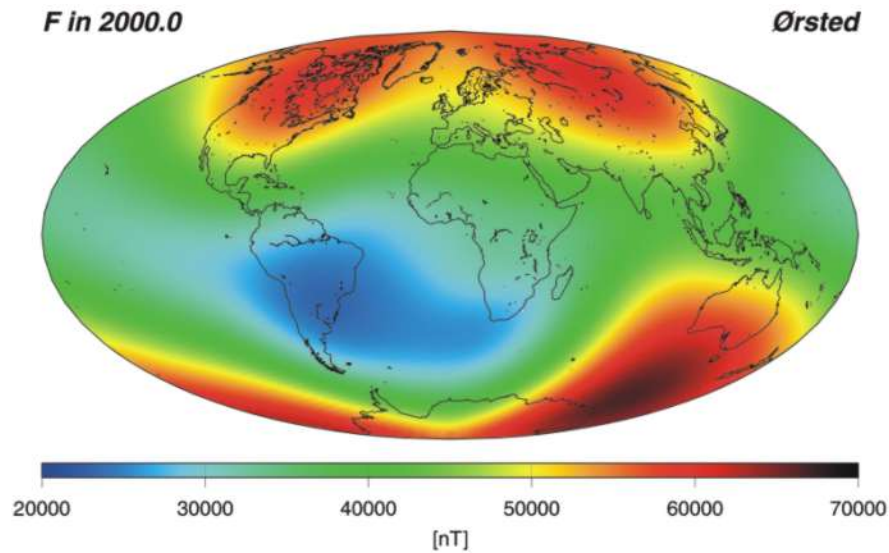


*Fig. 0.2: Total intensity  $F$  for the epoch 2000.0 from data delivered by the Danish satellite Ørstedt. The greatest difference from the field of a dipole that is inclined against the axis of the earth are the maximum in northern Siberia and the distinctive minimum in the Southern Atlantic and in South America.*

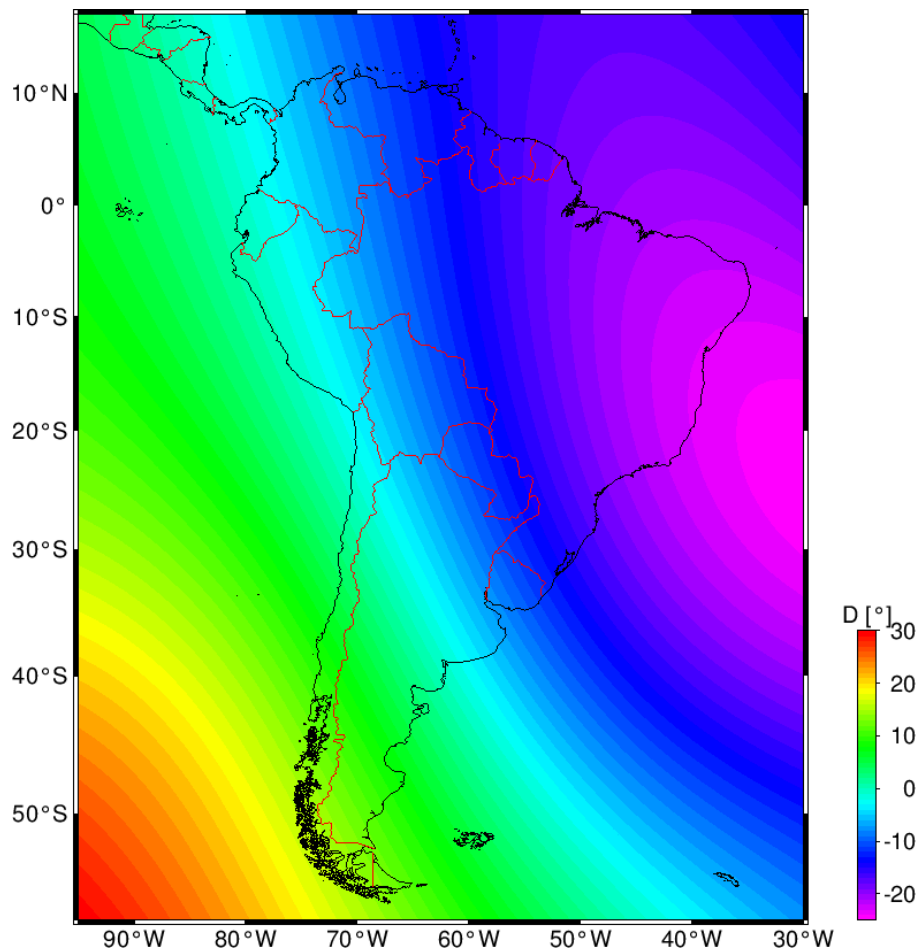


*Fig. 0.3: Declination (from IGRF) in South America 2005.0. The large deviation from  $0^\circ$  has to be taken into account when inferring strike directions, e.g., in magnetotellurics.*

**Some useful formulae from vector analysis**

1.  $\nabla(\varphi + \psi) = \nabla\varphi + \nabla\psi$
2.  $\nabla \cdot (\underline{A} + \underline{B}) = \nabla \cdot \underline{A} + \nabla \cdot \underline{B}$
3.  $\nabla \times (\underline{A} + \underline{B}) = \nabla \times \underline{A} + \nabla \times \underline{B}$
4.  $\nabla \cdot (\varphi \underline{A}) = \varphi \nabla \cdot \underline{A} + \underline{A} \cdot \nabla \varphi$
5.  $\nabla \times (\varphi \underline{A}) = \varphi \nabla \times \underline{A} + (\nabla \varphi) \times \underline{A} = \varphi \nabla \times \underline{A} - \underline{A} \times \nabla \varphi$
6.  $\nabla \cdot (\underline{A} \times \underline{B}) = \underline{B} \cdot \nabla \times \underline{A} - \underline{A} \cdot \nabla \times \underline{B}$
7.  $\nabla \times (\underline{A} \times \underline{B}) = \nabla \cdot \underline{B} \underline{A} - \nabla \cdot \underline{A} \underline{B}$   
$$= \underline{A} \nabla \cdot \underline{B} + \underline{B} \cdot \nabla \underline{A} - \underline{B} \nabla \cdot \underline{A} - \underline{A} \cdot \nabla \underline{B}$$
8.  $\nabla \times (\nabla \varphi) = 0$  A gradient field is rotation-free
9.  $\nabla \cdot (\nabla \times \underline{A}) = 0$  A rotational field is source-free

**Basic literature (text books)<sup>5</sup> and further reading**

- Berdichevsky, M.N. & Dimitriev, V.I. (2002): Magnetotellurics in the context of ill-posed problems, Society of Exploration Geophysicists, Tulsa.
- Berdichevsky, M.N. & Zhdanov, M.S. (1984): Advanced Theory of Deep Geomagnetic Sounding, Elsevier, Amsterdam. [BZ84]
- Chave, A. & Jones, A.G. (2012) The Magnetotelluric Method, Cambridge University Press.
- Grant, F.S. & West, G.F. (1965): Interpretation Theory in Applied Geophysics, McGraw-Hill, New York. [GW65]
- Kaufman, A.A. & Keller, G.V. (1981): The magnetotelluric sounding method, Elsevier, Amsterdam.
- Keary, P., Brooks, M. & Hill, I. (2002): An Introduction to Geophysical Exploration, Blackwell, Oxford.
- Keller, G.V. & Frischknecht, F.C. (1966): Electrical Methods in Geophysical Prospecting, Pergamon Press, Oxford.
- Koefoed, O. (1979): Geosounding Principles, Vol. I, Resistivity Sounding Measurements, Elsevier, Amsterdam.
- Nabighian, M.N. (ed., 1987 und 1991): Electromagnetic Methods in Applied Geophysics, Vol. 1 + 2, Society of Exploration Geophysicists, Tulsa. [N87] und [N91]
- Patra, H.P. & Mallick, K. (1980): Geosounding Principles, 2, Elsevier, Amsterdam.
- Porstendorfer, G. (1975): Principles of magneto-telluric sounding, Gebr. Bornträger, Berlin-Stuttgart.
- Rokityansky, I.I. (1982): Geoelectromagnetic Investigation of the Earth's Crust and Mantle, Springer-Verlag, Berlin.

---

<sup>5</sup> Some of the figures in this script are taken from these books. A detailed bibliography is given in a separate file (Literatur.pdf).

- Schmucker, U. & Weidelt, P. (1974): Aarhus Lecture Notes.
- Simpson, F. & Bahr, K. (2005): Practical Magnetotellurics, Cambridge Univ. Press.
- Telford, W.M., Geldart, L.P. & Sheriff, R.E. (1992): Applied Geophysics, 2nd edition, Cambridge University Press, Cambridge. [T92]
- Vozoff, K. (ed.) (1985): Magnetotelluric Methods, Geophysics Reprint Series, No. 5, Society of Exploration Geophysicists, Tulsa.
- Weaver, J.T. (1994): Mathematical Methods for Geo-Electromagnetic Induction, Wiley, New York.
- Whitall, K.P. & Oldenbourg, D.W. (1992): Inversion of Magnetotelluric Data for a One-Dimensional Conductivity, Society of Exploration Geophysicists, Tulsa.
- Zhdanov, M.S. & Keller, G.V. (1994): The Geoelectrical Methods in Geophysical Exploration, Elsevier, Amsterdam. [ZK94]
- Zhdanov, M.S. (2009): Geophysical Electromagnetic Theory and Methods, Methods in Geochemistry and Geophysics, 43, Elsevier, 868pp.

## 1 Basics

Electrical current  $I$  (measured in A = Ampère) and electrical voltage  $U$  (in V = Volt) are connected via Ohm's law:

$$U = R I \quad ; \quad (1.1)$$

here  $R$  is Ohm's *resistance*, measured in Ohm ( $1 \Omega = 1 \text{ V/A}$ ). Let's consider a cylindrical rock sample of length  $\ell$  and cross-section  $A$  (Fig. 1.1). If we apply a voltage  $U$  to its front surfaces, a current  $I$  will flow, and we get:

$$R = \rho \frac{\ell}{A} \quad . \quad (1.2)$$

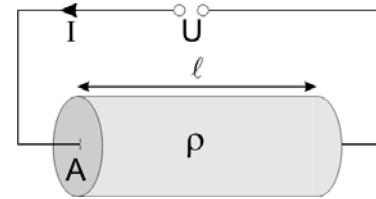


Fig. 1.1: Defining electrical resistivity

The *resistivity*  $\rho$  is a material property; it is measured in  $\Omega\text{m}$ .

Its reciprocal is *conductivity*  $\sigma$ , in units of  $1/\Omega\text{m} = \text{S/m}$  ( $\text{S} = \text{Siemens}^1$ ):

$$\sigma = \frac{1}{\rho} \quad . \quad (1.3)$$

The reciprocal of Ohm's resistance is called *conductance*  $\tau$ , measured accordingly in  $\text{S} = 1/\Omega$ . In geoelectric sounding one often calls this parameter *integrated conductivity*, which is obtained from the integral or the sum over the depth-dependent conductivity  $\sigma(z)$  or  $\sigma_i$ , respectively (in a  $n$ -layer case with layer thicknesses  $\Delta z_i$ ), and a certain depth interval:

$$\tau = \int_{z_1}^{z_2} \sigma(z) dz \quad \text{or} \quad \tau = \sum_{i=1}^n \sigma_i \Delta z_i \quad . \quad (1.4a)$$

As will be seen later,  $\tau$  is often the best resolved parameter in a geoelectric sounding. Similarly one defines a „transversal resistance“  $T$  (in  $\Omega\text{m}^2$ ):

$$T = \int_{z_1}^{z_2} \rho(z) dz \quad \text{or} \quad T = \sum_{i=1}^n \rho_i \Delta z_i \quad . \quad (1.4b)$$

$T$  and  $\tau$  are sometimes called *Dar-Zarrouk parameters*<sup>2</sup>.

Eq. (1.1) is a special case of the generalized Ohm's law:

$$\underline{J} = \sigma \underline{E} \quad ; \quad (1.5)$$

here  $\underline{J}$  denotes current density (current per area, in  $\text{A/m}^2$ ) and  $\underline{E}$  electrical field (voltage per unit length, in  $\text{V/m}$ )<sup>3</sup>.

When an electric field is applied to a conductor, an electric current flows with a density of:

$$\underline{J} = \sigma \underline{E} = en \underline{v} \quad , \quad (1.5a)$$

with  $n$  = number of charge carriers,  $v$  = velocity and  $e$  = elementary charge. With  $\mu_e = v/E$  as

<sup>1</sup> In Anglo-Saxon literature one occasionally encounters the term "mho" instead of Siemens (ohm read reversely, a very pragmatic unit...). Also ohm-feet for  $\rho$  exist.

<sup>2</sup> See Maillet (1947) for the origin of this name (which refers to a house in Sidi Bou Said, a little town next to Cartago near Tunis).

<sup>3</sup> In this manuscript vectors are underlined, matrices and tensors double-underlined.



mobility of charge carriers it follows for the conductivity:

$$\sigma = en\mu_e \quad . \quad (1.5b)$$

The continuity equation connects the temporal variation of charge density  $q$  with the divergence of the current density:

$$\nabla \cdot \underline{J} = -\frac{dq}{dt} \quad . \quad (1.5c)$$

There are basically 3 mechanisms for electrical conductivity: *semiconductor*, *electrolytic (ionic)* and *metallic (electronic)*; a special role plays the enhancement of conductivity at an *electrical double-layer*. Most rocks and minerals are normally bad electrical conductors; their nature as semiconductors becomes effective only at high temperatures, i.e., in deeper parts of the mantle. Conductivity of electrons and defect electrons follow an *Arrhenius law* (see Fig. 1.2)<sup>4</sup>:

$$\sigma = \sigma_0 \exp\left(-\frac{E_A}{kT}\right) , \quad (1.6a)$$

where  $E_A$  = activation energy and  $k$  = Boltzmann constant.

However, fluids in pore space or faults may significantly lower the overall resistivity<sup>5</sup>. To consider this *Archie* (1942) developed an empirical law – originally for rocks not containing any clay components – that takes into account the porosity and the fluid filling:

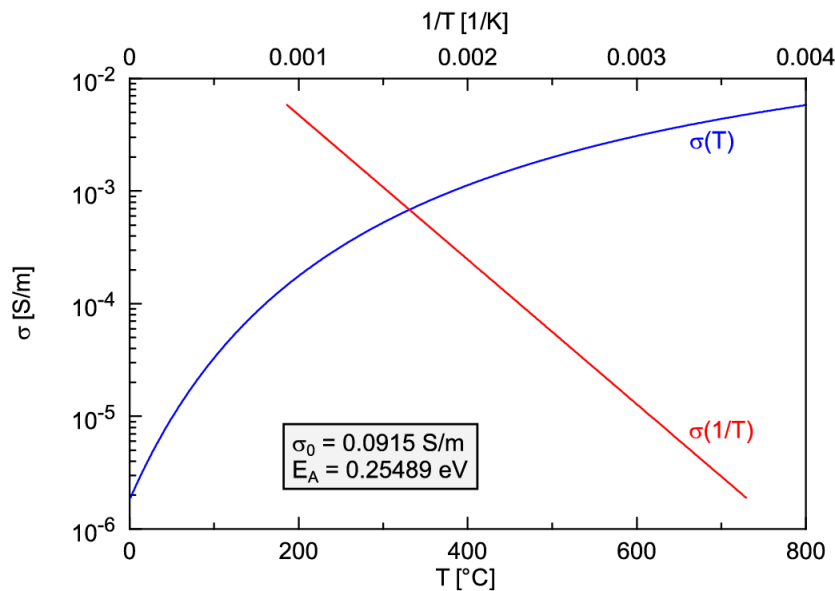


*Fig. 1.2: Temperature dependence of electrical conductivity, here for a dry granulite. Constants have been determined in laboratory experiments (Glover & Vine 1995). Therefore electrical anomalies with  $\sigma$  over 0.1 S/m in the earth's crust cannot be explained by higher temperatures.*

<sup>4</sup> In petrophysics the dependence of  $(1/T)$  is mostly applied as shown in fig. 1.2. In a semi-logarithmical plot we then obtain a straight line in the Arrhenius-diagram.

<sup>5</sup> In contrast to this, the conductivity dependence on the pressure is much lower in most cases. We obtain it by expanding equation (1.6a):  $H = E_A + PdV$  with  $P$  = pressure and  $dV$  = volume,  $H$  is enthalpy.

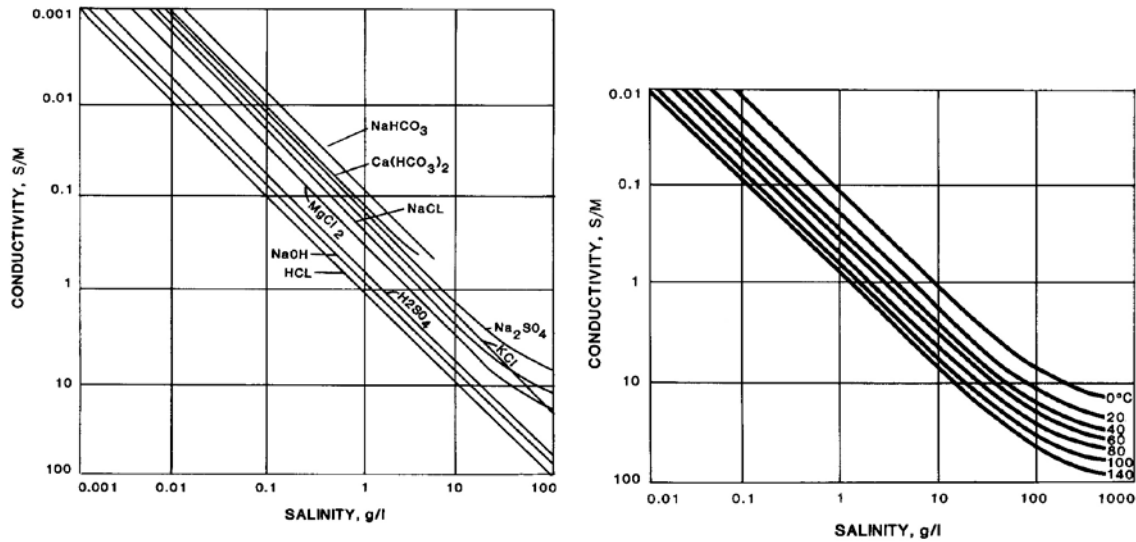


Fig. 1.3: Conductivity as salinity function for varying solutions (left) and varying temperatures of a mixed solution (right). After Palacky (1987), in [N87].

$$\rho_G = F\rho_f = a\Phi^n S^m \rho_f \quad (1.6b)$$

Here  $\rho_G$  denotes the total (bulk) resistivity of the rock,  $\rho_f$  is the resistivity of the fluid (e.g., water) and  $F$  is the (dimensionless) *formation factor*.  $\Phi$  is porosity and  $S$  that part of pores containing fluid. The constants  $a$ ,  $n$  and  $m$  are determined empirically<sup>6</sup>.

The conductivity of fluids is strongly dependent on their salinity and also their temperature (due to the higher mobility of charge carriers). Fig. 1.3 shows these dependencies for different salt solutions; temperature dependence is drawn for a mixed solution, which roughly corresponds to that of sea water. Sea water has an average salinity of 35 g/l (or 35 ‰), deep-crustal fluid often over 100 g/l.

The *connectivity* of the electrolytic phase or the pore space respectively is important. If the conductive component within the badly conductive rock matrix consists of pores or crevices which are not connected to each other it does not influence the total resistance of the rock. Some mixing laws and extremal models have been elaborated for multi-phase systems and the complete connectivity or non-connectivity of the pores, e.g., the *Hashin-Shtrikman (HS) bounds*.<sup>7</sup>

These marginal models consist of spheres with the same proportion of  $\sigma_f$  and  $\sigma_m$  (conductivity of the rock matrix) as the entire rock. For the HS lower bound  $\sigma_{\min}$  the well conductive core of the spheres is surrounded by a badly conductive mantle. For the HS upper bound  $\sigma_{\max}$  the outer shell is well conductive and connects the various spheres. The equations in their original form are as follows:

<sup>6</sup> Conductivity at the boundary layer is the decisive mechanism for clays. It will be discussed later in connection with induced polarization.

<sup>7</sup> According to Hashin & Shtrikman (1962); Maxwell already presented those models in 1881. Waff (1974) and Beekmans & Heyne (1976) or Macdonald (1987) developed other multi-phase models. The percolation theory, that describes the development of coherent areas in a random medium, provides another analysis of two-phase systems. To a certain degree of probability there will be conductive paths through the entire system from a certain percolation threshold on. Only from that point on the effective conductivity will grow significantly.

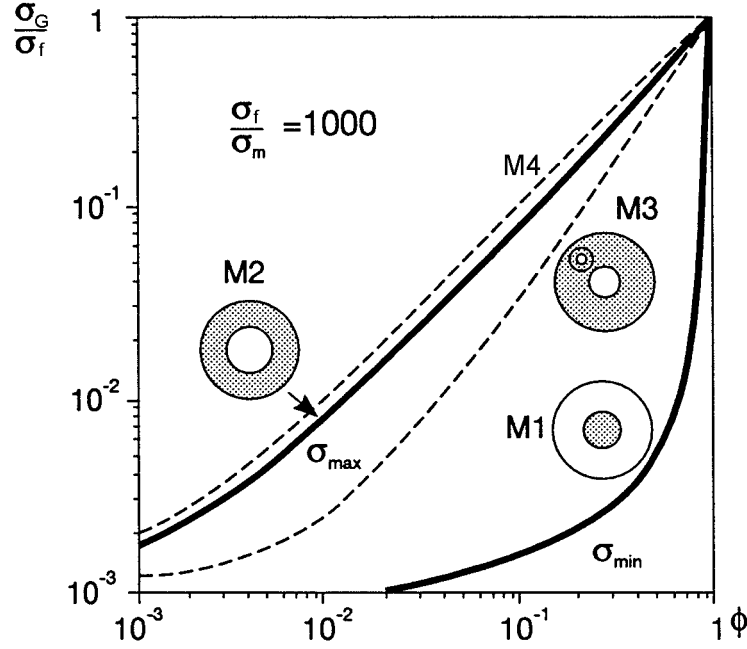


Fig. 1.4: Marginal models according to Hashin-Shtrikman and Sen, calculated for a conductivity proportion of 1:1000. M1: HS lower bound, M2: HS upper bound, M3: according to Sen, M4 (upper broken line): anisotropic (ellipsoids) model. Fig. from [KKL97].

$$\sigma_{\max} = \sigma_f \left( 1 - \frac{3(1-\phi)(\sigma_f - \sigma_m)}{3\sigma_f - \phi(\sigma_f - \sigma_m)} \right) \quad \sigma_{\min} = \sigma_m \left( 1 + \frac{3\phi(\sigma_f - \sigma_m)}{3\sigma_m + (1-\phi)(\sigma_f - \sigma_m)} \right) \quad (1.6c)$$

Alternatively, a mixing law can be described with a parallel or series connection of the phases, for example:

$$\sigma_{\max} = \phi \sigma_f + (1-\phi) \sigma_m \quad \text{and} \quad \sigma_{\min} = \left( \frac{\phi}{\sigma_f} + \frac{1-\phi}{\sigma_m} \right)^{-1} \quad (1.6d)$$

In this case the effective rock conductivity is between  $\sigma_{\min}$  and  $\sigma_{\max}$ :  $\sigma_{\min} \leq \sigma_G \leq \sigma_{\max}$  (s. Fig. 1.4). The upper bound for  $\sigma_f \gg \sigma_m$  is determined by (1.6c) to:

$$\sigma_{\max} = \frac{2\phi}{3-\phi} \sigma_f \quad (1.6e)$$

Sen et al. elaborated another model in which the well conductive spheres are not homogeneous but filled with self-similar smaller spheres which are invariant for changing scales (model M3 in fig. 1.4); here the effective conductivity is:

$$\frac{\sigma_G - \sigma_m}{\sigma_f - \sigma_m} \left( \frac{\sigma_f}{\sigma_G} \right)^{1/3} = \phi \quad (1.6f)$$

or

$$\sigma_G = \sigma_f \phi^{3/2} \quad \text{für} \quad \sigma_m = 0 \quad , \quad (1.6g)$$

i.e., an equation according to Archie's model.

Generalizing Sen's law by replacing spheres with ellipsoids we get an anisotropic model of conductivity (M4) with:

$$\frac{\sigma_G - \sigma_m}{\sigma_f - \sigma_m} \left( \frac{\sigma_f}{\sigma_G} \right)^N = \phi \quad (1.6h)$$

$N$  is the factor for de-electrization that describes the generated field on the body's surface. This field is generated by various charges and opposite the external field<sup>8</sup>. In the limiting cases the ellipsoids degenerate into needles ( $N \rightarrow 0$ ) or plates ( $N \rightarrow 1$ ) respectively.

From a mineralogical point of view the fluid (or melting) phase can be connected if the wetting (dihedral) angle  $\theta$  is below  $60^\circ$  (Fig. 1.5). The dihedral angle is defined by the proportion of the energies at the boundary layer:

$$\cos \frac{\theta}{2} = \frac{1}{2} \frac{\gamma_{ss}}{\gamma_{sf}} \quad (1.7)$$

here  $\gamma_{ss}$  denotes the energy at the bound mineral-mineral and  $\gamma_{sf}$  the energy at the bound mineral-fluid. With  $\theta > 60^\circ$  the fluid phase remains limited to isolated crevices, with  $\theta < 60^\circ$  the fluid phase will connect along the grain boundary even if there are only few parts of fluids in the total system. Even with a volume

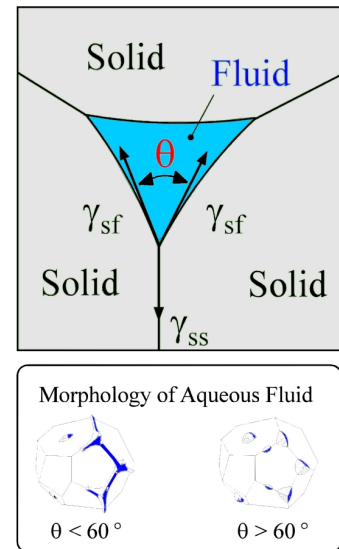


Fig. 1.5: dihedral (wetting) angle (according to Mibe, 2000).

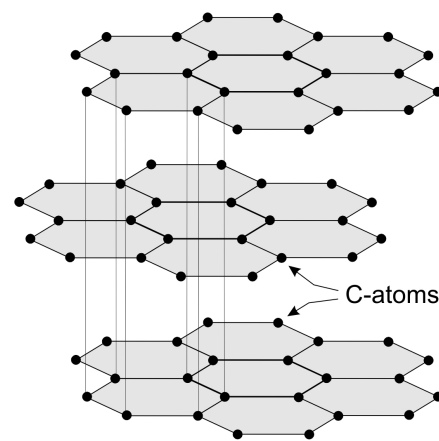
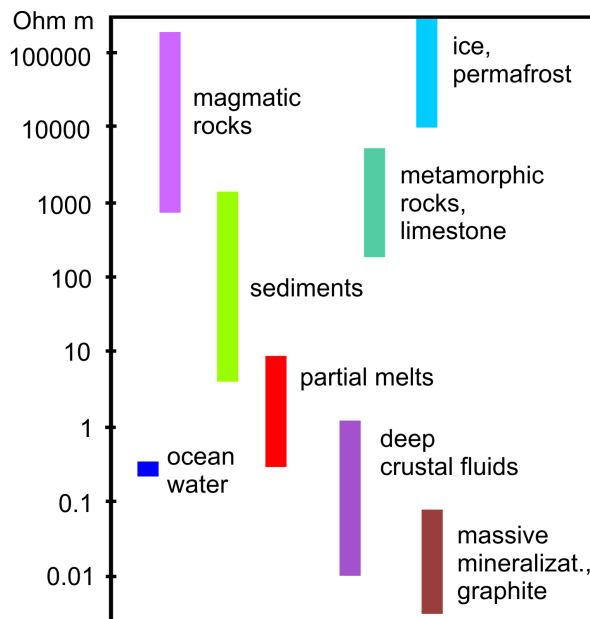


Fig. 1.6: left: Typical resistivity of some rocks and minerals. The resistivity of freshwater is about 10-100  $\Omega m$ , that of dry ice and (potash) salt over  $10^6 \Omega m$ . In the case of mineralization the conductivity largely depends on the mineral; only a small amount is needed to raise the conductivity of pyrrhotite, while there has to be a proportion of at least 60% in the rock matrix of pyrite. Right: Lattice structure of graphite.

<sup>8</sup> The entire electrical field is  $\underline{E} = \underline{E}_{ext} + \underline{E}_N$  with  $\underline{E}_N = -1/\epsilon_0 \nabla \underline{P}$ ,  $\underline{P}$  is the vector of the electrical polarisation.

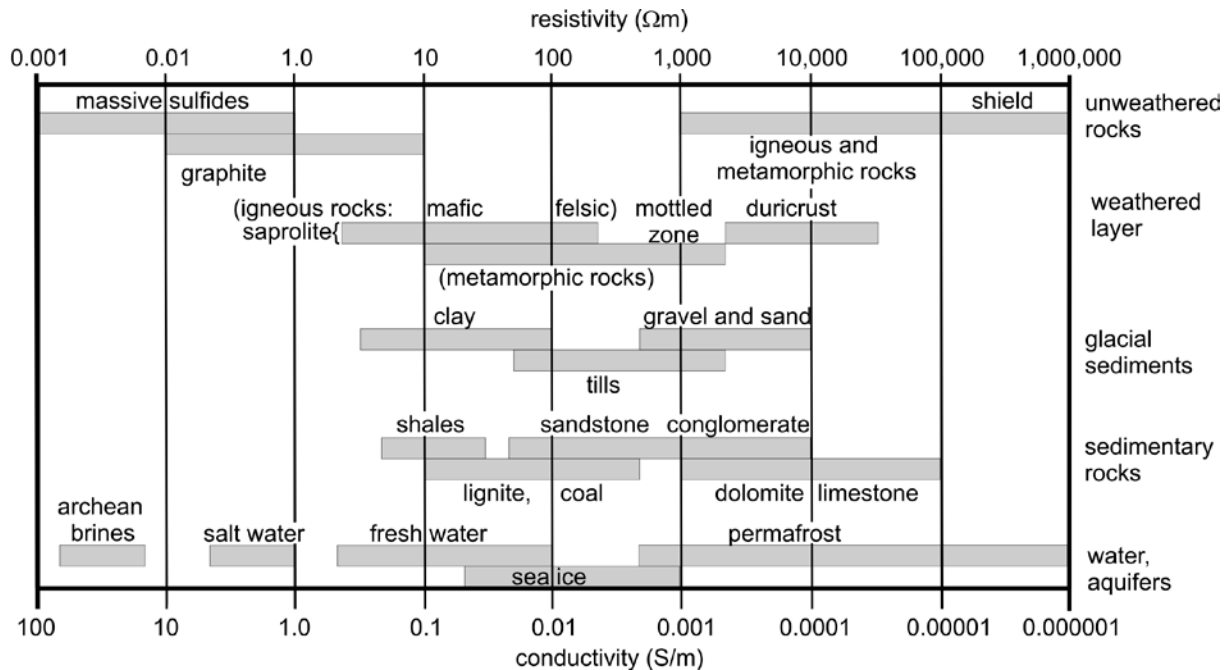


Fig. 1.7: conductivity dependence on the degree of weathering, modified according to Palacky (1987, in [N87]).

part of less than 1%, saline fluids for example might form a connected network which influences the electrical conductivity.

In Fig. 1.6 some characteristic values of the resistivity of rocks are listed. They cover a large area from  $10^{-7} \Omega\text{m}$  for pure metals up to  $10^{15} \Omega\text{m}$  for (dry) potash- and rock salts. They also have a wide range which mainly depends on the existence of fluids in the pores and crevices. Additionally, the weathering degree of the rocks near the surface (Fig. 1.7) is of great importance.

The good electrical conductivity of graphite is particularly interesting. Carbon belongs to the fourth main group and has four outer electrons. In the modification of diamond every C-atom has four neighbours (cubic lattice centred on the surface). Therefore it is a bad electrical conductor because no electron on the outer shell has weak bonds. In the modification of graphite the C-atoms form layered, hexagonal rings in which every atom has three neighbours. That means that there are always three electrons needed to bind the atoms (s. fig. 1.6). Then the surplus electron can bind with another surplus electron of a neighbouring atom (weak resonance bonding). Due to this weak bond it can easily be moved within the layer, i.e. carry electricity. The layers are kept together only by weak van der Waals forces (molecular forces with mutual induction of dipole moments), i.e. not by electronic bonds. The result is a high degree of conductivity in the direction of the layers (approximately  $10^5 \text{ S/m}$  for pure graphite) and thus a strong anisotropy.

If we expand the electrical conductivity that can occur in many other rock complexes and that we regarded as a scalar quantity up to now, we can mathematically describe the anisotropy as follows:

$$\underline{\underline{\sigma}} = \begin{pmatrix} \sigma_{xx} & \sigma_{xy} & \sigma_{xz} \\ \sigma_{yx} & \sigma_{yy} & \sigma_{yz} \\ \sigma_{zx} & \sigma_{zy} & \sigma_{zz} \end{pmatrix} , \quad (1.8a)$$

It becomes a 3 x 3 tensor. The off-diagonal elements, however, are pairwise equal:  $\sigma_{xy} = \sigma_{yx}$  etc. (the electric current does not care if it flows in xy- or yx-direction)<sup>9</sup>. The number of conductivities is therefore reduced to six. If we now turn the coordinate system in the direction of the main axis there are three elements

$$\underline{\underline{\sigma}} = \begin{pmatrix} \sigma_1 & 0 & 0 \\ 0 & \sigma_2 & 0 \\ 0 & 0 & \sigma_3 \end{pmatrix} \quad (1.8b)$$

and three directions (strike, dip, slant) remaining. In contrast to this intrinsic anisotropy, which is a characteristic of the rock, a structural, macro or pseudo anisotropy can be defined if the size of the volume prospecting methods integrate, let the structures *appear* to be anisotropic (e.g., faults that have a better conductivity in a poorly conductive rock ensemble). This reflects the reduced resolution of the methods (see also Fig. 1.8)<sup>10</sup>.

In cases of horizontal stratification we distinguish between conductivity flowing in vertical or horizontal direction<sup>11</sup>. We then define an *anisotropy coefficient*

$$\eta = \sqrt{\sigma_h / \sigma_v} = \sqrt{\rho_v / \rho_h} , \quad (1.8c)$$

which in practice varies between 1.4 and 2.5. As we will see later, this coefficient cannot be resolved by one single method, but only by a combination of different methods with different geometries of the electrical systems in the subsoil (e.g. DC geoelectrics and MT).

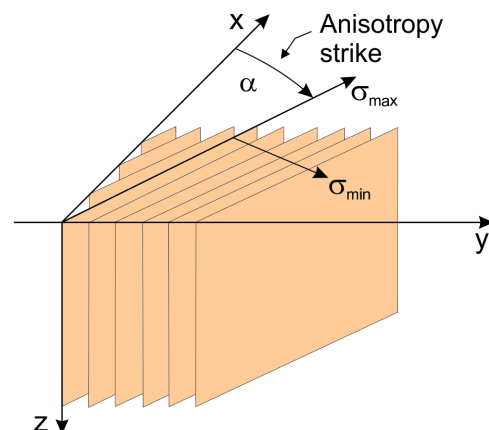


*Fig. 1.8: An inclined lacustrine sandstone (Humar Basin, North Sudan). Its fine layering reflects the different conditions of sedimentation in the course of time, and results in a macro-, pseudo- or structural anisotropy. The conductivity is larger along the conductive planes and smaller in the direction perpendicular to the layering.*

<sup>9</sup> This symmetry does not apply when the magnetic field is important, e.g., the Hall effect in a plasma.

<sup>10</sup> Already in the 1930s research about electrical anisotropy was carried out (Maillet & Doll 1932). In the following not much attention was paid on this subject until in the 1990s it became highly topical again.

<sup>11</sup> We often notice this kind of anisotropy caused by fine layering in marine or lacustrine sediments. One typical anisotropic rock is gneiss, which is already visually obvious due its banded structure.



In the following chapters we assume that the electrical conductivity is real and frequency-independent. To a large extent this applies to the frequency range taken into consideration here.

Ohm's Law (1.5) is only one of three material equations in electrodynamics. The other two equations for media that cannot be polarized and not be magnetized are:

$$\underline{D} = \epsilon_r \epsilon_0 \underline{E} \quad (1.9a)$$

$$\underline{B} = \mu_r \mu_0 \underline{H} \quad (1.9b)$$

Here  $\underline{D}$  is the vector of dielectric displacement;  $\underline{H}$  is the magnetic field strength.  $\epsilon_0 = 8.89 \times 10^{-12}$  As/Vm is the permittivity constant and  $\mu_0 = 4\pi \times 10^{-7}$  Vs/Am is the induction constant.

The natural maximum of the relative dielectricity  $\epsilon_r$  for water is approximately 81, for dry rocks we can assume 20 on average. Dielectricity is important only in high frequency processes (e.g. ground-penetrating radar) as we will see later. The permeability  $\mu_r$  differs significantly from 1 only for some titanium-magnetites. In most electromagnetic applications, however, we can equate it with 1 and neglect it (s. table 1.1).

Rock, mineral	Dielectric const.	Mineral	Permeability
Galena	18	Magnetite	5
Sphalerite	7.9–69.7	Pyrrhotite	2.55
Cassiterite	23	Titanomagnetite	1.55
Hematite	25	Hematite	1.05
Fluorite	6.2–6.8	Pyrite	1.0015
Calcite	7.8–8.5	Rutile	1.0000035
Apatite	7.4–11.7	Calcite	0.999987
Barite	7–12.2	Quartz	0.999985
Peridotite	8.6	Hornblende	1.00015
Norite	61		
Quartz porphyry	14–49.3		
Diabase	10.5–34.5		
Trap	18.9–39.8		
Dacite	6.8–8.2		
Obsidian	5.8–10.4		
Sulphur	3.6–4.7		
Rock salt	5.6		
Anthracite	5.6–6.3		
Gypsum	5–11.5		
Biotite	4.7–9.3		
Epidote	7.6–15.4		
Plagioclase feldspar	5.4–7.1		
Quartz	4.2–5		
Granite (dry)	4.8–18.9		
Gabbro	8.5–40		
Diorite	6.0		
Serpentine	6.6		
Gneiss	8.5		
Sandstone (dry to moist)	4.7–12		
Packed sand (dry to moist)	2.9–105		
Soil (dry to moist)	3.9–29.4		
Basalt	12		
Clays (dry to moist)	7–43		
Petroleum	2.07–2.14		
Water (20°C)	80.36		
Ice	3–4.3		

*Table 1.1: Permittivities (left) and permeabilities (above) of some minerals and rocks (from Telford et. al.1992).*

## 2 EM-fields in homogeneous and isotropic conductors

The classical electrodynamic theory generally emanates from Maxwell's equations. In addition to the material equations (1.5, 1.8, 1.9) all non-relativistic phenomena derive from them:

$$\nabla \times \underline{H} = \frac{\partial \underline{D}}{\partial t} + \underline{J} \quad \nabla \times \underline{E} = -\frac{\partial \underline{B}}{\partial t} \quad (2.1a,b)$$

$$\nabla \cdot \underline{B} = 0 \quad \nabla \cdot \underline{D} = Q \quad (2.1c,d)$$

Here  $Q$  denotes charge density. Depending on the geoelectric method these equations simplify: In DC geoelectrics all terms containing time derivations are 0, while in methods using low frequencies the displacement current  $\partial \underline{D} / \partial t$  is negligible, etc. Eq. (2.1a) is called *Ampère's law*; eq. (2.1b) is called *Faraday's law*.

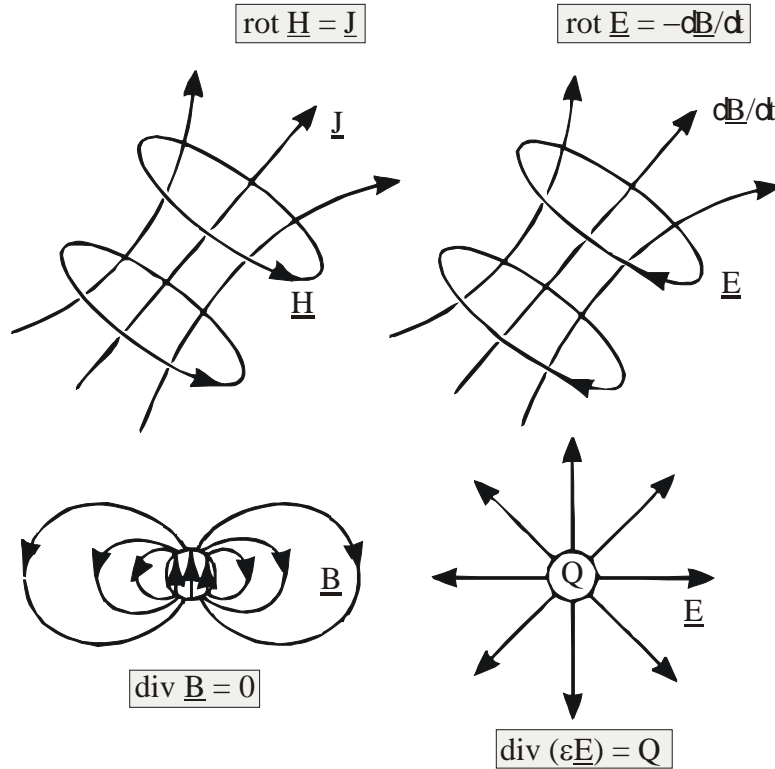


*Fig. 2.1: Illustration of Maxwell's equations. Upper left: an electric current causes a magnetic eddy current; upper right: a time varying magnetic field causes an electric eddy field; lower left: no magnetic monopoles exist; lower right: the electric charges are sources of the electric field.*

In this chapter, we assume a homogeneous and isotropic subsurface (conductivity  $\sigma$ , permeability  $\mu_r$  and dielectricity  $\epsilon_r$  are constant); furthermore this homogeneous halfspace shall only be “normally” polarizable and magnetizable, i.e., any polarization vector is zero. Additionally we only regard fields outside the sources.

From (2.1a) together with the material equations  $\underline{B} = \mu \underline{H}$ ,  $\underline{D} = \epsilon \underline{E}$  and  $\underline{J} = \sigma \underline{E}$  follows:

$$\nabla \times \underline{B} = \mu \sigma \underline{E} + \mu \epsilon \frac{\partial \underline{E}}{\partial t}$$

and with a theorem of vector calculus

$$\nabla \times (\nabla \times \underline{\mathbf{B}}) = \nabla \underbrace{(\nabla \cdot \underline{\mathbf{B}})}_0 - \nabla^2 \underline{\mathbf{B}} \quad :$$

$$\nabla \times (\nabla \times \underline{\mathbf{B}}) = \nabla \times \left( \mu\sigma \underline{\mathbf{E}} + \mu\varepsilon \frac{\partial \underline{\mathbf{E}}}{\partial t} \right) = -\mu\sigma \frac{\partial \underline{\mathbf{B}}}{\partial t} - \mu\varepsilon \frac{\partial^2 \underline{\mathbf{B}}}{\partial t^2} = -\nabla^2 \underline{\mathbf{B}} \quad ;$$

Accordingly, for the electric field in (2.1) one obtains an equation for the damped propagation of an electromagnetic wave, the *telegrapher's equation*:

$$\nabla^2 \underline{\mathbf{F}} = \mu\sigma \frac{\partial \underline{\mathbf{F}}}{\partial t} + \mu\varepsilon \frac{\partial^2 \underline{\mathbf{F}}}{\partial t^2} \quad , \quad (2.2)$$

where  $\underline{\mathbf{F}}$  represents one of the field quantities. The second term in (2.2) depicts wave propagation of the field; the first term contains the conductivity and describes a diffusion process.  $(\mu\sigma)^{-1}$  is called (magnetic) “diffusivity”, with the dimension  $\text{m}^2/\text{s}$  (area/time). The electrical conductor is assumed not to move; otherwise, in the case of a slowly time dependent variation, a Lorentz term ( $\underline{\mathbf{v}} \times \underline{\mathbf{B}}$ ,  $\underline{\mathbf{v}}$  = velocity) must be considered.

Now we regard fields with a periodic time dependency  $\underline{\mathbf{F}} \sim \exp(i\omega t)$  and a periodic space dependency  $\underline{\mathbf{F}} \sim \cos(vx)$ <sup>1</sup>.  $\omega$  is the angular frequency with  $\omega = 2\pi f$  and  $v$  is the horizontal wave number with  $v = 2\pi/\ell$ ,  $\ell$  is wavelength. Then from (2.2) follows:

$$\left( \frac{\partial^2 \underline{\mathbf{F}}}{\partial x^2} + \frac{\partial^2 \underline{\mathbf{F}}}{\partial y^2} + \frac{\partial^2 \underline{\mathbf{F}}}{\partial z^2} \right) = i\omega\mu\sigma \underline{\mathbf{F}} - \mu\varepsilon\omega^2 \underline{\mathbf{F}} \quad \text{and, as } \underline{\mathbf{F}} = \underline{\mathbf{F}}(x,z,t):$$

$$-v^2 \underline{\mathbf{F}} + \frac{\partial^2 \underline{\mathbf{F}}}{\partial z^2} = i\omega\mu\sigma \underline{\mathbf{F}} - \mu\varepsilon\omega^2 \underline{\mathbf{F}} \quad \text{and therefore the Helmholtz equation:}$$

$$\frac{\partial^2 \underline{\mathbf{F}}}{\partial z^2} = \gamma^2 \underline{\mathbf{F}} \quad . \quad (2.3)$$

$\gamma$  is the complex propagation constant with the dimension of a *wave number* ( $\text{m}^{-1}$ ):

$$\gamma^2 = v^2 + i\omega\mu\sigma - \mu\varepsilon\omega^2 = v^2 + k^2 - \kappa^2 \quad . \quad (2.4)$$

With these equations (2.3, 2.4) we assigned the description of the fields from the time-space domain to the frequency-wave-length domain.

The undamped part<sup>2</sup> of the wave (3. term in (2.4)) is described by the wave number  $\kappa$ , the wave length is  $\lambda_0 = 2\pi/\kappa = 2\pi/[\omega(\mu\varepsilon)^{1/2}] = c_0/f$  with  $c_0$  = speed of light.

Regarding the diffusion process alone, the Helmholtz equation is given by:

$$\frac{\partial^2 \underline{\mathbf{F}}}{\partial z^2} = k^2 \underline{\mathbf{F}} \quad (2.5)$$

---

<sup>1</sup>  $\underline{\mathbf{F}}$  is only a function of  $x$ ,  $z$  and  $t$ . Constraining lateral variations to the  $x$ -direction is only to keep the following calculations simple, and constitutes no loss of generality. The periodic site dependency of  $v$  is only a special case; in the near field of a dipole, the lateral term is to modify. The case  $v = 0$  describes a plane wave. Note that time dependency is often set to  $\exp(-i\omega t)$ .

<sup>2</sup> See comment on page 2-5.

with the now *complex wave number*:

$$k = \sqrt{i\omega\mu\sigma} \quad . \quad (2.6a)$$

This wave number can also be expressed as:

$$k = (1+i)\sqrt{\frac{\omega\mu\sigma}{2}} = \sqrt{\frac{\omega\mu\sigma}{2}} + i\sqrt{\frac{\omega\mu\sigma}{2}} \quad , \quad \text{because} \quad (2.6b)$$

$$\sqrt{i} = \sqrt{(-1)^{1/2}} = \sqrt{e^{i\pi/2}} = e^{i\pi/4} = \left(\frac{1}{\sqrt{2}} + i\frac{1}{\sqrt{2}}\right) = \frac{1+i}{\sqrt{2}} \quad .$$

Here the Euler formula  $e^{i\phi} = \cos\phi + i\sin\phi$  together with

$$\cos\frac{\pi}{4} = \sin\frac{\pi}{4} = \frac{1}{\sqrt{2}}$$

were used. In eq. (2.5)  $F$  only depends on the depth  $z$  (and the frequency), (2.5) has the general solution:

$$\underline{F}(z) = \underline{F}_0 e^{-kz} + \underline{F}_1 e^{+kz} \quad . \quad (2.7)$$

$\underline{F}_0$  and  $\underline{F}_1$  are the values of the fields at the surface. To understand the behavior of the fields in the subsurface, the exponential expressions are separated into real and imaginary parts (see eq. (2.6b)):

$$e^{kz} = e^{gz} e^{igz} \quad \text{und} \quad e^{-kz} = e^{-gz} e^{-igz} \quad \text{mit} \quad g = \text{Re } k = \text{Im } k = \sqrt{\frac{\omega\mu\sigma}{2}}$$

The imaginary part has an absolute value of 1, which results from the Euler formula and the Moivre formula:

$$e^{\pm igz} = \cos gz \pm i \sin gz \quad .$$

Consequently, the absolute value of the complex exponential function is

$$|e^{kz}| = e^{\text{Re } kz} = e^{gz} \quad .$$

The term  $\exp(+gz)$  describes an exponential increase with depth, which is physically absurd, while the term  $\exp(-gz)$  describes an exponential decrease for  $z \rightarrow \infty$ . Substituting  $\underline{F}_1 = 0$  in solution (2.7) one obtains:

$$\underline{F}(z) = \underline{F}_0 e^{-kz} \quad . \quad (2.9)$$

Consider that this limitation of the variety of solutions only applies for a homogeneous space. In a layered half space, on the other hand, reflections at the interfaces occur, leading to the other solution.

The depth, where the absolute value of the field

$$F(z) = |\underline{F}_0 e^{-kz}| = F_0 e^{-gz}$$

is attenuated to 1/e-th of the value at the surface is defined as the *penetration depth* or *skin depth*  $\delta$  of an electromagnetic plane wave (with  $v = 0$ ) in a conductive material:

$$\delta = \sqrt{\frac{2}{\mu\omega\sigma}} = \frac{1}{g} \quad \text{with} \quad (2.10a)$$

$$F(\delta) = \frac{1}{e} F_0 = \frac{1}{e} F(z=0) \quad . \quad (2.10b)$$

The evidence can easily be provided by substitution:

$$F(\delta) = F_0 e^{-g\delta} = F_0 e^{-1} = \frac{1}{e} F_0 \quad .$$

By substituting  $\mu = \mu_0$ ,  $\mu_0 = 4\pi \times 10^{-7}$  Vs/Am,  $\omega = 2\pi/T$  and  $\rho = 1/\sigma$ , one obtains:

$$\delta \approx 0.5\sqrt{\rho T} \quad \text{oder} \quad \delta \approx 0.5\sqrt{\rho/f} \quad [\text{km}] \quad . \quad (2.10c)$$

Consequently penetration depth is a function of both resistivity and period or frequency of the fields, respectively (see fig. 2.2). A numerical example: In a granite body ( $\rho = 1000 \Omega\text{m}$ ) there is  $\delta = 500$  km for  $T = 1000$  s and  $\delta = 5$  km for  $T = 0.1$  s, while the penetration depth in well conducting sediments ( $\rho = 10 \Omega\text{m}$ ) is only 50 or 0.5 km for the same periods.

We define the wave length  $\Lambda$  of the diffusing field as:

$$\Lambda = \frac{2\pi}{g} = 2\pi\delta \quad , \quad \text{thus} \quad k = (1+i)\frac{2\pi}{\Lambda} = \frac{(1+i)}{\delta} \quad \text{and} \quad k^2 = \frac{2i}{\delta^2} \quad . \quad (2.10d)$$

As the damping term is complex, it causes a different decay for the real and imaginary parts

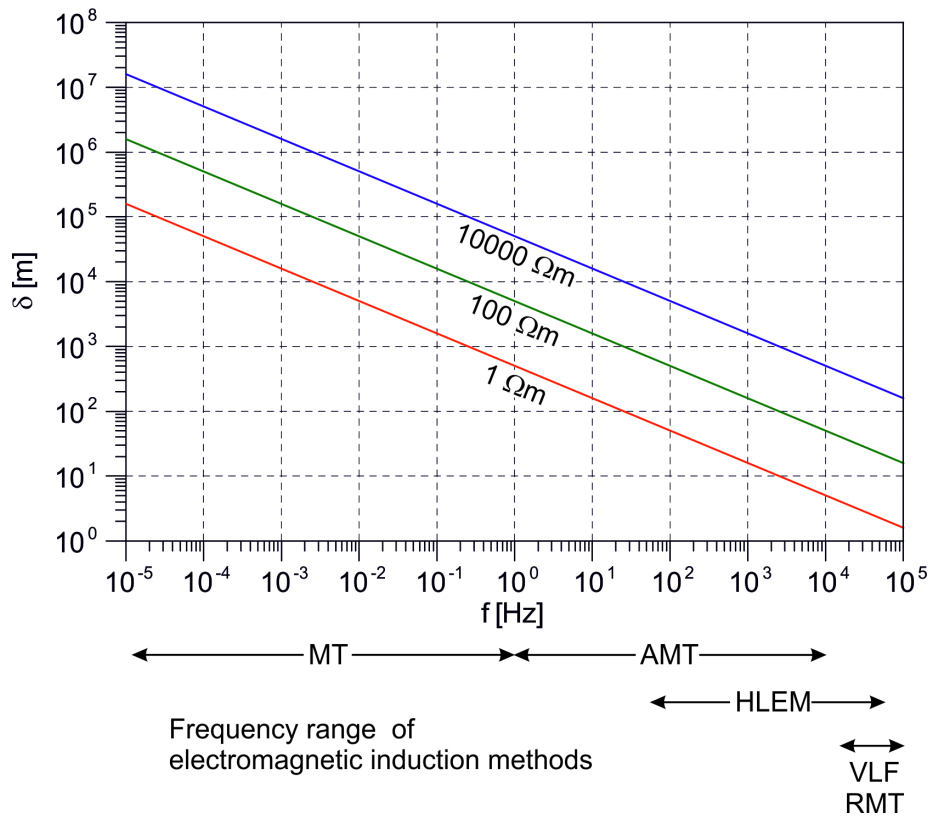


Fig. 2.2: Penetration depth as a function of frequency for different resistivities and the frequency range of the induction methods. For active methods, e.g. HLEM (Slingram), the effective penetration depth is lower due to the geometric damping in the near field.

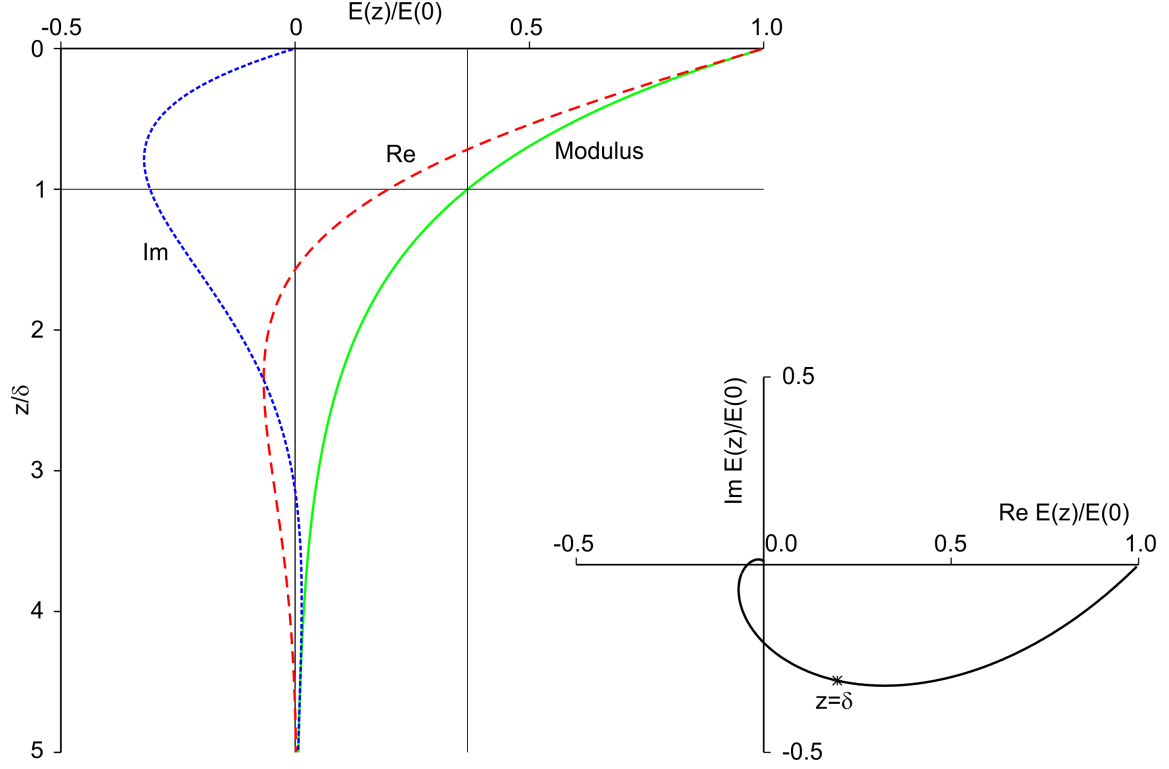


Fig. 2.3: Descent of the strength  $E$  with depth for the modulus, the real and the imaginary part. Lower right: Argand diagram of this relation.

of the field and therefore a phase shift compared to the field at the surface (see fig. 2.3).

The propagation constant or wave number of the total field  $\gamma$  from eq. (2.4) can be expressed by three characteristic lengths  $\ell$ ,  $\delta$  and  $\lambda$ :

$$\gamma^2 = \frac{4\pi^2}{\ell^2} + \frac{2i}{\delta^2} - \frac{4\pi^2}{\lambda^2}. \quad (2.11)$$

The smallest of these lengths basically defines the value of  $\gamma$  and consequently the character of the field. Now we investigate the three marginal cases:

- I.  $\ell \ll \delta, \lambda$ . Under excitation at very low frequencies by a highly inhomogeneous source (the observation point is located in the near field of the transmitter dipole such as in the Slingram method; the DC geoelectric method constitutes the extreme case) one gets  $\gamma \approx v$ , i.e. the variation of the field is determined by the – now purely geometric – term  $\exp(-vz) = \exp(-2\pi z/\ell)$ . That means the more inhomogeneous the field is in horizontal direction, the faster it decays with depth  $z$ .
- II.  $\lambda \ll \delta, \ell$ . For high frequencies and plane waves the propagation in a poor conductor is undamped<sup>3</sup>. This is the case of the georadar, whereas in practice the frequencies can not be chosen high enough that the contribution of  $k$  can totally be neglected. This is also mostly the case for the geometric term.

<sup>3</sup> This penetration term causes an additional damping when  $\mu_r \neq 1$  and/or  $\epsilon_r \neq 1$ . In this case it is real and does not cause any phase shift. The exploration of  $\epsilon$  is the aim of the ground penetrating radar (GPR) method.



III.  $\delta \ll \lambda, \ell$ . The field is *quasi homogeneous (far field approximation)* and the *charge current outweighs the displacement current*. This is the case for magnetotelluric and geomagnetic deep sounding; we examine only quasi-homogeneous and quasi-stationary fields here.

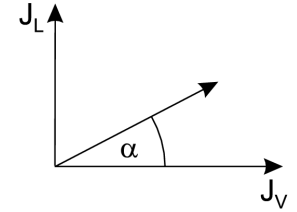
Case III of the diffusion of the field takes a central position between the purely geometrically damped and the undamped propagation. For plain waves ( $v \equiv 0$ ) the displacement current

$$J_v = \frac{\partial D}{\partial t} = \epsilon \frac{\partial E}{\partial t} = i\omega\epsilon E \quad (2.12)$$

can be neglected with respect to the charge current  $J_L = \sigma E$  if the relaxation time  $\tau_0$  – that means the average decay time of free electric charges in an observed volume – is small compared to the oscillation period:

$$\omega \ll \frac{\sigma}{\epsilon_r \epsilon_0} = \frac{1}{\tau_0} \quad \text{or} \quad (2.13a)$$

$$\tan \alpha = \frac{J_L}{|J_v|} = \frac{\sigma}{\epsilon \omega} = 1.8 \times 10^{10} \frac{\sigma}{\epsilon_r f} \gg 1, \quad (2.13b)$$



here  $\epsilon_0 = 8.8543 \times 10^{-12}$  As/Vm was inserted;  $f$  is measured in Hz and  $\sigma$  in S/m (see fig. 2.4). A field that satisfies this condition is called *quasi-stationary*. The quantity  $\alpha$  is often referred to as loss angle (because of Ohm's losses resulting from  $J_L$ ) and  $\tan \alpha$  as “loss tangent”.

Furthermore it is assumed that the phase variation of the incoming “plain” wave in the investigation area is negligible. With a frequency of, e.g., 1 kHz wave length is  $\lambda_0 = c_0/f = 10^5$  m, with 1 Hz it's  $\lambda_0 = 10^8$  m, etc. ( $c_0 = 10^8$  m/s). Consequently, it is always much larger than the observed target (fig. 2.5).

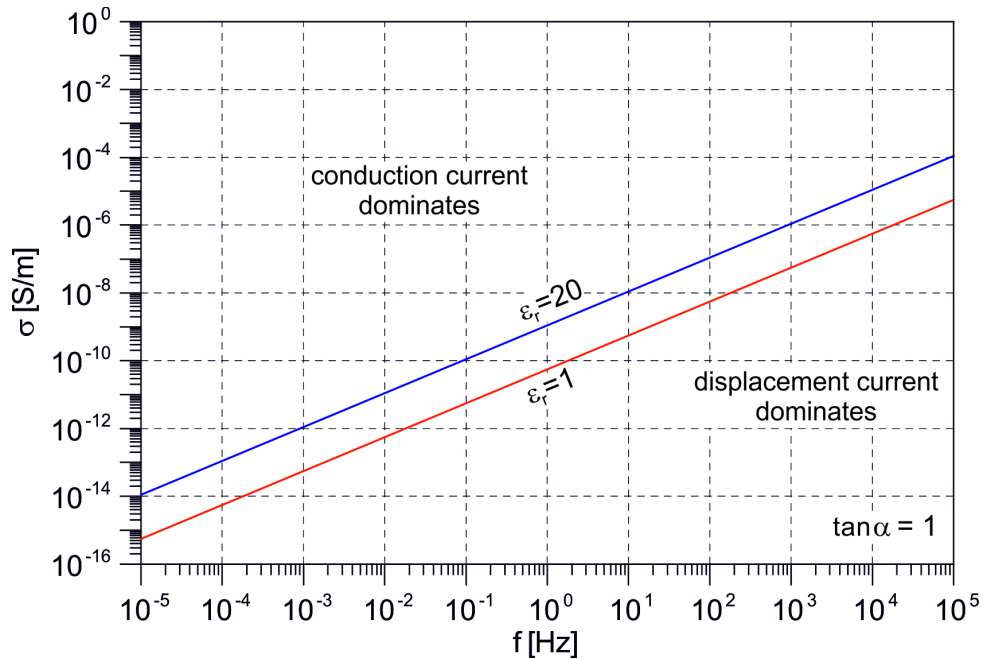


Fig. 2.4: The relation between diffusion current and displacement current ( $\tan \alpha = 1$ ) for different dielectric constants  $\epsilon_r$ .

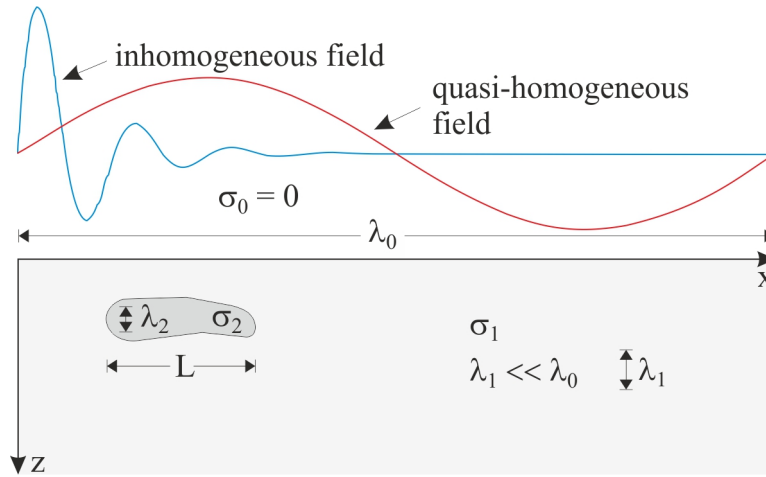


Fig. 2.5: The lateral wavelength  $\lambda_0$  must be much larger than the wavelength in the subsurface  $\lambda_1$  and therefore it must also be larger than the dimension  $L$  of a possible anomaly ( $\sigma_2 > \sigma_1$ ,  $\lambda_2$ ).

One may think of course think of MT signals simply as an electromagnetic wave arriving at some angle at the earth's surface. Due to the enormous conductivity contrast, even a wave under grazing incidence will propagate vertically down into the earth (Fig. 2.6a).

In the earth, the wave changes its physical character: It's severely attenuated and a complex quantity, i.e., suffers a phase shift against its surface value. It now turns into a diffusion process. This holds for E and B fields in the same manner. But E and B have now a phase shift of  $45^\circ$ . Note the dimensions of wavelength in free space, which make it difficult to imagine these processes as wave propagation.

Thus, instead of thinking of plane waves, we better look at an excitation as in figure 2.6b: Currents in outer space (in the magnetosphere or in the ionosphere) are accompanied by a magnetic field. Like in a transformer this magnetic field induces electrical currents in the conducting earth. Wherever these external fields come from, the only important thing is that they are quasi-homogeneous, i.e., the spatial wave number  $v = 0$  !

If we regard now without loss of generality only one component, e.g., the magnetic field  $B_y$ , the solution (2.7) of the Helmholtz equation simplifies to:

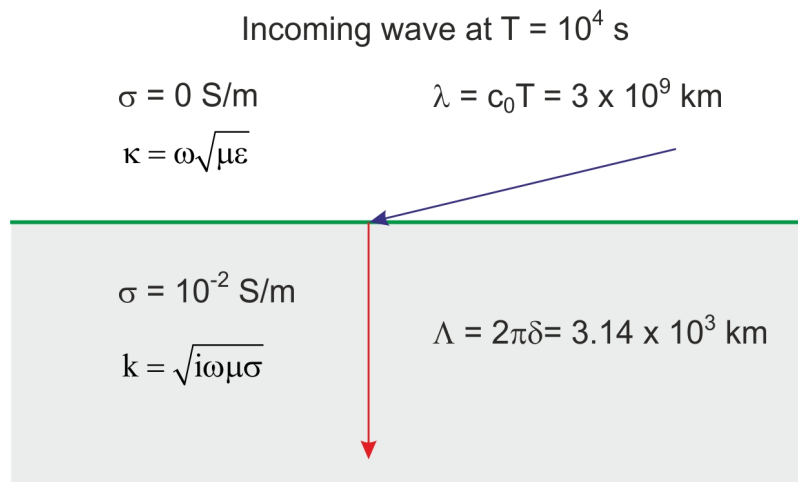


Fig. 2.6a: An incoming wave is always refracted perpendicularly into the ground due to the huge conductivity contrast between air and the earth.

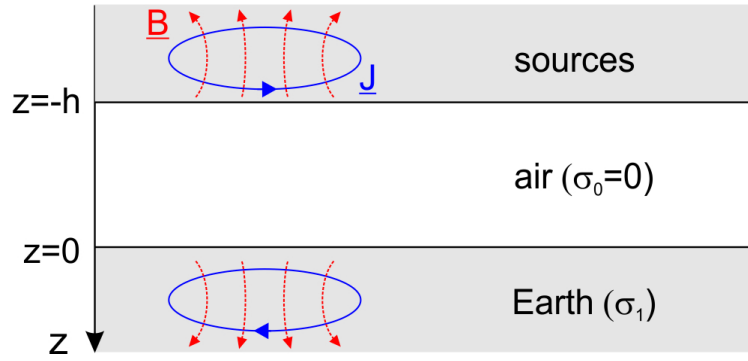


Fig. 2.6b: The general model of geomagnetic induction without wave analogy.

$$B_y = B_{y0} e^{-kz} . \quad (2.14)$$

As a result from (2.5) and (2.1b) we get:

$$\frac{\partial E_x}{\partial z} = -E_{x0} k e^{-kz} = -i\omega B_y = -i\omega B_{y0} e^{-kz} . \quad (2.15)$$

Hence, we obtain the relation between the electric and the magnetic field:

$$Z = Z(\omega) = \frac{E_{x0}}{B_{y0}} = \frac{i\omega}{k} = \frac{i\omega}{\sqrt{i\omega\mu\sigma}} = \sqrt{\frac{i\omega}{\mu\sigma}} = \sqrt{\frac{\omega}{\mu\sigma}} \sqrt{i} . \quad (2.16a)$$

$Z$  is known as the “*magnetotelluric impedance*” and contains the required information about conductivity of the subsurface. As a complex number  $Z = |Z|e^{i\varphi}$  it has the norm

$$|Z| = \sqrt{\frac{\omega}{\mu\sigma}} . \quad (2.16b)$$

As a result we obtain resistivity<sup>4</sup>:

$$\rho = \rho(\omega) = \frac{\mu}{\omega} |Z|^2 \quad (2.17a)$$

or, if we put in the numerical value for  $\mu_0 = 4\pi \times 10^{-7}$  Vs/Am and  $\omega = 2\pi/T$  with  $T$  in s and  $Z$  in (mV/km)/nT =  $10^{-3}$  (V/m)/T, we get:

$$\rho = \rho(T) = 0.2 T |Z|^2 . \quad (2.17b)$$

Here we already set  $\mu = \mu_0$ , as is adequate in most cases (except for measurements on huge iron ore deposits and perhaps for measurements on the sea bottom on top of the upper basaltic, oceanic crust). According to (2.16a,b) the impedance changes by  $\mu_r^{-1/2}$ , the resistivity according to (2.17a) by  $\mu_r^{1/2}$  if the relative permeability is  $\mu_r \neq 1$ . The skin depth changes accordingly.

$Z$  has the *phase*  $\varphi = i^{1/2}$ , so:

$$\varphi = \varphi(T) = e^{i\pi/4} = 45^\circ . \quad (2.18)$$

<sup>4</sup> The period or frequency dependence of the resistivity is given explicitly as well as implicitly by the period dependency of  $Z$ .

The electric field leads the magnetic field by  $45^\circ$ <sup>5</sup>. If  $Z$  is calculated by the orthogonal components  $E_y$  and  $B_x$ , this yields to a phase shift of  $\varphi = -135^\circ$  (Fig. 2.7)<sup>6</sup>. Usually,  $180^\circ$  are added to this value for reasons of clarity, so that  $\varphi_{xy}$  and  $\varphi_{yx}$  are in the same quadrant. If the approach  $\exp(-i\omega t)$  for time dependency had been used, the result would have been the complex conjugate impedance and phases of  $-45^\circ$  or  $135^\circ$  respectively. A function like the impedance is also called *transfer function*, a term originating in filter theory: The information about the subsoil (here resistivity) is transferred from the input signal (magnetic field) to the output signal (telluric signal) by means of a linear operator. The real part of an electromagnetic transfer function (like the impedance) is often called "*in-phase*", the imaginary part "*out-of-phase*" or "*quadrature*".

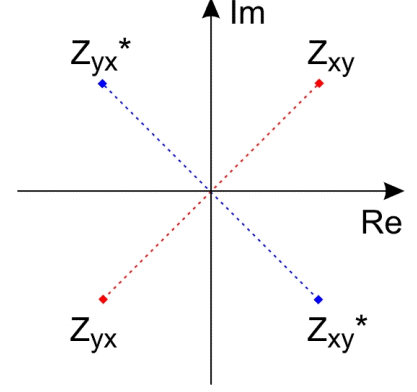


Fig. 2.7: The impedance in the complex plane.

This “impedance” measured in [m/s] has the dimension of a velocity. If the magnetic field  $H$  instead of the magnetic induction  $B$  would have been used, the result would have been a quantity of the expected dimension of an impedance or resistance of waves [ $\Omega$ ]:

$$\zeta = \frac{E_x}{H_y} \quad (2.19)$$

But the actually measured quantity (e.g., in an induction coil) is the magnetic flux density (or a voltage that is proportional to the derivative of  $B$  with respect to time  $\partial B/\partial t$ ), thus we obtain the above, somehow curious definition. Of course, this definition does not only apply to the damped case. The wave resistance is one of the quantities that characterize the electromagnetic field in a particular medium. In vacuum wave resistance is

$$|\zeta| = \left| \frac{E_x}{H_y} \right| = \mu_0 \left| \frac{E_x}{B_y} \right| = \mu_0 \frac{|i|\omega}{\sqrt{\mu_0 \epsilon_0} \omega^2} = \sqrt{\frac{\mu_0}{\epsilon_0}} \approx 377 \, \Omega \quad .$$

In the *time domain method (TEM)* we cannot use a harmonic approach for the field quantities. Now the solution of the diffusion equation

$$\nabla^2 F = \mu_0 \sigma \frac{\partial F}{\partial t} \quad (2.20)$$

is the error function (see later in this manuscript):

$$F = F_0 \operatorname{erf} \left( z \sqrt{\frac{\mu_0 \sigma}{4t}} \right) \quad (2.21)$$

<sup>5</sup> The lead of the phase of the electric field does not create a “causality problem” as it is sometimes assumed, because neither the  $B$ - nor the  $E$ -field dies exist “earlier”, both are connected inseparably. A time varying  $B$ -field always causes an  $E$ -field – and vice versa; the one cannot exist without the other. The phase relation between them only depends on the electric quantities of the medium at a given frequency. Cf. the phase relation between current and voltage at complex resistors, as they appear in series and parallel connection with  $R$  and  $C$  or  $L$ , respectively.

<sup>6</sup> This phase in the „other“ quadrant often appears in the time series, e.g. a positive peak in  $B_x$  or in  $B_y$  induces a positive  $E_x$ , but a negative  $E_y$

### 3 Geomagnetic Variations - an overview

Magnetotellurics makes use of natural geomagnetic variations which cover a wide range of frequencies of about  $10^{-4}$  -  $10^4$  Hz (see fig. 3.1). Variations with high frequencies are caused by electromagnetic radiation of lightning and propagation within the wave guide earth/ionosphere. In contrast, current systems in the ionosphere and magnetosphere below  $\sim 3$  Hz, which are caused by solar wave and corpuscular radiation, make up the essential part of the excitation energy. These natural signals are often superimposed by artificial disturbances, i.e., straying currents stemming from technical sources which become a problem if - and only

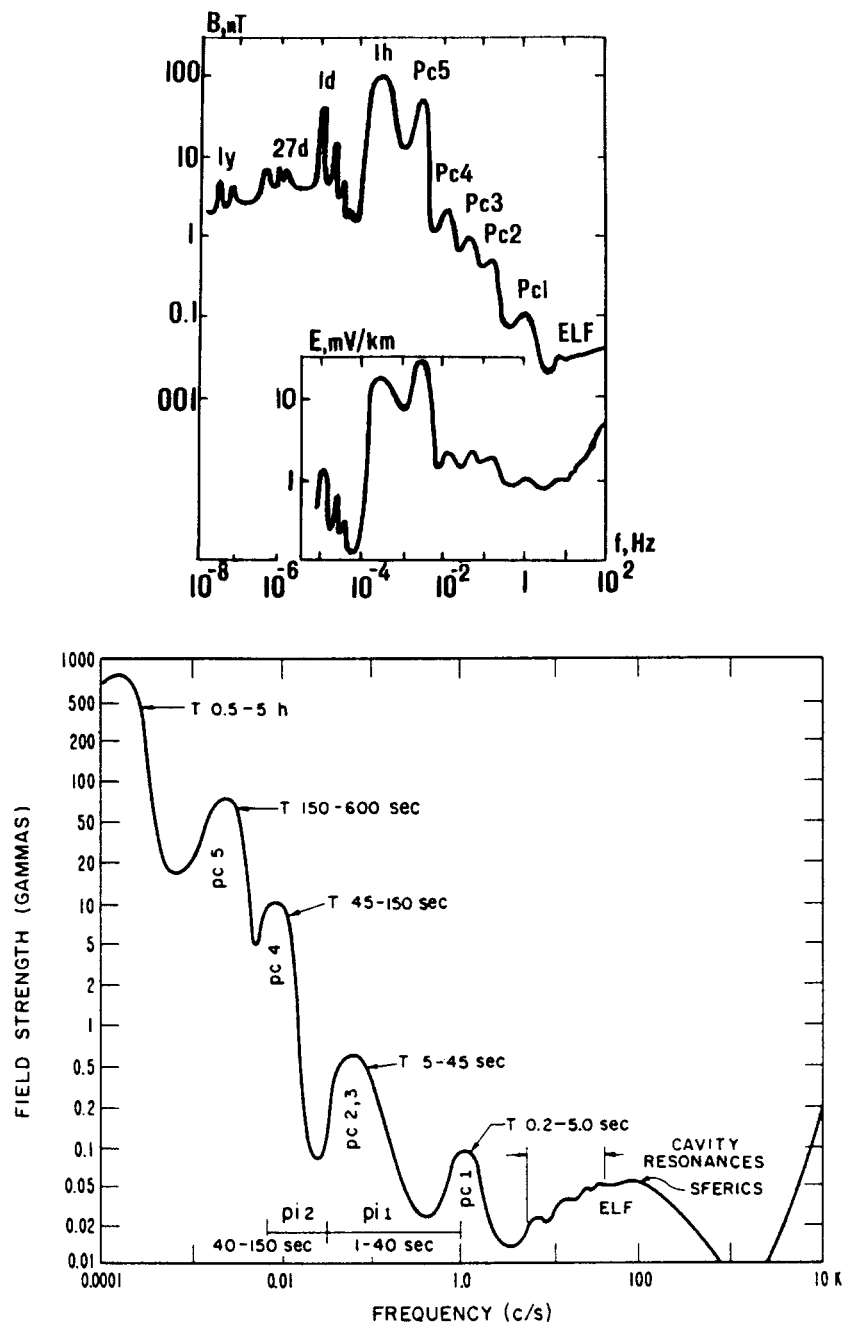


Fig. 3.1: Spectrum of geomagnetic variations. The observed field largely depends on the observer's position, in particular on geomagnetic latitude, and on time. Above: after Ser-son (1973), below: after Campbell (1966). The unit c/s means "cycles per second" = Hz.

if - the observation site is located in the near field of the source. We then need special processing methods to separate the perturbing signals from the natural ones.

Figs. 3.2 - 3.3 show synoptically the structure of the atmosphere, the shell structure of the ionosphere for the day- and night side and the magnetosphere.

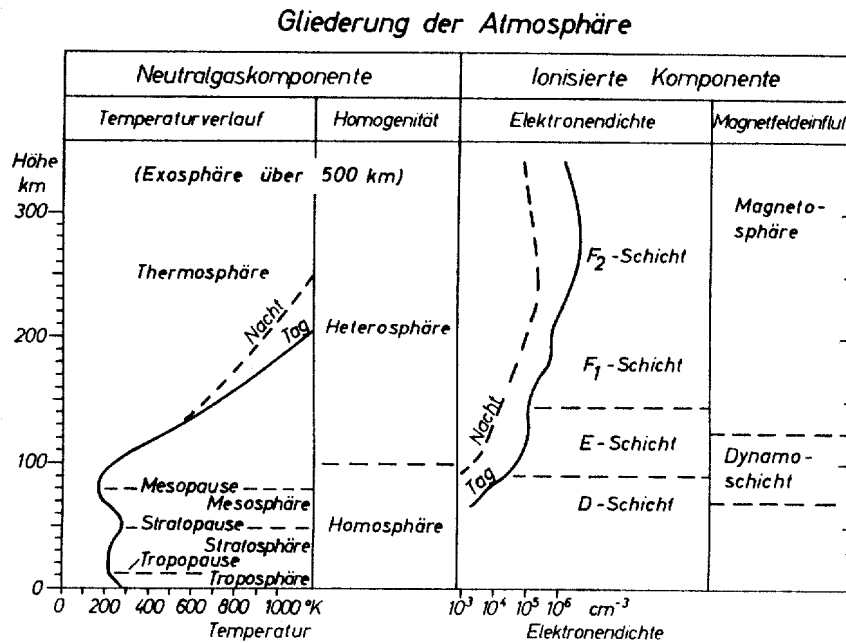


Fig. 3.2: Structure of the atmosphere subdivided according to their proportion of neutral gas and their ionized components (Kertz 1971).

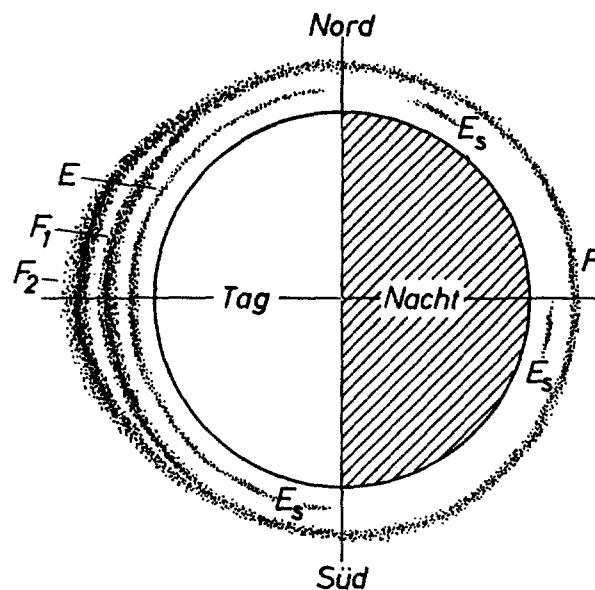


Fig. 3.3: The outer layers of the ionosphere on the day and night side of the earth (Kertz 1971). The D-layer, which is not marked in this figure, also degrades nearly completely at night.



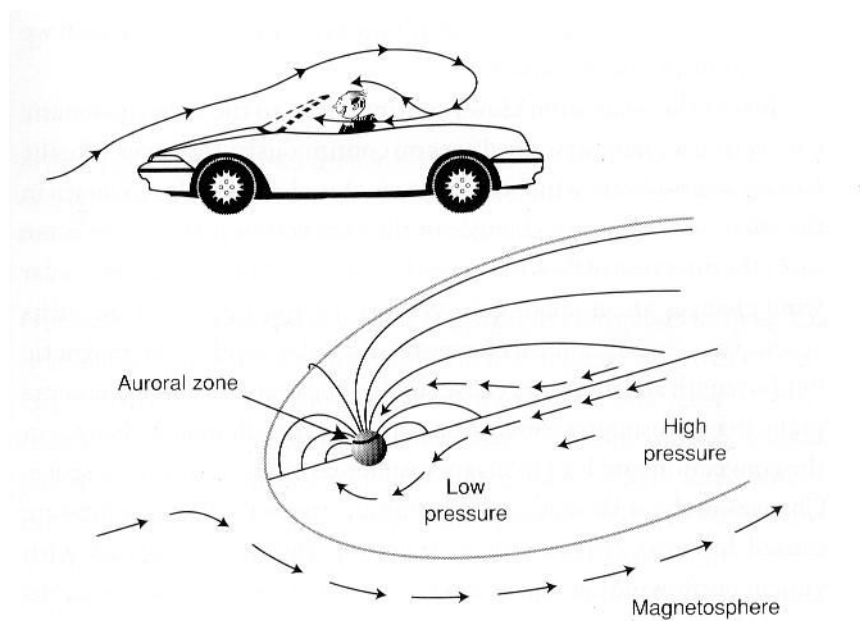
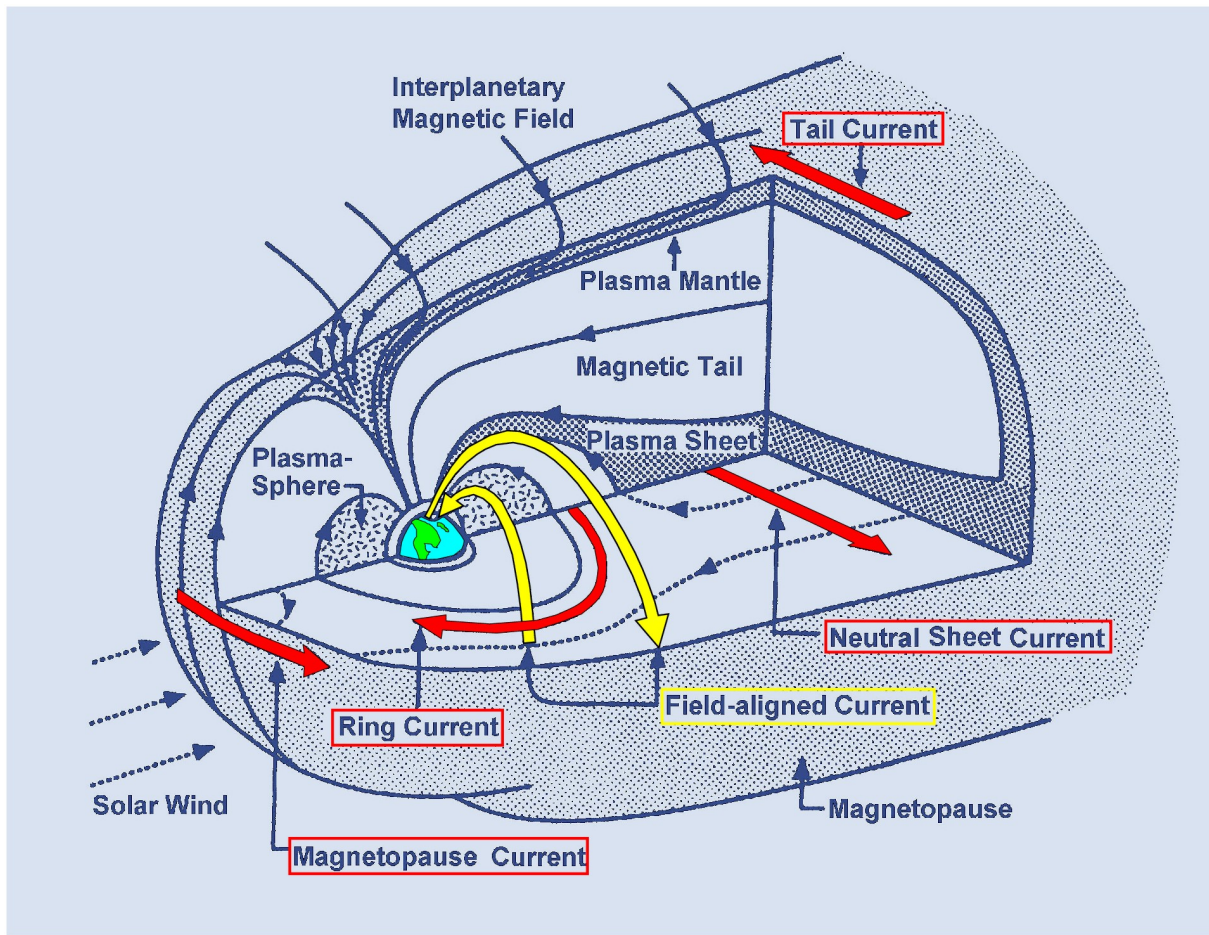


Fig. 3.4: Schematic structure of the magnetosphere (above). Source: geomag.us. Below: Explanation of the charged particles of the solar wind penetrating in the magnetosphere on its reverse side (V. Haak, pers. comm.).

### 3.1 Conductivities in the Ionosphere

For a charged particle in a ionized gas or plasma, such as the ionosphere and the magnetosphere, the equation of motion (without considering gravity) is used:

$$m \frac{d\mathbf{v}}{dt} = e(\mathbf{E} + [\mathbf{v} \times \mathbf{B}]) \quad , \quad (3.1)$$

here  $m$  denotes the mass of a particle,  $e$  its charge and  $\mathbf{v}$  its velocity. The term

$$\mathbf{F}_L = e[\mathbf{v} \times \mathbf{B}] \quad , \quad (3.2)$$

is the Lorentz force.

In a plasma a current flows with a density of (see eq. 1.5)

$$\mathbf{J} = \sigma \mathbf{E} = (n_i \mathbf{v}_i - n_e \mathbf{v}_e) e = (n_i \mu_i - n_e \mu_e) e \mathbf{E} \quad (3.3).$$

This current is generated by an electrical field  $\mathbf{E}$ <sup>1</sup>. Here  $n_i$  and  $n_e$  are the number of ions or electrons per  $\text{m}^3$ ,  $\mathbf{v}_i$ ,  $\mathbf{v}_e$  are the velocities,  $\mu_i$ ,  $\mu_e$  are the mobilities, and  $e$  indicates elementary charge. We now have to define different conductivities depending on the motion of the charged particles that can be parallel or vertical (with the velocities  $\mathbf{v}_{\parallel}$  and  $\mathbf{v}_{\perp}$ ) to the magnetic field. The conductivity becomes anisotropic, however.<sup>2</sup>

If the electrical field is statistically distributed the total current density is

$$\mathbf{J} = \sigma_0 \mathbf{E}_{\parallel} + \sigma_1 \mathbf{E}_{\perp} + \sigma_2 \frac{(\mathbf{B} \times \mathbf{E}_{\perp})}{B} \quad . \quad (3.5)$$

If the electrical field is parallel to the magnetic field the "parallel conductivity"<sup>3</sup> is:

$$\sigma_0 = e^2 \left( \frac{n_e}{m_e v_e} + \frac{n_i}{m_i v_i} \right) \quad (3.6)$$

with  $n_{i,e}$  = number of the positively or negatively charged ions or electrons,  $v_i$  and  $v_e$  = collision frequency,  $m_i$  and  $m_e$  = mass of ions and electrons and  $e$  = elementary charge.

If we consider the electrical field  $\mathbf{E} = 0$  and the motion being vertical to the magnetic field, only the Lorentz force (3.2) is orthogonal to  $\mathbf{v}$  and the particles are in a circular motion with the gyro-frequency.

$$\omega_g = \frac{|e|}{m} B$$

The centrifugal acceleration and the Lorentz acceleration are identical:

$$\frac{v_{\perp}^2}{r} = \frac{|e|}{m} v_{\perp} B$$

with  $r$  = radius of the orbit.

---

<sup>1</sup> Both ions and electrons (as well as anions and cations in an electrolyte) contribute positively to the total current. This results from (3.3) if  $e$  is signed.

<sup>2</sup> For more information on the different conductivities see e.g. Kertz, vol. II.

<sup>3</sup> This conductivity also leads to the observed "field-aligned currents".

With an additional  $\underline{E}_\perp$  the motion of the particles consists of this gyration and a shift of the gyration centre (drift):

$$\underline{v} = \underline{v}_D + \underline{v}_g \quad \text{with} \quad \underline{v}_D = \frac{[\underline{E}_\perp \times \underline{B}]}{B^2} \quad .$$

After collisions took place in the ionosphere the charged particles first move in parallel direction to  $\underline{E}_\perp$ . This leads to a "*transversal*" or "*Pedersen conductivity*":

$$\sigma_1 = e^2 \left( \frac{n_e v_e}{m_e (v_e^2 + \omega_{ge}^2)} + \frac{n_i v_i}{m_i (v_i^2 + \omega_{gi}^2)} \right) \quad . \quad (3.7)$$

The conductivity vertical to  $\underline{E}$  and  $\underline{B}$  is the "*Hall conductivity*":

$$\sigma_2 = e^2 \left( \frac{n_e \omega_{ge}}{m_e (v_e^2 + \omega_{ge}^2)} + \frac{n_i \omega_{gi}}{m_i (v_i^2 + \omega_{gi}^2)} \right) \quad . \quad (3.8)$$

These different conductivities play an important role in the formation of ionospheric current systems. Therefore they are also important for the magnetic variations that can be observed on the surface of the earth. However, first we want to explain the signals with short periods, which have their origins between the earth's surface and the ionosphere.

### 3.2 Atmospherics

In the frequency domain of AMT (audiomagnetotellurics), atmospherics (or atmosferics or shortly sferics) are the most important form of excitation. They are produced through radiation of electromagnetic waves caused by lightnings and propagate within the wave guide earth/ionosphere. The frequency of lightning worldwide is approximately 100/s with a strong emphasis on the tropical areas in Asia, Africa and Latin America. Lightning arises from different charges between clouds and the earth's surface or separate cloud areas (cloud-cloud-lightning), the latter ones make up ca. 75 - 90% of the total number of lightnings. The charge distribution in a thundercloud of cumulonimbus type is shown in fig.3.5, fig. 3.6.shows the temporal sequence of a cloud-earth lightning. The "Return Stroke" with current magnitudes of up to 200 kA makes up the biggest part by far. Often the charges will be balanced only after several return strokes. Fig. 3.7 and 3.8 show the global distribution of lightning depending on time (UT). This distribution is also connected with the formation of convergence cells in the afternoon, particularly in tropical areas.<sup>4</sup>

During their propagation in the wave guide the electromagnetic waves are attenuated depending on the time of day. It is important to take into consideration that on the night side the absorbing D-layer disappears. At far away observation locations this leads to characteristic day curves of activities which are shown as an example in fig. 3.8. Therefore late afternoon or early evening are, often the best times to record AMT signals in many areas worldwide.

<sup>4</sup> A cloud-ground lightning is a vertical electrical dipole and therefore a TM source. However, at observation stations that are far away, TE parts caused by mode conversions may also occur. In contrast to this, a cloud-cloud lightning is a horizontal dipole and therefore source of TE and TM waves.

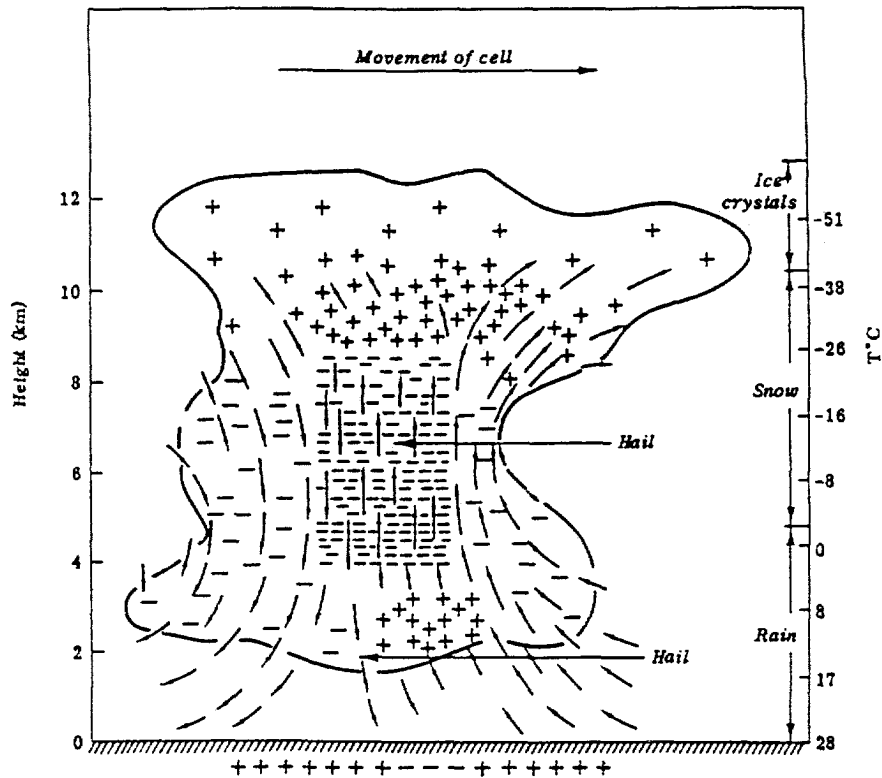


Fig. 3.5: Charge distribution in a cumulonimbus cloud (Uman 1987).

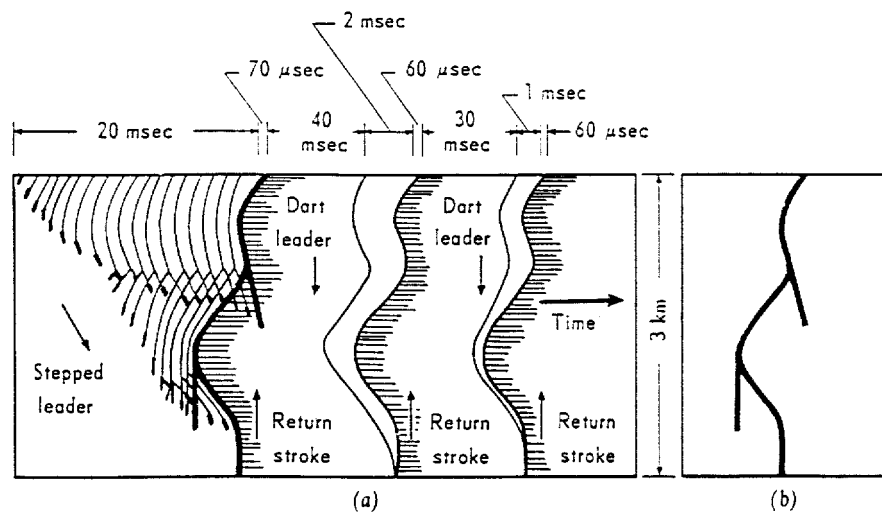


Fig. 3.6: Temporal sequence of a cloud-earth lightning (Uman 1987).

The absorption in the D-layer results in a dispersion of the signal, parts around  $f = 2-3$  kHz are more strongly absorbed and a characteristic "slow tail" is formed (fig. 3.9). The obtained spectrum with the typical "excitation gap" is shown in fig. 3.10. Until today (2003) it is not possible to obtain standard high quality registration of AMT for this part of the spectrum.

Sferics with a propagation of several thousand km and therefore a strong dispersion are also called "tweeks". "Whistler" also arise from lightning and propagate along the lines of force of the geomagnetic field to the conjugated point and sometimes back to the source ("one hop-" and "two hop-whistler"). Using an antenna and an audio amplifier they can become audible. For the frequency domain of 7-60 Hz, fig. 3.10 (C) shows sharp spectral peaks known as

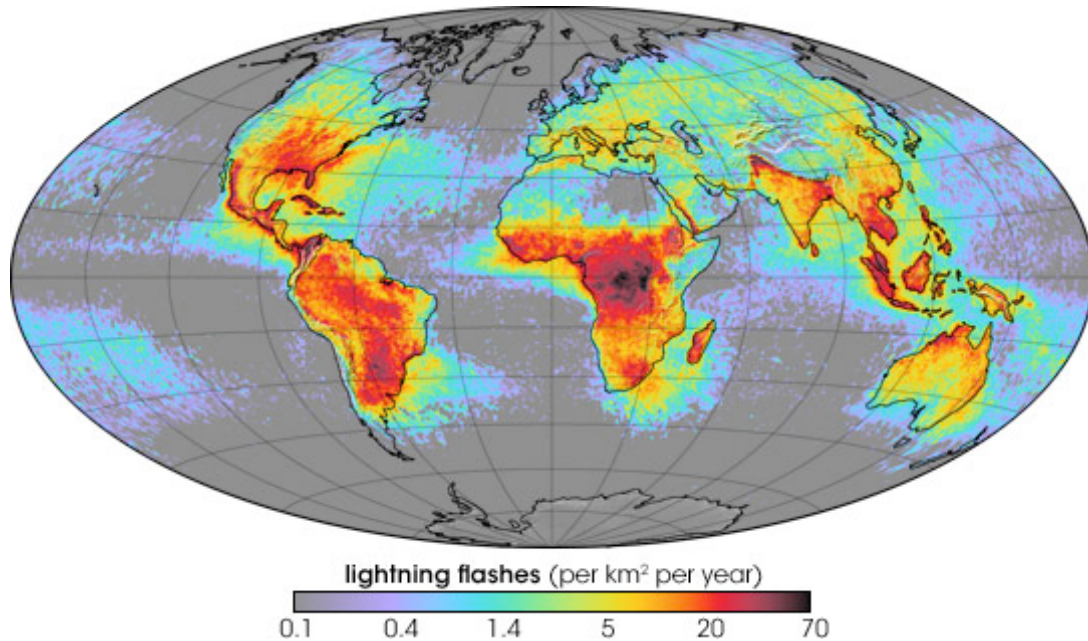


Fig. 3.7: Frequency of lightning (number per km<sup>2</sup> and year), source: <http://earthobservatory.nasa.gov>

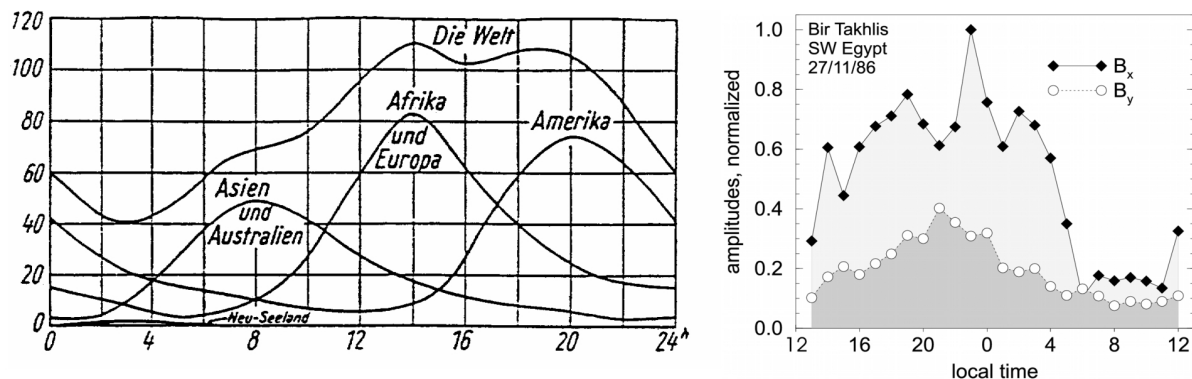
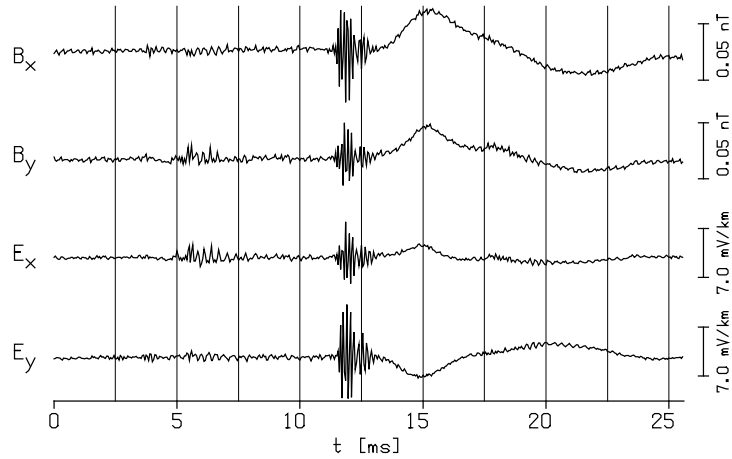


Fig. 3.8 (left): Global distribution of lightning (area covered by thunderstorms in 1000 km<sup>2</sup> depending on UT), according to Israel (1961). Right: Day curve of atmospheric magnetic components measured at a station in the Western Desert (Egypt) for the magnetic northern and eastern components. The dominance of the eastern component indicates that the sources are located in the South (equatorial Africa).

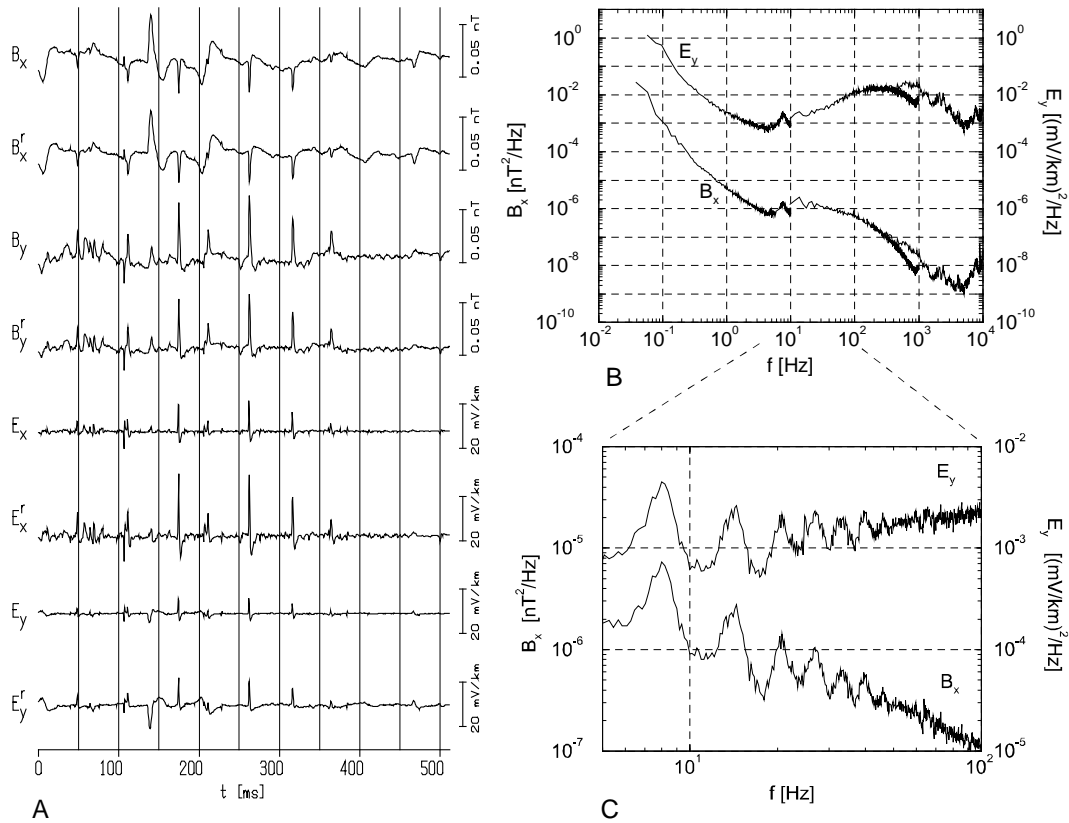
*Schumann resonances*, which are resonance waves in the wave guide earth/ionosphere at a frequency of  $f \approx 7.8, 14.1, 20.3, 26.4, \dots$  Hz<sup>5</sup>.

Fig. 3.10 shows time series in areas of the earth which are completely unpopulated and are therefore free of any technical disturbances. In populated regions the extraction of a stable magnetotelluric transfer-function can be impossible due to disturbances that always superimpose the natural signals. Fig. 3.11 shows two examples in which the natural atmospherics are nearly unrecognizable. Sources of perturbances are particularly electric trains and the network of power cables.

<sup>5</sup> A simple estimation without considering the curvature of the earth leads to a realistic frequency for the ground mode: wave length  $\lambda = 2\pi R = 40,000$  km and  $f = c/\lambda = 7.5$  Hz with earth radius  $R$  and speed of light  $c$ . However, often these resonances cannot be observed directly in the recorded wide-band time series. They then disappear in the background noise of the sferics.



*Fig. 3.9: Characteristic slow tail of an atmospheric that can be explained by the frequency-dependent damping in the ionosphere; later "ultra slow tails" which are connected with sprites can be observed, too (see below).*



*Fig. 3.10: Example of signal shapes of atmospherics (A) and their spectra (B) as well as the Schumann resonances (C), measured in the north-eastern Sahara. The time series in A are obtained at a base station and one movable station (superscript r). The differences are caused by the distribution of conductivity in the interior of the earth. The different courses of the spectra of E and B also reflect the conductivity in the subsoil. Therefore the conductivity in C is smaller (larger E-field compared to B) at high frequencies, i.e., at smaller depths.*

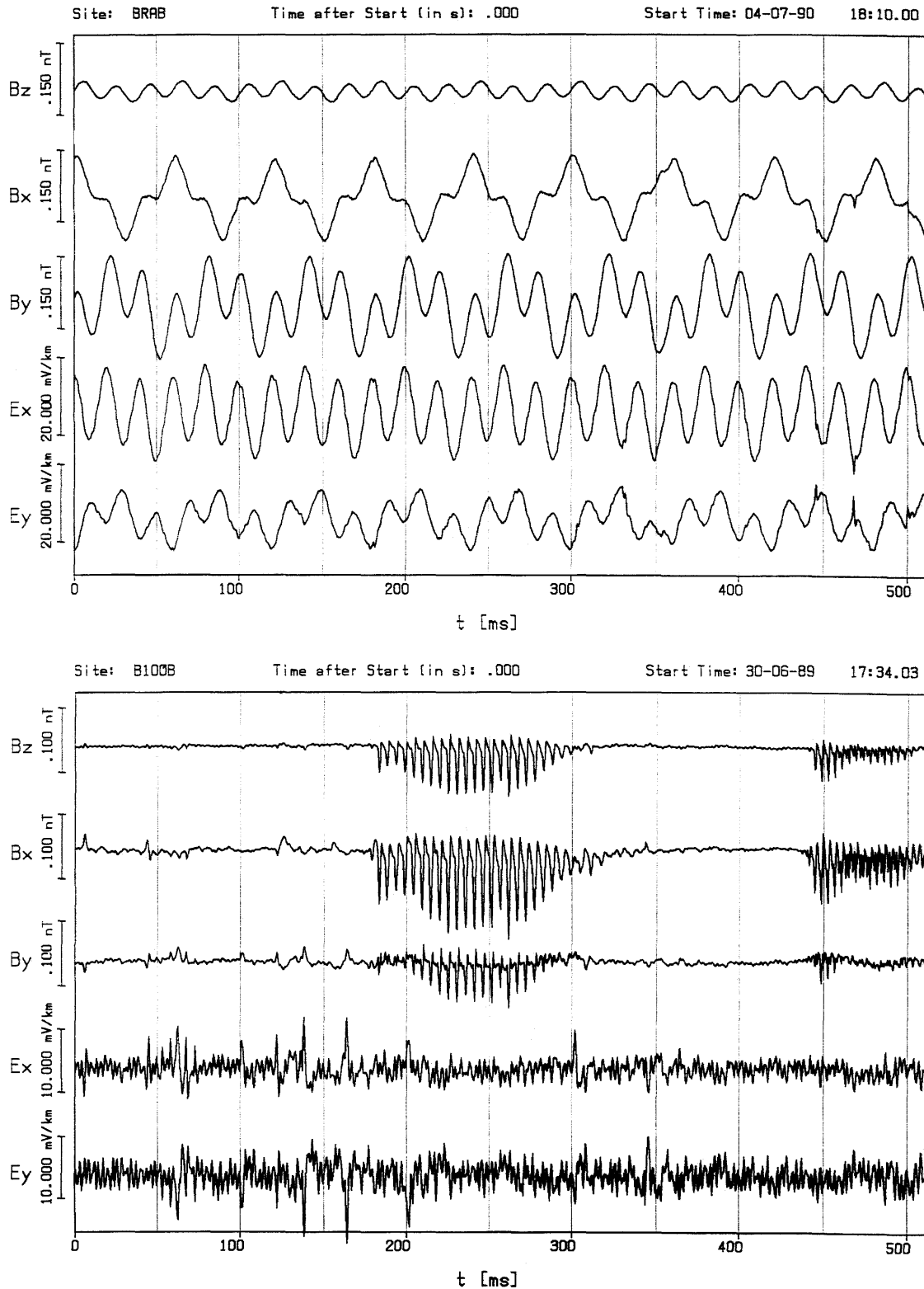
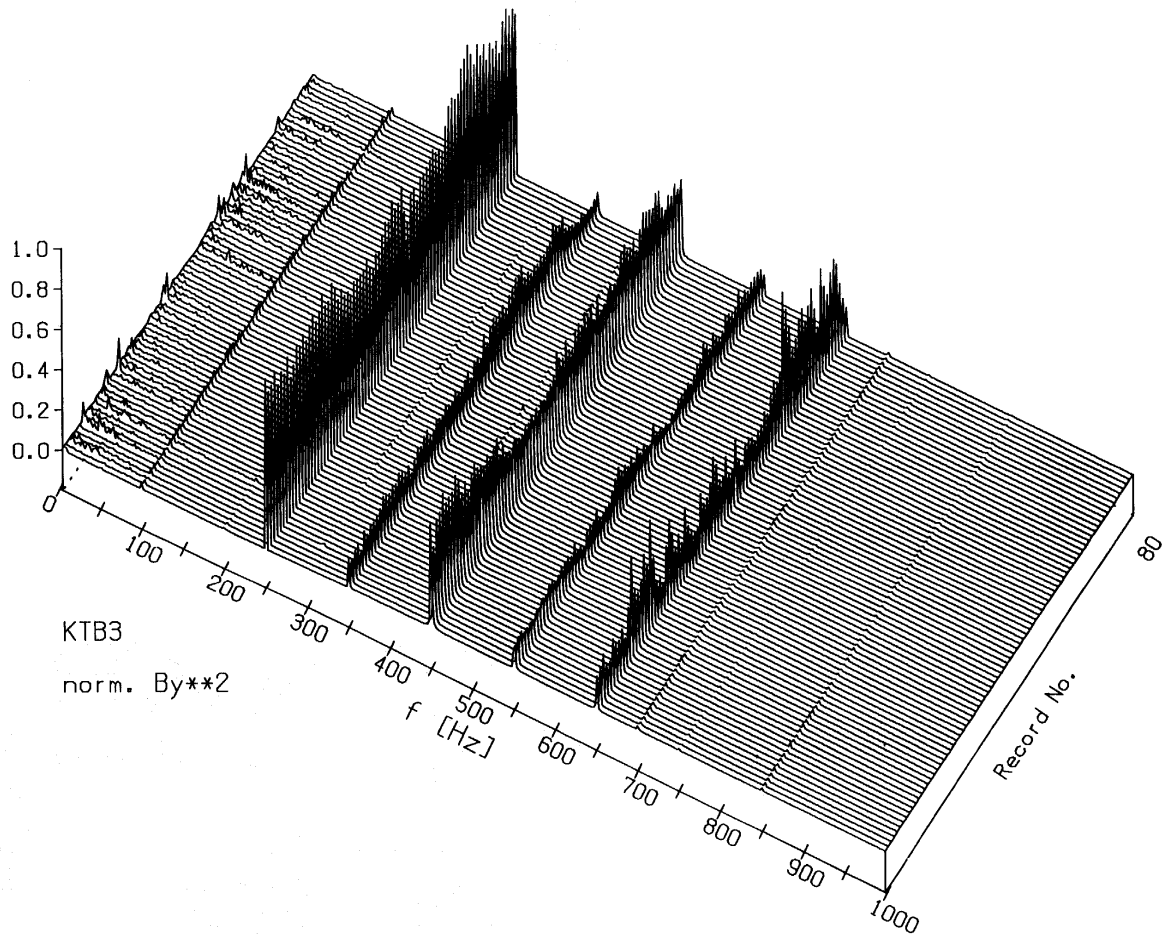


Fig. 3.11: AMT time series with disturbances. Above: Interspersion of  $16^{2/3}$  and 50 Hz of electric railway and overhead power cables. Below: radiation of a pulse radar.

The influence of quasi harmonic disturbances can be reduced by notch filters for  $16^{2/3}$  Hz (railway) and 50 Hz (frequency of the German electricity network, 60 Hz in North America and Brazil) as well as harmonics (see next chapter); however, this is not always successful.





*Fig. 3.12: Variation of harmonics with time. Every track corresponds to a recording time of 512 ms. The example is taken from the KTB-location before a pre-drilling took place; the notch filters at  $16^{2/3}$ , 50 and 150 Hz were turned on.*

Disturbances of single pulses, e.g. resulting from systems being turned on, and DC railways, e.g. in Poland, Italy, Spain or the S-Bahn in Berlin, cause much more problems.

Finally there are the recently discovered sprites, elves and jets which are optical phenomena in the high atmosphere (see fig. 3.13 a,b). They are also caused by discharges of thunderclouds and can sometimes radiate strong geomagnetic variations. They appear less frequently than atmospheric and are therefore less important in audiomagneto-tellurics. Another unusual and only recently discovered source is vortexes ("dust devils") that can also radiate ELF signals.



*Fig. 3.13a: A sprite, filmed by the space shuttle Columbia in January 2003. Photo taken from Spiegel-Online.*



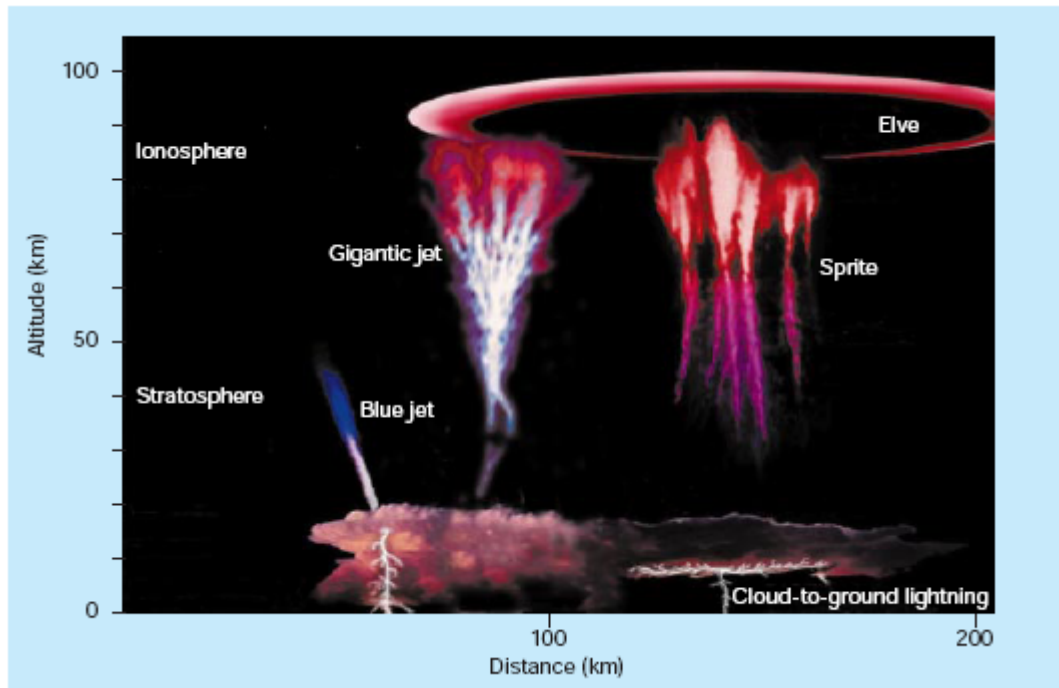


*Fig. 3.13b: Schematic depiction of sprites and elves, according to: Williams, E.R. (2001): Sprites, Elves, and Glow Discharge Tubes, Physics Today, 54 (11) as well as Pasko, V.P. (2004): Electric jets, Nature, 423, 927-929.*

An exotic source of atmospherics are clouds of charged ash particles from volcanic eruptions, as they were observed at Chaitén (2008, South Chile), Puyehue (2011, South Chile) or Eyjafjalla (2010, Iceland) volcanoes (Fig. 3.13c).



*Abb. 3.13c: Exotic source of atmospherics: lightnings in a cloud of volcanic ash, here at the eruption of Chaitén, South Chile in May 2008 (Source: nature.com).*

### 3.3 Variations of long periods

As already shown in fig. 3.1 amplitudes of geomagnetic variations grow with periods from  $T \approx 1$  s. These approximately regular variations that appear on “quiet days” are often superimposed by irregular fluctuations which result from disturbances of the geomagnetic field caused by solar influences. Solar winds carry a "frozen magnetic field" that interacts with the earth's magnetic field. Frozen magnetic field (see appendix) means that the magnetic flux through an area  $F(t)$  remains preserved if there is a motion of the (ideal) plasma:

$$\frac{d}{dt} \oint_{F(t)} \underline{B} \cdot d\underline{f} = 0 \quad .$$

A global quasi-logarithmic measure for geomagnetic activity is the planetary number  $K_p$  that is obtained from several geomagnetic observatories worldwide (e.g. Niemegk south of Berlin) and that is shown in a "musical diagram" (fig. 3.14). The magnetic activity is determined by eruptions on the sun (sunspots, flares and coronal mass ejections). Therefore  $K_p$  numbers are always marked for one solar rotation interval (27 d). This repetition tendency of magnetic activity every 27 days can actually be observed in fig. 3.14, although it is only weak. The half-year cycle of activity is often strong (see also fig. 3.14). However, the normal case is the quiet sun. The 11-year cycle of sun activity is marked in fig. 3.15a, while fig. 3.15b shows several groups of spots in October 2003. The relative sunspot number  $R$  (after Rudolf Wolf, 1848) is determined by  $R = k(10g+s)$ ; with  $g$  indicating the number of spot groups,  $s$  is the total number of spots and  $k$  is a factor depending on the observation conditions and instruments.

Link to Niemegk observatory:

<http://www.gfz-potsdam.de/portal/gfz/Struktur/Departments/Department+2/sec23/infrastructure/observatories/niemegk>

Space weather:

[www.spaceweather.com](http://www.spaceweather.com)

<http://www.swpc.noaa.gov/SWN/>

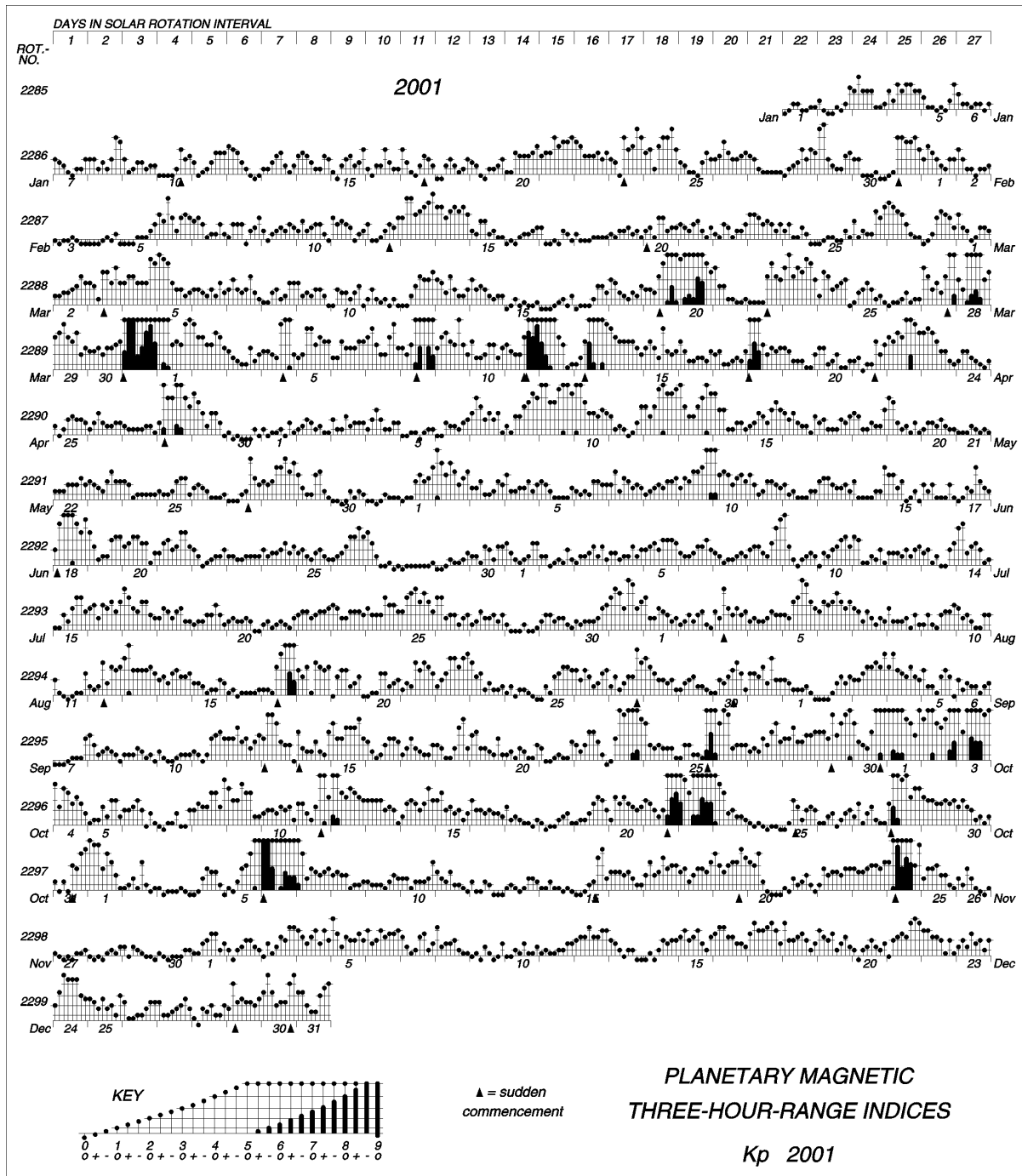
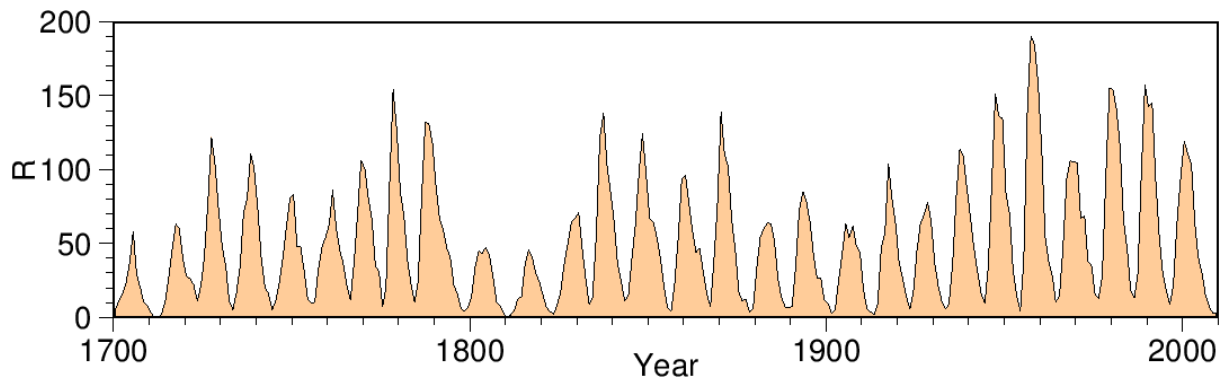


Fig. 3.14: Kp-numbers (music-diagram) for the year 2001. Source: Homepage of the geomagnetic observatory in Niemegk, Germany.

Pulsations ( $T = 0.2 - 600$  s, fig. 3.16), variations ( $T > 10$  min) and Sq ( $T = 1$  d and harmonics) are of particular importance for the geomagnetic depth sounding. In addition there are lunar variations (L), Bay-disturbances (duration of ca. 0.5 h), ring current variations (DR, the main phase of a magnetic storm with a duration of several days) and solar flare effects (sfe, duration of 0.2 - 2 h); see Kertz (1971), Rokityanski (1982) or the various web sites on "Space Weather" to get an overview. Current magnetograms are published on the web pages of different observatories. Geomagnetic storms are caused by large eruptions on the sun (Coronal Mass Ejections, CME) whose flow of particles is directed towards the earth.



*Fig. 3.15a: Relative number of sunspots  $R$  to measure solar activity from 1700-2010. Plotted from data of the World Data Center for the Sunspot Index, Royal Observatory of Belgium (<http://sidc.oma.be/>). In the second half of the 17th century hardly any spots could be observed (Maunder minimum). This correlated with a global cooling of the earth.*



*Fig. 3.15b: Several large spot groups on the surface of the sun in October 2003. Source: NASA.*

Variations with very long periods are only of secondary importance for the practice of deep sounding. However, they are necessary to achieve information about the upper-mid mantle. Today only pure magnetic measurements are used because the stability of telluric probes for periods  $T > 1$  d cannot be guaranteed any more.

Sq-variations are inhomogeneous excitations. Therefore the magnetotelluric assumption of plane waves does not lead to a result here. This is the same thing with electrojets in polar and equatorial areas (see paragraphs 3.4 and 3.5).

Extremely long period variations and correspondingly very large penetration depths are usually analyzed with data from magnetic observatories. This is shown in fig. 3.17 that particularly displays the high conductivity of the mantle.

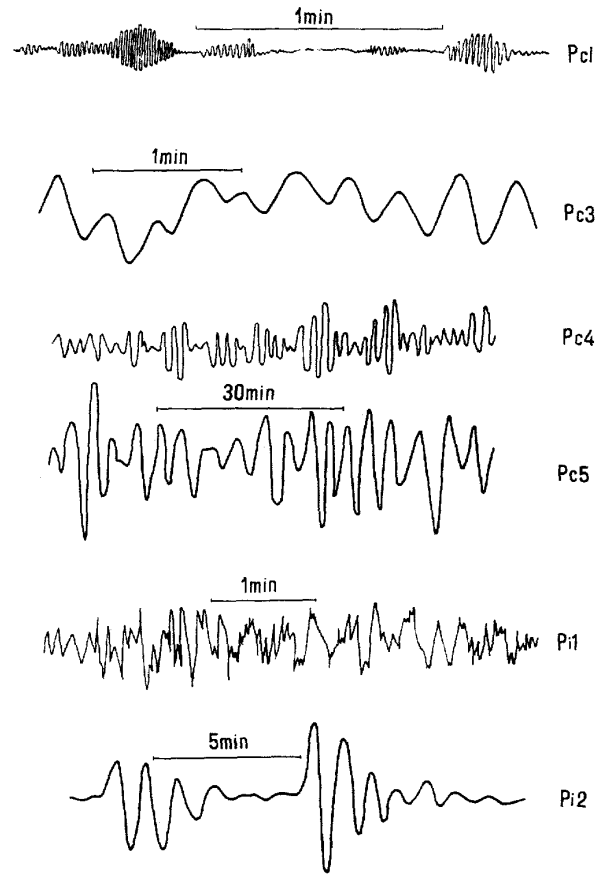


Fig. 3.16: Typical signal shapes of pulsations, according to Rokityanski (1982). There are continuous (Pc1 - Pc5) and irregular pulsations (Pi1, Pi2) that have to be distinguished.

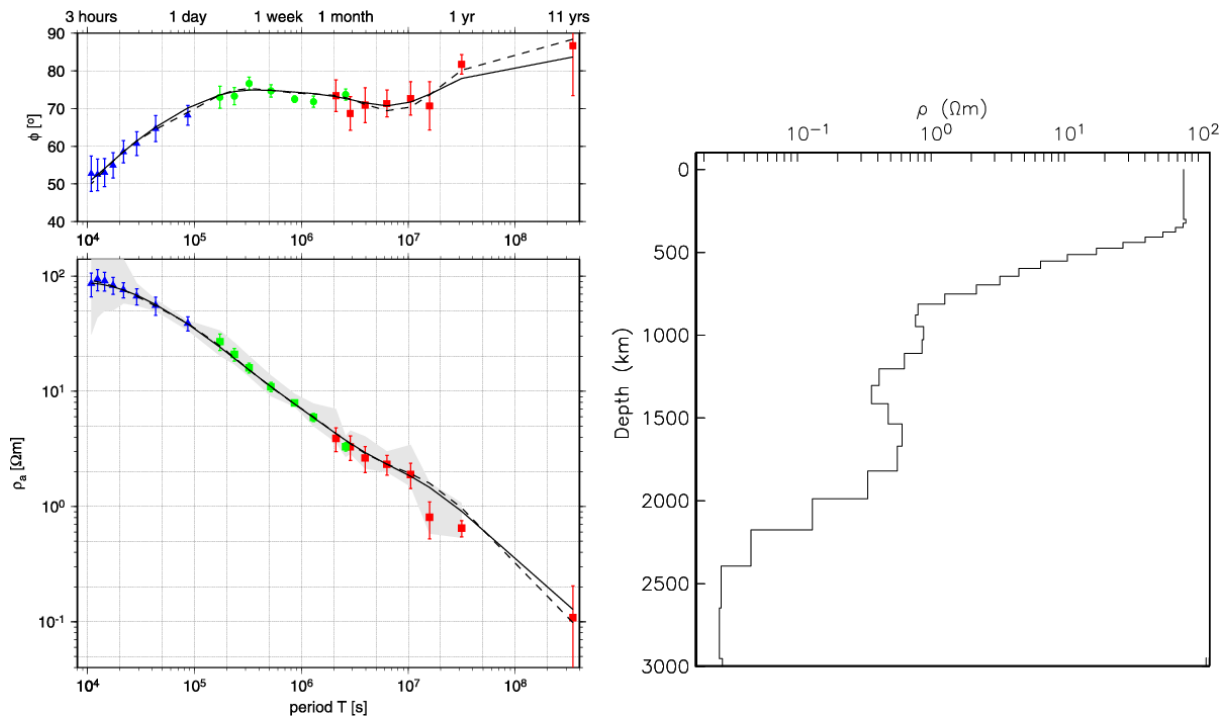


Fig. 3.17: Above: Example of a  $\rho_a$ - and phase curve for extremely long periods. Below the resistivity model calculated from these data is shown (N. Olsen, pers. comm., modified). The high conductivity of the mantle becomes particularly obvious.

### 3.4 Sq-Variations

Variations with periods of one day ( $T = 24\text{h} + \text{harmonics}$ ) can be observed on days without magnetic perturbations. For this reason they are called Sq (solar quiet). They are the result of current eddies in the ionosphere on the day side and they strongly depend on the latitude. These variations are an inhomogeneous source for normal magnetotellurics. Fig. 3.19 shows a registration example.

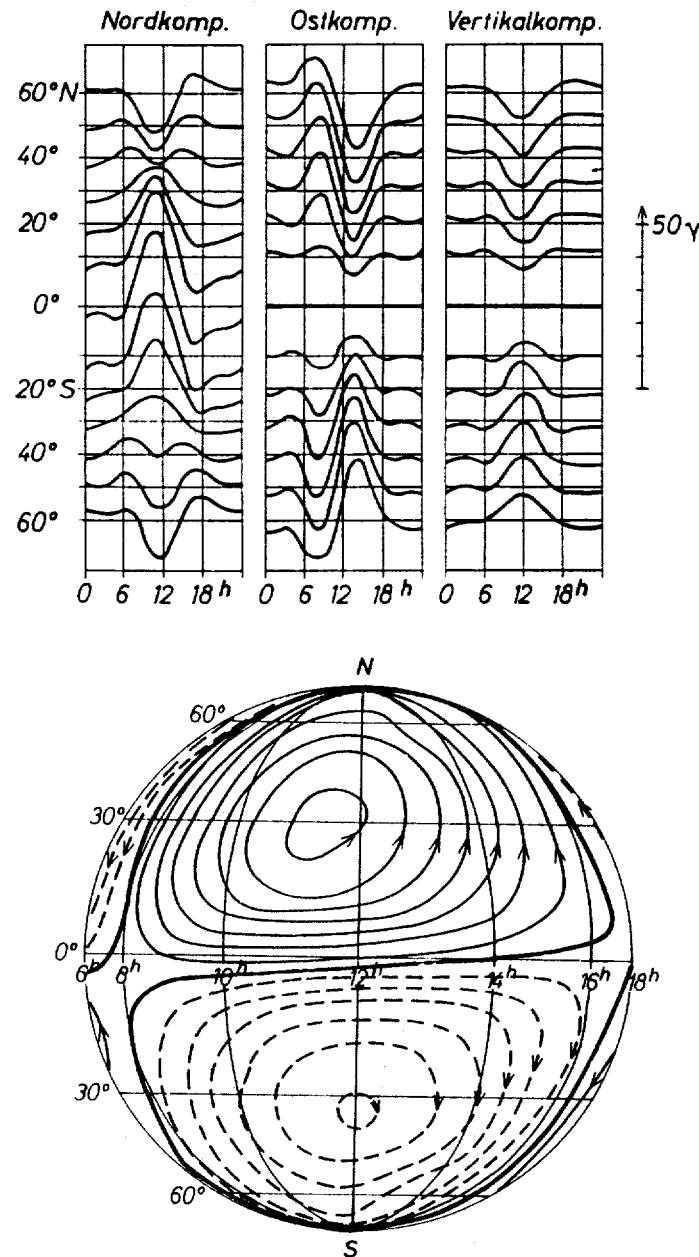
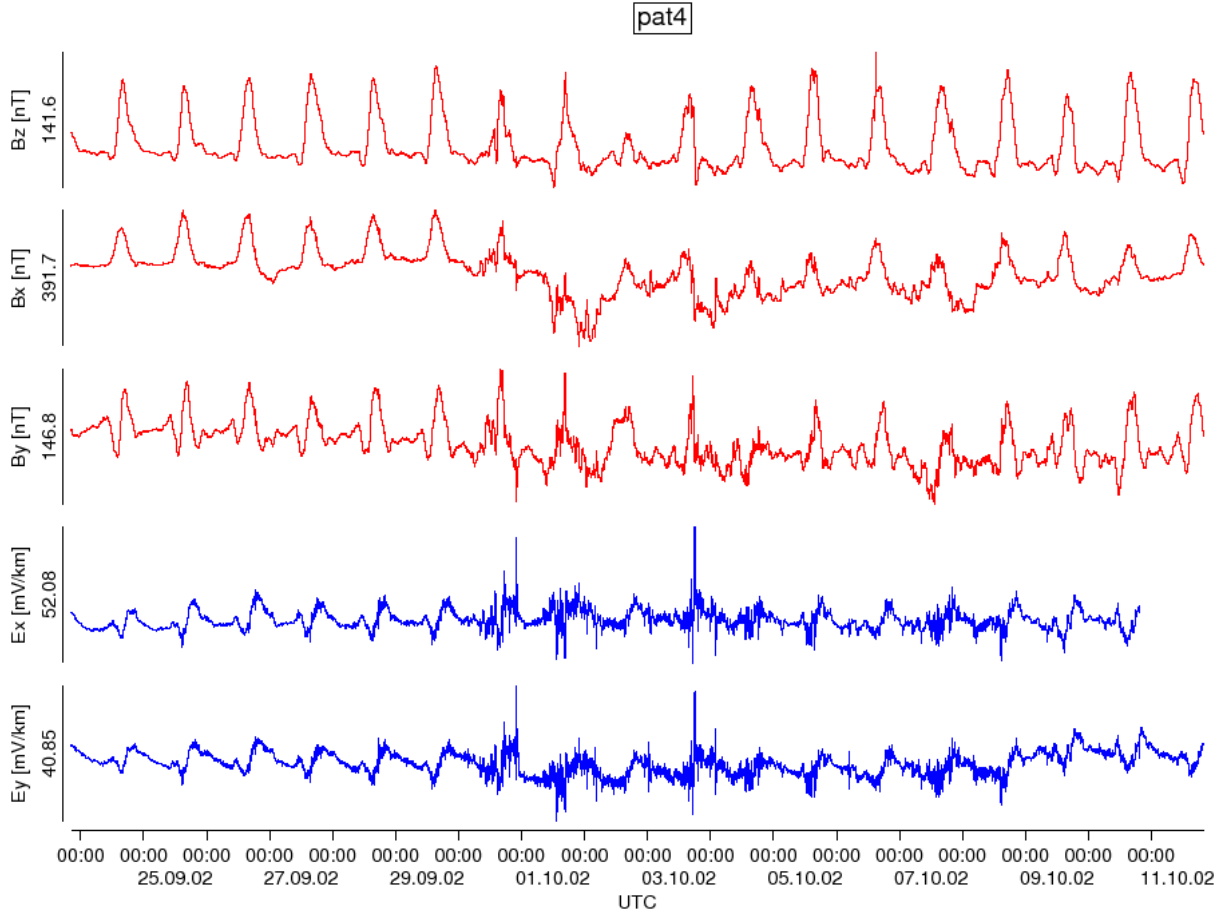


Fig. 3.18: Geomagnetic variations on quiet days (above). Sq-current system as a function of magnetic latitude and local time (below). From Kertz (1971).



*Fig. 3.19: Registration example of magnetic and telluric variations with long periods in Bolivia. The daily variations and a magnetic storm that began on 30.9.02, time in UTC, are clearly discernible. It's strongest expressed in the northern component of the magnetic field. On the last day the  $E_x$ -channel broke down because the cable was cut. On 6.10.02, there is a spike in the  $B_z$ -channel (astonishingly only in this one) that is supposedly caused by a person approaching the station.*

### 3.5 Electrojets

At the magnetic equator (in magnetic coordinates: inclination  $I = 0^\circ$ , vertical field  $B_z = 0$  and eastern component  $B_y = 0$ ) at an altitude of slightly more than 100 km there is an increasing electrical conductivity in the ionosphere caused by space charge effects on the day side. A primary electrical field in y-direction  $\underline{E}_{py}$  causes flows in y- and z-direction as shown in eq. (3.7) and (3.8):

$$\underline{J}_{py} = \sigma_1 \underline{E}_{py} \text{ and } \underline{J}_{pz} = \sigma_2 \underline{E}_{py} \quad .$$

A secondary field  $\underline{E}_{sz}$  is generated due to the vertical current that charges the upper and lower side of the ionosphere. The vertical charge balancing will take place until the primary vertical current is compensated:

$$\underline{J}_z = \sigma_2 \underline{E}_{py} + \sigma_1 \underline{E}_{sz} = 0, \quad \text{thus} \quad \underline{E}_{sz} = -\frac{\sigma_2}{\sigma_1} \underline{E}_{py} \quad .$$

$\underline{E}_{sz}$  also causes a Hall-current in y-direction:

$$\underline{J}_{sy} = -\sigma_2 \underline{E}_{sz} = \frac{\sigma_2^2}{\sigma_1} \underline{E}_{py} \quad ;$$

consequently the total current is

$$\underline{J}_y = \underline{J}_{py} + \underline{J}_{sy} = \left( \sigma_1 + \frac{\sigma_2^2}{\sigma_1} \right) \underline{E}_{py} = \sigma_3 \underline{E}_{py} \quad . \quad (3.9)$$

The actual conductivity  $\sigma_3$  is also known as Cowling-conductivity. This increase is limited to a small area around the magnetic equator and the resulting quasi line current (equatorial electrojet EEJ) is superimposed on the Sq-current system (fig. 3.20). Then there is a diffuse flow back on the night side. For further information on EEJ see Onwumechili (1997).

The polar electrojets (PEJ) in the aurora areas are generated similarly. Both PEJ and EEJ lead to an increase in the variations of the geomagnetic field for variations that are shorter than one day. These current systems are an inhomogeneous source and therefore they cause problems for magnetotellurics, which assumes plain waves. Therefore in polar or equatorial areas only night effects have to be taken into consideration.

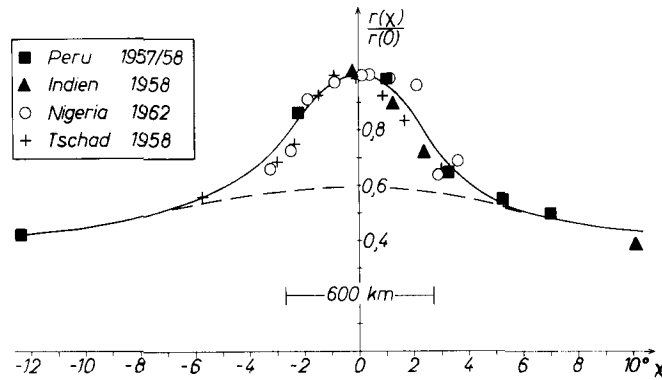


Fig. 3.20: Equatorial electrojet (EEJ). Relation between the values obtained at noon for the horizontal intensity  $r(x)$  to the level at night  $r(0)$  as a function of distance  $x$  from the equator in degrees. According to Untiedt (1968).



## 4 Instruments and time series analysis

### 4.1 Fundamental setup

The main problem in installing a magnetotelluric station often consists of the space needed. As the voltages at the input of the telluric amplifiers must not become too small the distance between the probes should be in the order of 50 - 100 m, which corresponds to the area of a soccer field. This might lead to considerably more difficult working conditions in e.g. high mountains or woods. The components are measured in magnetic coordinates. This requires the approximate knowledge of declination, as e.g. known from the International Geomagnetic Reference Field (IGRF). A cross layout of the probes is preferable to the L-configuration (Fig. 4.1), because then the differential input of the preamplifiers can be used. In most cases the ground of the loggers will be earthed separately by a grounding electrode or by another probe. MT stations should be installed as far away as possible from villages or technical installations due to perturbing signals. For measurements with long periods the stations must often be installed for several weeks which sets high demands on the devices concerning power consumption. In areas with a high level of sunshine, solar panels are often used so that a change of batteries might become unnecessary. For time synchronization DCF77 (in Central Europe) or GPS are frequently used.

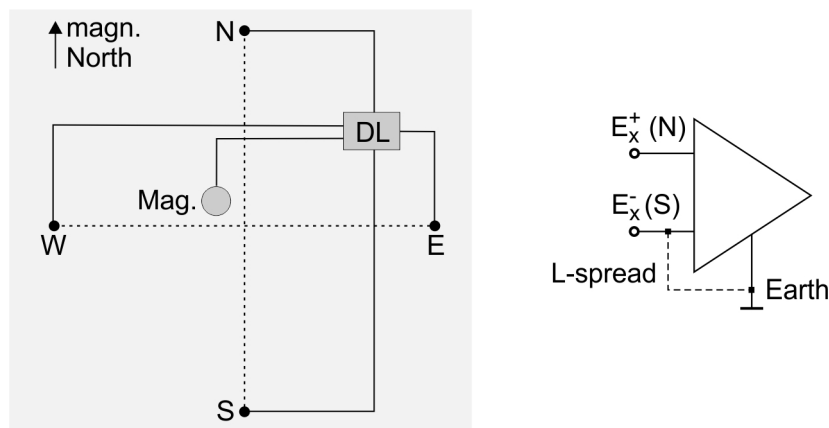


*Fig. 4.1: Above left: Fundamental layout in the field (DL: data logger). The probes are in a cross layout. Above right: Connection of the telluric probes at the input of an operational amplifier. Below left: Layout of telluric cables. Below right: View on data logger, electronics for controlling the fluxgate magnetometer, external GPS for time synchronization and solar panel. The instruments should be buried to protect them from the influence of temperature variations.*

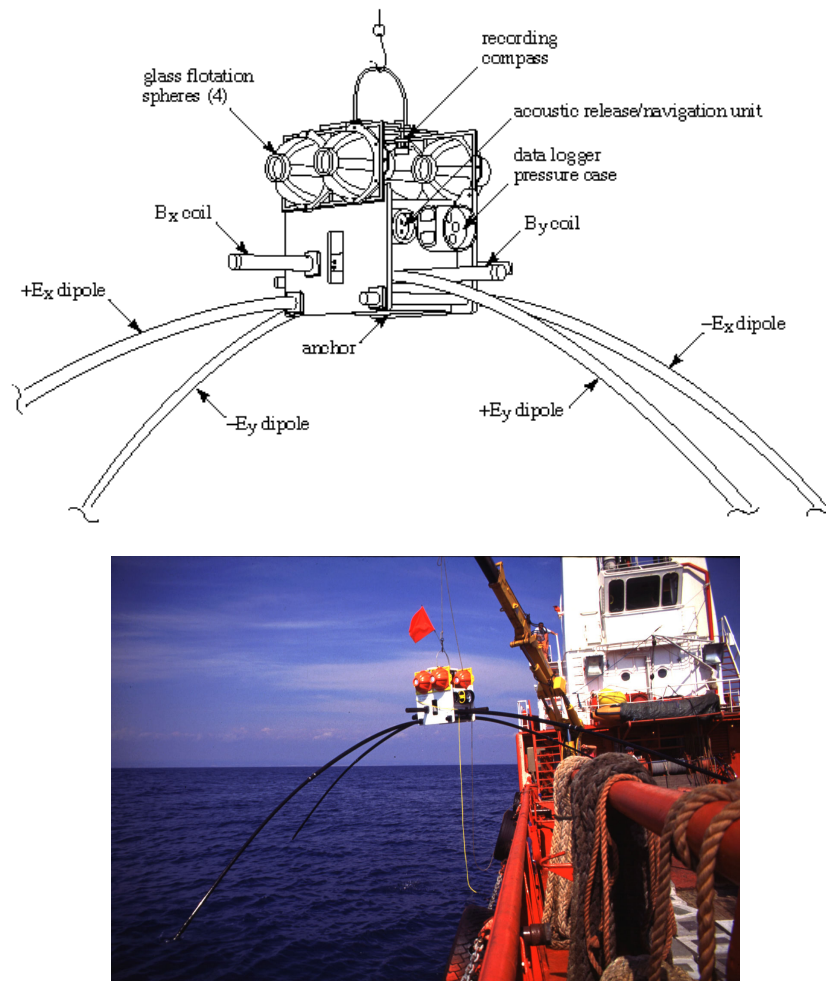


Fig. 4.2: Scheme and deployment of an instrument for the sea bottom, in this version with induction coils. Source: Web site Scripps Institution of Oceanography, S. Constable.

Magnetotellurics can also be carried out on the bottom of the sea (which is also possible and done with other geoelectric methods). Fig. 4.2 shows the scheme of a corresponding instrument. At great depths, however, only long periods can be recorded because the electromagnetic fields are severely attenuated by the very well-conductive sea water. The measuring of (small) electric fields causes particular problems because for practical reasons these fields have to be registered with short spreads (5-10 m).

## 4.2 Magnetometers

In magnetotelluric and geomagnetic depth sounding, proton magnetometers cannot be used to record geomagnetic field variations due to their large polarization time (approximately 1 s) as well as the difficulty in measuring components. Therefore, depending on the frequency range, induction coils and fluxgate magnetometers are used nearly exclusively today. For the use of passive methods, high temperature squids<sup>1</sup> are still not low-noise enough (2010).

<sup>1</sup> From Superconducting Quantum Interference Device.

The smallest variations which are to be resolved are in the order of approximately 1 pT (at least for the field of AMT) while the "static" geomagnetic main field comprises values from  $2 \times 10^4$  (at the equator) up to  $6 \times 10^4$  nT (at the poles)<sup>2</sup>. Therefore the dynamics measured in decibel<sup>3</sup> is approximately 155 dB which is still significantly beyond the values of modern measuring instruments (in the range of 120 dB). However, there are often lower requirements on the dynamics of the measuring instruments because the absolute value of the field components in MT is not relevant and can be removed with a high-pass filter.

Dynamics and resolution of a measuring instrument are limited considerably by the used analogue/digital converter (ADC), because today recording is nearly always digitally with a data logger. Therefore a 16 Bit-ADC (dynamics of 48 dB) and an input voltage in the range of  $\pm 5V$  can theoretically resolve 0.153 mV ( $10 V/2^{16}$ ) opposed to 0.6  $\mu V$  for a 24 Bit-ADC (dynamics 144 dB). Here limitations caused by the circuit technology have not been taken into consideration.

*Induction coil magnetometers* basically consist of a large number of windings wrapped around a highly-permeable  $\mu$ -metal core. The induced voltage in a single loop is

$$U = -nA \frac{\partial B}{\partial t} \cos \vartheta \quad . \quad (4.1)$$

Consequently, voltage is proportional to frequency. In (4.1)  $n$  indicates the number of coils,  $A$  the enclosed area and  $\vartheta$  is the angle of the surface normal to the magnetic field lines. A simple estimation with  $B = 1$  nT,  $T = 1$  s,  $\vartheta = 0^\circ$ ,  $n = 1$  and  $A = 0.01$  m<sup>2</sup> results in a voltage  $U = 10^{-11}$  V! However, voltages in the order of mV are necessary. For this reason, in practice, coils with  $10^4$  to  $10^5$  windings are used. It is not possible to extend the area  $A$  significantly, but the same effect can be achieved by coiling on a highly permeable core (superpermalloy). Instead of (4.1) and with  $\vartheta = 0^\circ$ , then follows:

$$U \approx -nA \frac{\partial B}{\partial t} \mu_r \quad , \quad (4.2)$$

with  $\mu_r$  that can reach values of up to  $10^5$  (superpermalloy).

The number of turns cannot be extended at will because they increase the inner resistance and the capacity of the coils which result in a characteristic resonance curve (see Fig. 4.3) with the following resonance frequency:

$$\omega_0 = \sqrt{\frac{1 + R/R_e}{LC}} \quad , \quad (4.3).$$

Here  $R_e$  indicates the input resistance of the instrument.

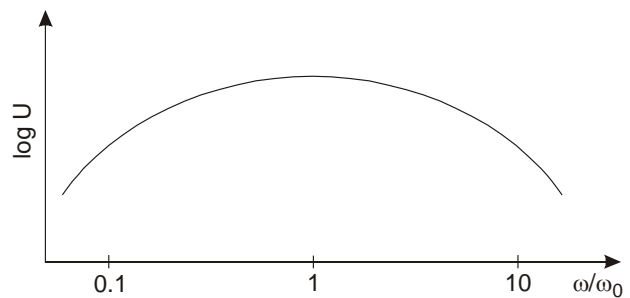


Fig. 4.3: Fundamental course of the resonance curve of an induction coil.

<sup>2</sup> See also Fig. 0.2 in the introductory notes.

<sup>3</sup>  $20 \log U_1/U_2$

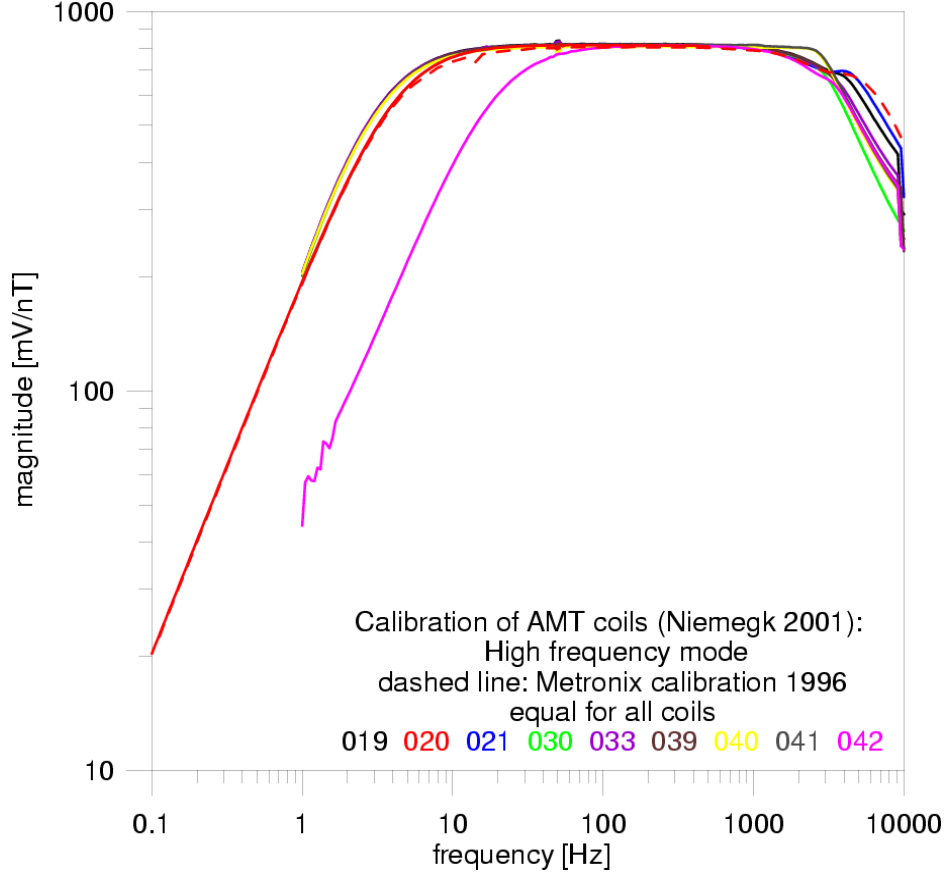


Fig. 4.4: Example of the calibration of several induction coils. The different coils should have the same transfer function. In coil no. 42 (pink line) one element of the filter seems to be broken down.

Of course, we prefer a flat curve, i.e. a constant sensitivity<sup>4</sup> for a large frequency range (Fig. 4.4). This can be achieved by an additional bucking coil. Using an electronic *chopper*- or *lock-in-amplifier* it is possible to extend the frequency range of induction coils far into the range of long periods. In this case the weak low-frequency signal is modulated (multiplied by an alternating rectangle function), intensified, demodulated and finally filtered with a low-pass filter.

For long periods ( $T \approx 10$  s – DC) *fluxgate magnetometers* are used. These fluxgate magnetometers have a special method of measuring: the outer magnetic field  $B_0$  is superimposed by a harmonic signal so that the non-linear part of the hysteresis curve of a ferrite core<sup>5</sup> is reached. The resulting field contains harmonics in which one harmonic, that is proportional to  $B_0$ , is filtered out electronically (see Fig. 4.5).

A hysteresis curve can be described as a third-degree polynomial:

$$B(H) = \mu_0(3H - H^3) \text{ for } H \leq 1 = H_s, \quad (4.4a)$$

with  $H$  normalized to the saturation field strength  $H_s$ . If we apply an exciting field  $H_e(t) = a \sin \omega t$  to a coil then the resulting field is

<sup>4</sup> A typical value for the sensitivity of coils is e.g. 100mV/nT. At FUB we use MFS05 coils from Metronix which have a frequency range from 8 kHz to 4,000 s.

<sup>5</sup> The magnetometers used at the FUB are manufactures by Magson and have a ring ferrite core.

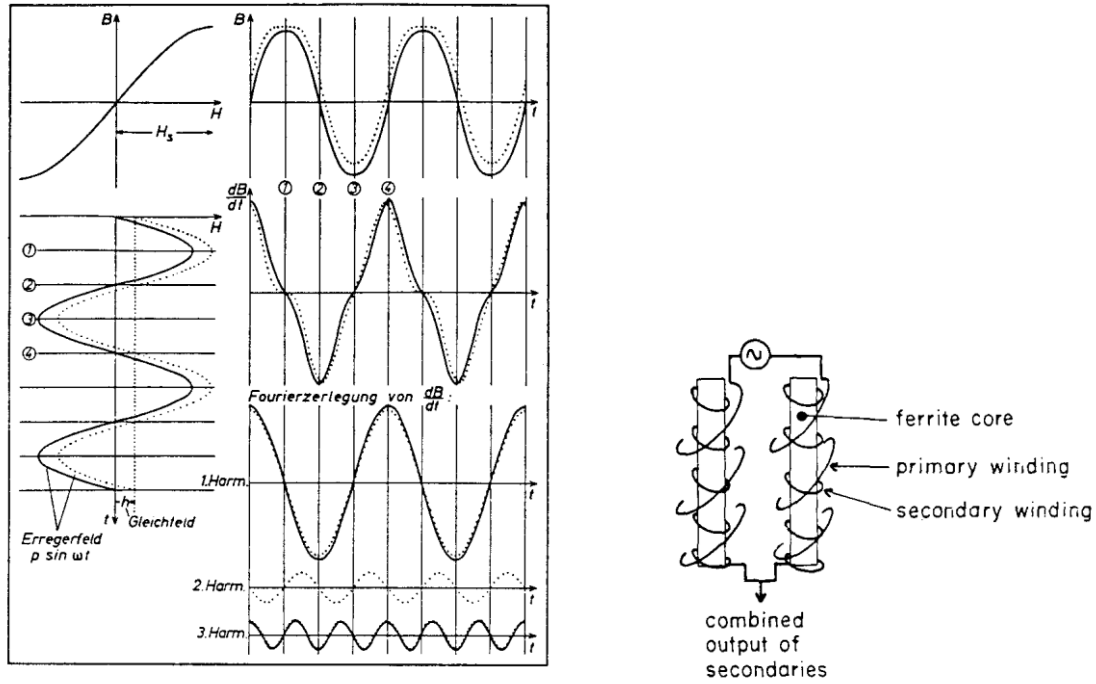


Fig. 4.5: Principle of a fluxgate magnetometer.

$$H(t) = H_e + H_-(t) = H_e + a \sin \omega t \quad ; \quad (4.4b)$$

with  $H_e$  indicating the relevant external field. Then the voltage in a coil around the excitation coil is induced

$$U_{\text{ind}} \sim \frac{\partial B}{\partial t} = 3a \left(1 - H_e^2 - \frac{1}{4}a^2\right) \omega \cos \omega t - 3H_e a^2 \omega \sin 2\omega t + \frac{3}{4}a^3 \omega \cos 3\omega t \quad (4.4c).$$

The second harmonic only occurs in the case of  $H_e = 0$ . It is filtered out and measured. The frequency of the excitation field is around several kHz. The excitation coils are wrapped in opposite direction around a double core (or a ring core). The induction coil encloses both and the harmonics with odd numbers complement each other to zero.

### 4.3 Some remarks on time series analysis in magnetotellurics

The aim of time series analysis in magnetotellurics (and in geomagnetic depth sounding) is the estimation of elements of the impedance tensor  $\underline{Z}$  or the tipper  $\underline{T}$  as a function of frequency (see chapter 6):

$$\begin{pmatrix} E_x(\omega) \\ E_y(\omega) \end{pmatrix} = \begin{pmatrix} Z_{xx}(\omega) & Z_{xy}(\omega) \\ Z_{yx}(\omega) & Z_{yy}(\omega) \end{pmatrix} \begin{pmatrix} B_x(\omega) \\ B_y(\omega) \end{pmatrix} \quad \text{and} \quad (4.5)$$

$$B_z(\omega) = \begin{pmatrix} T_x(\omega) & T_y(\omega) \end{pmatrix} \begin{pmatrix} B_x(\omega) \\ B_y(\omega) \end{pmatrix} \quad (4.6)$$

By observing nature we obtain several series of digitally recorded voltage values (time series) which represent the fields  $B(t)$  and  $E(t)$ . These fields are subject to irregular processes (and consequently random numbers) and they are analyzed statistically.

In deterministic processes the distribution of amplitudes and phases as a function of frequency is established by a Fourier transformation. This procedure is not possible for irregular processes which are not limited in time  $x(t)$  and we are restricted to average values for the amplitudes. The condition for the existence of Fourier transforms, i.e., the finiteness of the integral

$$\int_{-\infty}^{\infty} |x(t)| dt \leq c < \infty$$

is not given any more. These processes have a finite average power instead

$$\lim_{T \rightarrow \infty} \frac{1}{2T} \int_{-T}^T |x(t)|^2 dt \leq c < \infty$$

We are looking for a function  $G(f)$  that indicates the power per frequency interval (power density spectrum, short also power spectrum). The integral over this function then results in the total power

$$\overline{x^2(t)} = \lim_{T \rightarrow \infty} \frac{1}{2T} \int_{-T}^T x(t)^2 dt = \int_{-\infty}^{\infty} G(f) df \quad .$$

The average square value in the frequency interval  $\Delta f$  is

$$P_x(f, \Delta f) = \lim_{T \rightarrow \infty} \frac{1}{2T} \int_{-T}^T x(t, f, \Delta f)^2 dt \quad ,$$

as a result the spectral density is:

$$G(f) = \lim_{\Delta f \rightarrow 0} \frac{P_x(f, \Delta f)}{\Delta f} \quad .$$

The squared spectrum is real,  $\geq 0$  and a linear function:  $G(f) = G(-f)$ , for the connection with the autocovariance function (ACV) the Wiener-Khintchine relation applies

$$R_{xx}(\tau) = \int_{-\infty}^{\infty} G(f) e^{2\pi i f \tau} df \quad \text{und} \quad G(f) = \int_{-\infty}^{\infty} R_{xx}(\tau) e^{-2\pi i f \tau} d\tau \quad .$$

The square spectrum does not contain any information on phase relations. The ACV itself is defined as the average value in time of all products of function values which differ in time  $\tau$ ; in each case after subtraction of the average value of the function. If this value is = zero the conditional equation is:

$$R_{xx}(\tau) = \lim_{T \rightarrow \infty} \frac{1}{2T} \int_{-T}^T x(t) x(t + \tau) dz \quad .$$

Consequently  $R_{xx}$  indicates the inner connection of the process.

To characterize two irregular processes  $x(t)$  and  $y(t)$  the complex cross power spectrum (or

cross spectrum) is defined analogously as a Fourier transform of the cross covariance function

$$G_{xy}(f) = \int_{-\infty}^{\infty} R_{xy}(\tau) e^{-2\pi i f \tau} d\tau \quad .$$

with

$$G_{xy}(f) = C_{xy}(f) - iQ_{xy}(f) = |G_{xy}(f)| e^{i\Theta_{xy}(f)}$$

and

$$\Theta_{xy}(f) = -\tan^{-1} \left( \frac{Q_{xy}(f)}{C_{xy}(f)} \right)$$

as phase. The coherence of both processes is determined by:

$$K_{xy}^2(f) = \frac{C_{xy}^2(f) + Q_{xy}^2(f)}{G_{xx}(f) G_{yy}(f)} \quad . \quad (4.7)$$

In magnetotellurics the power spectrum is usually determined by the periodogram estimate

$$\bar{P}_T(t) = \frac{1}{T} \left| \int_0^T x_T(t) e^{2\pi i f t} dt \right|^2 \quad .$$

#### 4.4 Processing method

The most important part is the transformation into the frequency domain by Fourier transformation<sup>6</sup>. Consequently the different steps of the working process of a routine analysis are:

- pre-treatment in the time domain (tapering, pre-whitening)
- transformation into the frequency domain, FFT
- correction of transfer functions of the instruments
- calculation of power spectra, stacking
- calculation of the impedance tensor with variance estimates
- calculation of derived quantities, e.g.  $\rho_a(\omega)$  and  $\phi(\omega)$ , with error bounds.

In the following some of these steps will be explained, particularly those that are different from the process in seismics.

##### *Pre-treatment in the time domain and Fourier transformation*

For later Fourier analysis the time series are subdivided into segments with a value of  $N=2^k$ <sup>7</sup>, e.g. 1024 when  $k=10$ . The aim is to bring the characteristics of the recorded time series in line with those of a white noise ("pre-whitening"), i.e. to remove trends and peaks from the spectrum. Usually, the beginning and the end (approximately 10%) of the time series are

<sup>6</sup> An analysis in the time domain is possible (Kunetz 1972), but is rarely applied.

<sup>7</sup> There are, however, FFT-algorithms without any limitations to the power of two.

superimposed by a  $\cos^2$ - weighting function ("tapering") to avoid boundary effects. The next step is to remove the average value and a linear trend or, in general, the use of a high-pass filter to weigh down very long periods. These are often assumed to be caused by a drift of the instruments (e.g. the probes). There is a peculiarity in the audio frequency domain where in populated areas strong spectral peaks can be observed at  $16^{2/3}$  Hz, 50 Hz + harmonics (even after the use of an electronic band-stop filter). They can be removed by a comb filter. This is realized by the non- recursive difference equation

$$y(k) = x(k) - x(k - n'), k = 0, 1, \dots, N - 1$$

with the transfer function

$$H(f) = 1 - \exp(2\pi i n' f) \quad .$$

### *Smoothing of the spectra*

The Fourier transform of  $M$  time series segments is achieved by a Fast Fourier Transformation (FFT). After correction of instrument responses, the power spectra, e.g.  $|B_x|^2 = B_x B_x^*$ , are calculated and normalized to  $\Delta f$  by multiplication with the length of the time series segments. Regarding the frequency the Fourier coefficients are equidistant; however, here the transfer functions are described logarithmically equidistant (at approximately 8 points per decade). The determination takes place by a Parzen-window function for example.

### *Calculation of the impedance tensor*

Usually the elements of the impedance tensor are calculated by a method of error minimization, the least squares method. We have a number of independent measurements  $j = 1, \dots, N$  and we assume that the values of the magnetic field are free of errors while those of the electrical field shall have errors<sup>8</sup>.

$$\begin{aligned} E_x^j &= Z_{xx} B_x^j + Z_{xy} B_y^j + \delta E_x^j \\ E_y^j &= Z_{yx} B_x^j + Z_{yy} B_y^j + \delta E_y^j \end{aligned}$$

with  $\delta E$  as residuals. Now the sum of the error squares is minimized

$$\begin{aligned} \sum_{j=1}^N \delta E_x^j \delta E_x^{j*} &= \sum_{j=1}^N (E_x^j - Z_{xx} B_x^j - Z_{xy} B_y^j)(E_x^{j*} - Z_{xx}^* B_x^{j*} - Z_{xy}^* B_y^{j*}) = \text{Min!} \\ \sum_{j=1}^N \delta E_y^j \delta E_y^{j*} &= \sum_{j=1}^N (E_y^j - Z_{yx} B_x^j - Z_{yy} B_y^j)(E_y^{j*} - Z_{yx}^* B_x^{j*} - Z_{yy}^* B_y^{j*}) = \text{Min!} \end{aligned}$$

by equating the derivations with zero according to their real and imaginary parts. Consequently we get

<sup>8</sup> Correspondingly this approach is called "Minimization of the error in E" which can be used in particular at long periods, mostly due to noise (particularly drift) of the telluric probes. In contrast, the noise of the magnetic fields can be ignored. This does not apply for very high frequencies from approximately 500 Hz up. For this reason the formulation then must be modified correspondingly via an admittance.



$$\begin{aligned}
\sum_{j=1}^N E_x^j B_x^{*j} &= Z_{xx} \sum_{j=1}^N B_x^j B_x^{*j} + Z_{xy} \sum_{j=1}^N B_y^j B_x^{*j} \\
\sum_{j=1}^N E_x^j B_y^{*j} &= Z_{xx} \sum_{j=1}^N B_x^j B_y^{*j} + Z_{xy} \sum_{j=1}^N B_y^j B_y^{*j} \\
\sum_{j=1}^N E_y^j B_x^{*j} &= Z_{yx} \sum_{j=1}^N B_x^j B_x^{*j} + Z_{yy} \sum_{j=1}^N B_y^j B_x^{*j} \\
\sum_{j=1}^N E_y^j B_y^{*j} &= Z_{yx} \sum_{j=1}^N B_x^j B_y^{*j} + Z_{yy} \sum_{j=1}^N B_y^j B_y^{*j}
\end{aligned}$$

With:

$$[XY^*] = \frac{1}{N} \sum_{j=1}^N X_j Y_j^*$$

the average value of N power spectra is described. The equations above are thus written as:

$$\begin{aligned}
[E_x B_x^*] &= Z_{xx} [B_x B_x^*] + Z_{xy} [B_y B_x^*] \\
[E_x B_y^*] &= Z_{xx} [B_x B_y^*] + Z_{xy} [B_y B_y^*] \\
[E_y B_x^*] &= Z_{yx} [B_x B_x^*] + Z_{yy} [B_y B_x^*] \\
[E_y B_y^*] &= Z_{yx} [B_x B_y^*] + Z_{yy} [B_y B_y^*]
\end{aligned}$$

Now the components of the tensors can be calculated:

$$\begin{aligned}
Z_{xx} &= \frac{[E_x B_x^*][B_y B_y^*] - [B_y B_x^*][E_x B_y^*]}{D} \\
Z_{xy} &= \frac{[B_x B_x^*][E_x B_y^*] - [B_x B_y^*][E_x B_x^*]}{D} \\
Z_{yx} &= \frac{[E_y B_x^*][B_y B_y^*] - [B_y B_x^*][E_y B_y^*]}{D} \\
Z_{yy} &= \frac{[B_x B_x^*][E_y B_y^*] - [B_x B_y^*][E_y B_x^*]}{D}
\end{aligned} \tag{4.8a}$$

with

$$D = [B_x B_x^*][B_y B_y^*] - [B_x B_y^*][B_y B_x^*] \tag{4.8b}$$

These relations have to be used for all target frequencies for which the transfer functions shall be determined (usually those are spread logarithmically and equidistantly in the frequency domain). The average value is determined by adjacent frequencies in a frequency band (Fig. 4.6) as well as by the set of the time series segments.

The derivation described here contains the

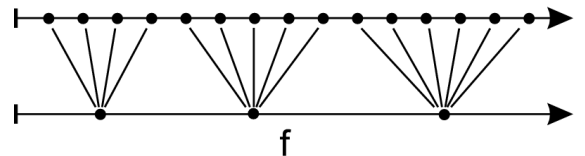


Fig. 4.6: Schematic representation of spectra that are equidistantly spread in a line and that are combined to a frequency band.

complete bivariate approach, i.e. each component of the electrical field is a function of the two magnetic components.

For a one-dimensional subsoil, however, only univariate equations  $E_x = Z B_y + \delta E_x$  or  $E_y = Z B_x + \delta E_y$  may be solved. If the components of the B-field are not polarized (i.e. not correlated) the terms become

$$\left[ E_x E_y^* \right] = 0 \quad , \quad \left[ E_x B_x^* \right] = 0 \quad \text{and} \quad \left[ B_x B_y^* \right] = 0$$

in (4.7a,b) and the following simple relations are obtained:

$$Z = \frac{\left[ E_x B_y^* \right]}{\left[ B_y B_y^* \right]} \quad \text{or} \quad Z = \frac{\left[ E_y B_x^* \right]}{\left[ B_x B_x^* \right]} . \quad (4.8c)$$

The transfer functions determined in that way are sometimes called "Cagniard impedances". However (4.8a,b) should always be used because the characteristics of the subsoil are often unknown.

The errors of the impedances are real numbers  $\delta Z$  (see Fig. 4.7) from which the errors of apparent resistivity can be calculated by using the law of error propagation:

$$\delta \rho_a = 0.4T |Z| \delta Z \quad . \quad (4.9a)$$

According to Fig. 4.7 the phase error is easily determined:

$$\delta \phi = \arcsin \frac{\delta Z}{|Z|} \approx \frac{\delta Z}{|Z|} \quad \text{for } \delta Z \ll |Z|. \quad (4.9b)$$

As it is a passive method, errors occur easily in magnetotellurics because of technical disturbances and noise in the time series in general. Besides the visual selection of "good" time series segments robust methods have been developed. For further information concerning these methods see, e.g., Egbert & Booker (1986).

The quantity D in the denominator of equation (4.8a) particularly contains the autospectra of the magnetic fields. If they contain strong noise (contrary to the initial assumption) the impedances (and therefore the resistivities) will be estimated as being too small. This can be resolved by the *Remote-Reference* technique (Gamble et. al 1979). Here the local magnetic fields are replaced by those of a (remote) reference station that is located far away but records synchronously<sup>9</sup>. If r as super- or subscript indicates the remote station we consequently obtain e.g.

$$Z_{xy}^r = \frac{\left[ B_x B_{xr}^* \right] \left[ E_x B_{yr}^* \right] - \left[ B_x B_{yr}^* \right] \left[ E_x B_{xr}^* \right]}{\left[ B_x B_{xr}^* \right] \left[ B_y B_{yr}^* \right] - \left[ B_x B_{yr}^* \right] \left[ B_y B_{xr}^* \right]} \quad (4.10)$$

etc. Fig 4.8 shows an example.

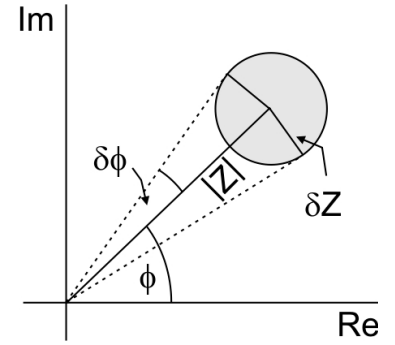


Fig. 4.7: The error of the impedance is a circle with the radius  $\delta Z$ .

<sup>9</sup> In this context "far away" means that the reference station should be located in an area with different noise. Depending on the frequency range and local conditions this can vary from several hundred m up to many km. Today the time-synchronization is mostly achieved by GPS.

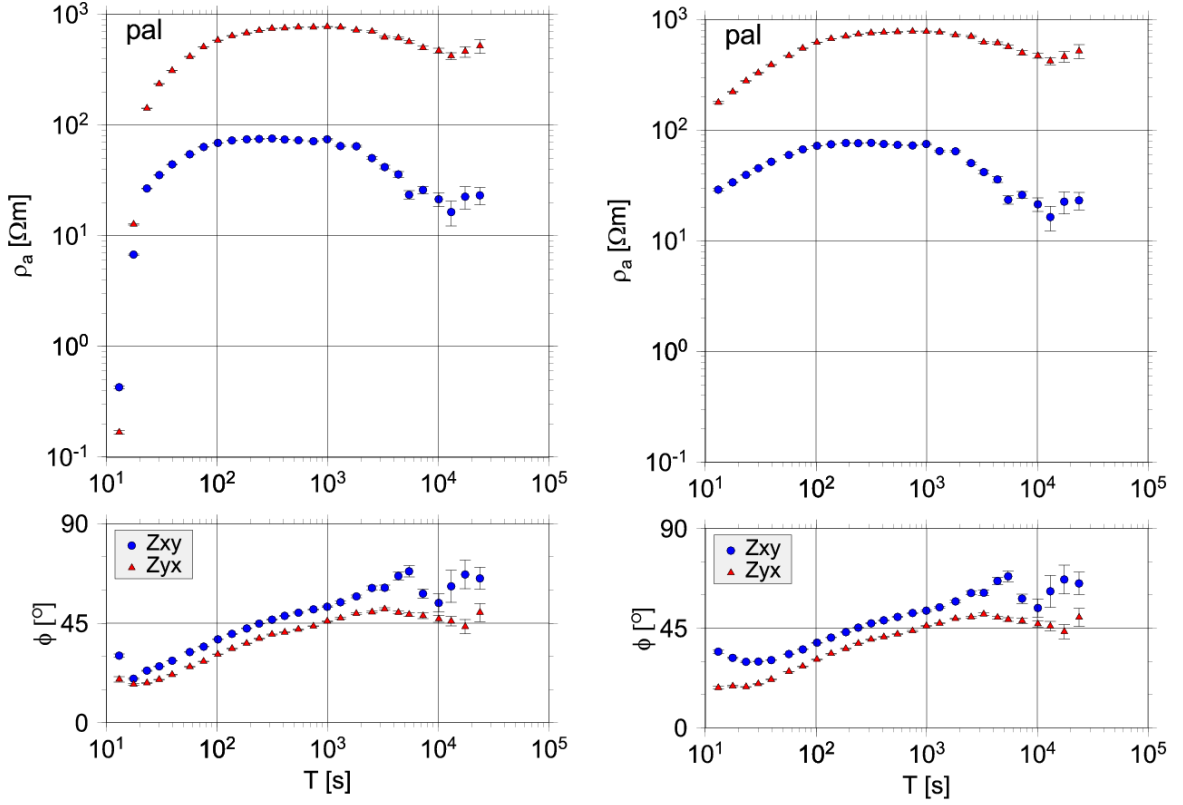


Fig. 4.8: Effects of Remote-Reference Processing for data of a station in Bolivia. Left: Single Site-Processing, right: with Remote Reference for the period range of 10 - 500 s. In the single processing the low sensitivity of the used fluxgate magnetometer is manifested, in particular in apparent resistivities. For long periods there was no improvement.

An exact synchronization of both stations is not necessary which also results from eq. (4.8). An time error at the reference station causes a phase difference  $\Delta\phi$  at a certain frequency, that means  $B_{xr} = B_{xr,0} \exp(i\Delta\phi)$ ,  $B_{yr} = B_{yr,0} \exp(i\Delta\phi)$  etc. Inserted into (4.8) this constant phase error will be eliminated. However, the error in time does not remain constant due to the drift of the internal logger clocks.

One selection criterion for stable transfer functions can be the coherence, e.g.:

$$K_p^2 = \frac{Z_{xx} [B_x E_x^*] + Z_{xy} [B_y E_x^*]}{[E_x E_x^*]} \quad (4.11a)$$

This is the (squared) multiple or predictive coherence; the simple or univariate coherence among the input processes (here  $B_x$ ,  $B_y$ ) is:

$$K_{xy}^2 = \frac{[B_x B_y^*][B_y B_x^*]}{[B_x B_x^*][B_y B_y^*]} \quad (4.11b)$$

For  $K_{xy}^2 = 1$  the denominator in the conditional equations (4.8a,b) becomes identical to zero and the bivariate problem becomes a univariate one. This means for example that a stable estimate of the transfer functions according to (4.8) is not possible for strongly correlated components of the magnetic field ( $B_x$ ,  $B_y$ ). Furthermore, if there is correlated noise (e.g. near a technical disturbance) a pure coherence criterion will fail.

## 5 Magnetotellurics over a layered half space

### 5.1 Boundary conditions<sup>1</sup>

The *boundary conditions* at an interface between two layers of conductivity  $\sigma_1$  and  $\sigma_2$  can be deduced from the Maxwell-equations in their integral form, which are achieved from (2.1a-d) with the aid of Stokes theorem

$$\int_{S'} (\nabla \times \underline{E}) \cdot \underline{n} \, ds = \oint_C \underline{E} \cdot d\underline{\ell} \quad (5.1a)$$

and Gauß theorem:

$$\int_V \nabla \cdot \underline{E} \, dv = \int_S \underline{E} \cdot \underline{n} \, ds \quad . \quad (5.1b)$$

Here  $V$  denotes a volume;  $S$  the area which encloses this volume,  $\underline{n}$  is the normalized vector on this area and  $C$  an enclosed curve around the area  $S'$ .

Then Ampère's and Faraday's law (2.1a,b) is:

$$\oint_C \underline{H} \cdot d\underline{\ell} = I + \frac{\partial}{\partial t} \int_S \underline{D} \cdot \underline{n} \, ds \quad \oint_C \underline{E} \cdot d\underline{\ell} = - \frac{\partial}{\partial t} \int_S \underline{B} \cdot \underline{n} \, ds \quad (5.2a,b)$$

with the total current:

$$I = \int_S \underline{J} \cdot \underline{n} \, ds \quad .$$

Analogically equations (2.1c,d) become:

$$\int_S \underline{B} \cdot \underline{n} \, ds = 0 \quad \int_S \underline{D} \cdot \underline{n} \, ds = \int_V Q \, dv = q \quad . \quad (5.2c,d)$$

The equation of continuity

$$\nabla \cdot \underline{J} + \frac{\partial Q}{\partial t} = 0 \quad (5.3a)$$

written in integral form is:

$$I = \int_S \underline{J} \cdot \underline{n} \, ds = - \frac{\partial}{\partial t} \int_V Q \, dv = \frac{\partial q}{\partial t} \quad . \quad (5.3b)$$

Now the following boundary conditions apply at the interface of two media:

1. *The normal component of  $\underline{B}$  is continuous.*

Let us look at a small cylinder (pillbox) with the base area  $\Delta a$  and the height  $\Delta \ell$  (Fig. 5.1) inside the interface  $S$ . If  $\Delta a$  is very small, the induction  $\underline{B}$  on the upper side has the constant value  $\underline{B}_1$ , on the lower side the constant value  $\underline{B}_2$ . We can approximate the integral (5.2a) with:

$$(\underline{B}_1 \cdot \underline{n}_1 + \underline{B}_2 \cdot \underline{n}_2) \Delta a + \text{contributions from margins} = 0$$

<sup>1</sup> The boundary conditions for the electrical field and the current density are already described in the chapter about DC geoelectrics and are recapitulated here.

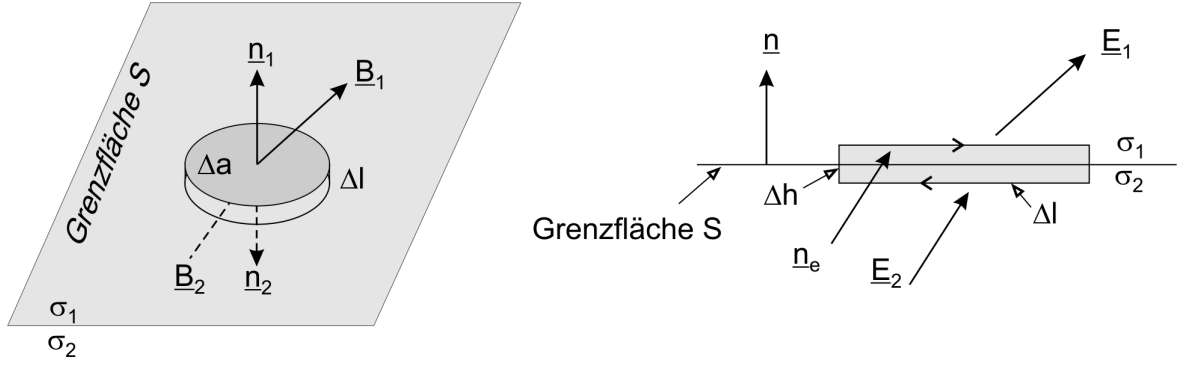


Fig. 5.1: Illustration of the continuity of the normal component of  $\underline{B}$  (left) and the tangential component of  $\underline{E}$  (right). The  $\underline{E}$ -fields and the normal vector  $\underline{n}_e$  is located in the plane of projection.

The contribution of the boundary areas to the integral over the surface (5.2a) is proportional to  $\Delta \ell$  and can be ignored or  $\Delta \ell \rightarrow 0$ . Consequently there is:

$$(\underline{B}_1 \cdot \underline{n}_1 + \underline{B}_2 \cdot \underline{n}_2) \Delta a = 0 \quad \text{and with} \quad \underline{n} = \underline{n}_1 = -\underline{n}_2 \quad :$$

$$\underline{n} \cdot (\underline{B}_1 - \underline{B}_2) = 0 \quad . \quad (5.4a)$$

2. *The normal component of  $\underline{D}$  is discontinuous.* The argumentation is simultaneous to the one before: The integral over the charge density in (5.3b) is approximated by:

$$\int_V Q dV = Q \Delta \ell \Delta a \quad .$$

$Q \Delta \ell = Q_s$  is charge density per area (charge/area); so (5.3b) becomes:

$$(\underline{D}_1 \cdot \underline{n}_1 + \underline{D}_2 \cdot \underline{n}_2) \Delta a = Q_s \Delta a \quad , \quad \text{and therefore}$$

$$\underline{n} \cdot (\underline{D}_1 - \underline{D}_2) = Q_s \quad . \quad (5.4b)$$

$D$  jumps by the value of the charge density per area.

3. Then *the normal component of  $\underline{E}$  is discontinuous*, too. In that case both dielectricity and conductivity influence the discontinuity. Due to Ohm's law and if  $\varepsilon_1 = \varepsilon_2$ ,  $\underline{E}_n$  jumps proportionally to the resistivity contrast.

4. *The tangential component of  $\underline{E}$  is continuous.*

If one determines the line integral (5.2b) according to Fig. 5.1 (right) with  $\underline{n}_e$  as the normal vector on the plotted rectangle:

$$\begin{aligned} -\frac{\partial}{\partial t} \int_S \underline{B} \cdot \underline{n}_e ds &= -\frac{\partial \underline{B}}{\partial t} \cdot \underline{n}_e \Delta h \Delta \ell \\ &= \oint_C \underline{E} \cdot d\underline{\ell} = \underline{E}_1 \cdot \Delta \underline{\ell} + \underline{E}_2 \cdot (-\Delta \underline{\ell}) + \text{contributions of left and right margins} \end{aligned}$$

With  $\Delta h \rightarrow 0$  follows

$$(\underline{E}_1 - \underline{E}_2) \Delta \ell \quad \text{or:}$$

$$\underline{n} \times (\underline{E}_1 - \underline{E}_2) = 0 \quad . \quad (5.4c)$$

5. The tangential component of  $\underline{H}$  is continuous.

Similarly to the prior consideration of the  $\underline{E}$  field with  $\Delta h \rightarrow 0$  the integral (5.2a) together with the integral over the current density then becomes:

$$\underline{n} \times (\underline{H}_1 - \underline{H}_2) = \lim_{\Delta h \rightarrow 0} \left( \frac{\partial \underline{D}}{\partial t} + \underline{J} \right) \Delta \underline{h}$$

For finite displacement- and charge current densities, the terms on the right side become zero. If a surface current  $\underline{J}_s$  exists, with

$$\underline{J}_s = \lim_{\Delta h \rightarrow 0, J \rightarrow \infty} \underline{J} \Delta h \quad ,$$

the boundary condition is

$$\underline{n} \times (\underline{H}_1 - \underline{H}_2) = \underline{J}_s \quad .$$

However, if the conductivities of both media are finite, the surface current density must disappear, because  $\underline{E} = \underline{J}/\sigma$  is always finite. So:

$$\underline{n} \times (\underline{H}_1 - \underline{H}_2) = 0 \quad . \quad (5.4d)$$

6. Consequently, the *tangential component of  $\underline{B}$  is continuous*, too if  $\mu_1 = \mu_2$ , as it was assumed. With an infinite conductivity the current density also becomes infinite, so  $\underline{E} = \underline{J}/\sigma$  stays finite and the tangential component of  $\underline{H}$  jumps by the value  $\underline{J}_s$ .

7. The normal component of  $\underline{J}$  is continuous:

For  $\Delta h \rightarrow 0$  a current

$$I = \underline{J}_1 \cdot \underline{n} \Delta a = \underline{J}_2 \cdot \underline{n} \Delta a$$

flows through the boundary layer and from this results:

$$\underline{n} \cdot (\underline{J}_1 - \underline{J}_2) = 0 \quad . \quad (5.4e)$$

From these boundary conditions the laws of refraction for the current lines shall be derived (see Fig. 5.2). With  $\phi_1$  as angle of incident and  $\phi_2$  as emergent angle,  $\underline{J}_n$  as normal and  $\underline{J}_t$  as tangential component we obtain:

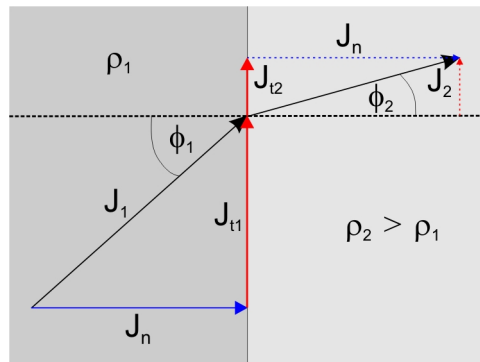


Fig. 5.2: The continuity and jump conditions of the current density at a boundary layer.

$$\begin{aligned}
 J_{n1} &= J_{n2} = J_n \\
 \frac{J_{t1}}{J_n} &= \tan \phi_1 \\
 \frac{J_{t2}}{J_n} &= \tan \phi_2
 \end{aligned} \quad (5.5)$$

The continuity of the normal component (it has the same value at both sides of the boundary layer) means that the current penetrates deeper into the poor conductor.

8. For the *components of the electric field strength* the reverse is the case (caused by the generalized Ohm's law). *The tangential component is continuous, the normal component jumps proportionally to the resistivity contrast:*

$$\begin{aligned}
 J_n &= \sigma_1 E_{n1} = \sigma_2 E_{n2} \\
 J_{t1} &= \sigma_1 E_t \\
 J_{t2} &= \sigma_2 E_t \\
 \text{thus } E_t &= \frac{J_{t1}}{\sigma_1} = \frac{J_{t2}}{\sigma_2}
 \end{aligned} \quad (5.6)$$

Consequently, the law of refraction for the current lines is:

$$\frac{J_{t1}}{J_{t2}} = \frac{\sigma_1 E_t}{\sigma_2 E_t} = \frac{\sigma_1}{\sigma_2} = \frac{\rho_2}{\rho_1} = \frac{\tan \phi_1}{\tan \phi_2} \quad (5.7)$$

This is illustrated in Figs. 5.3 and 5.4.

Equations 5.5 to 5.7 are just a transcription of Snell's law of refraction, which correlates the directions of the normal vectors of the waves in both media:

$$\underline{k}_1 \times \underline{n} = \underline{k}_2 \times \underline{n} \quad ; \quad (5.8a)$$

Here  $\underline{k}_1$  and  $\underline{k}_2$  are the wave number vectors ( $\parallel$  to the relative direction of propagation in medium 1 or 2),  $\underline{n}$  is the normal vector. From this follows:

$$k_1 \sin \phi_1 = k_2 \sin \phi_2 \quad (5.8b)$$

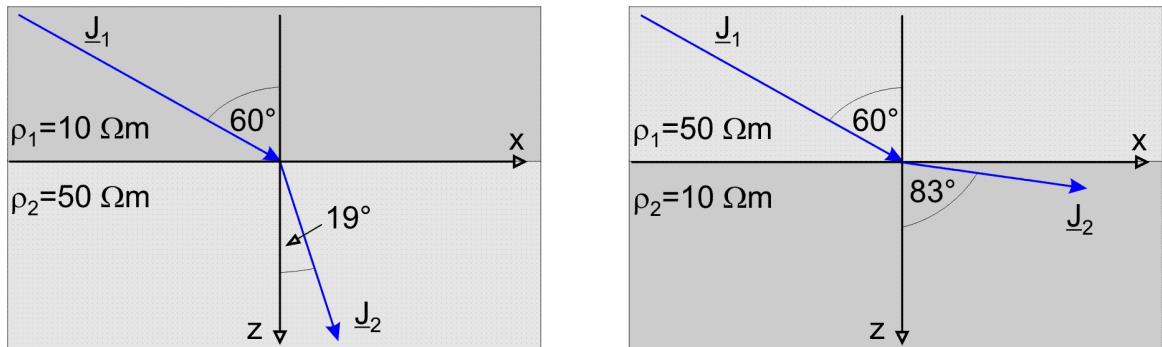


Fig. 5.3: Refraction of current lines at a resistivity interface; the angle of incidence is  $60^\circ$  in both cases. Left: poor conductor under good conductor, the refraction angle constitutes  $19^\circ$  and the current lines penetrate deeper into the poor conductor. Right: If the current lines penetrate into a good conductor, a current concentration takes place at the interface, and the angle of refraction is  $83^\circ$ . See eq. (5.6).

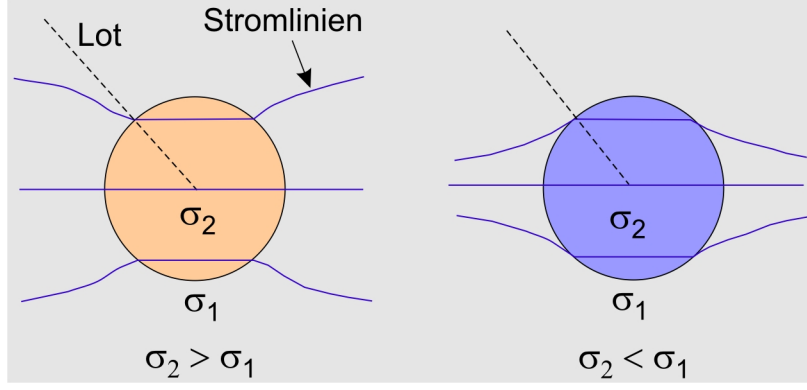


Fig. 5.4: Concentration and expulsion of current in a sphere.

The high conductivity contrast at the earth's surface causes a perpendicular refraction in the subsoil even under grazing incidence. Consequently all fields in the homogeneous (and also in the layered) subsoil are parallel to the earth's surface.

## 5.2 General induction fields, TE and TM modes

Let us first treat an idealized model of geomagnetic induction. Over the earth's surface ( $z = 0$ ) we locate the non-conducting air space ( $\sigma_0 = 0$ ) and at height  $z = -h$  the region of sources (ionosphere and magnetosphere), with a (plasma-) conductivity that is irrelevant in this context. The conductivity of the earth is  $\sigma_1$ , which again is assumed to be homogeneous (Fig. 5.5).

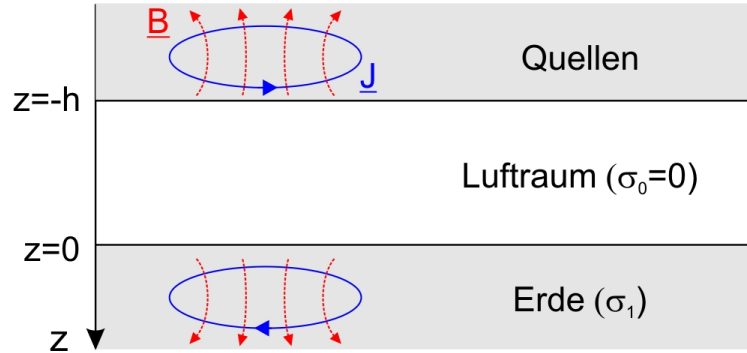


Fig. 5.5: Model of geomagnetic induction. Current systems in outer space induce secondary currents inside the earth.

The magnetic field is always divergence-free:  $\nabla \cdot \underline{B} = 0$ . Divergence-free fields can be divided into a part that is rotation-free and another one that contains rotation. The second one can again be divided into a *toroidal* and a *poloidal* part:

$$\underline{B}(\underline{r}) = \underline{B}_1(\underline{r}) + \underline{B}_2(\underline{r}) + \underline{B}_3(\underline{r})$$

with

$$\underline{B}_1(\underline{r}) = \nabla \times (\phi \underline{r}) \quad \text{and} \quad \underline{B}_2(\underline{r}) = \nabla \times \nabla \times (\psi \underline{r})$$

for the part with rotation and



$$\underline{B}_3(\underline{r}) = \nabla U$$

for the curl-free.  $\underline{r}$  is the position vector.  $\phi$ ,  $\psi$  and  $U$  are scalar functions of position.

$\phi$  and  $\psi$  satisfy the equation of induction

$$\Delta\phi = i\omega\mu_0\sigma\phi \quad , \quad \Delta\psi = i\omega\mu_0\sigma\psi \quad .$$

From

$$\nabla \times (\phi \underline{r}) = \phi \nabla \times \underline{r} - \underline{r} \times \nabla \phi = -\underline{r} \times \nabla \phi \quad \text{due to } \nabla \times \underline{r} = 0$$

results  $\underline{B}_1 \perp \underline{r}$  and  $\underline{B}_1 \perp \nabla \phi$ , so especially  $\underline{B}_1 \parallel (z = 0)$ . Consequently,  $\underline{B}_1$  is tangential to the earth's surface and describes the toroidal part.  $\underline{B}_2$  on the other hand has no limitation in direction, so that it represents the poloidal part.  $\underline{B}_3$  is a static field and has no relevance in the following. From this follows:

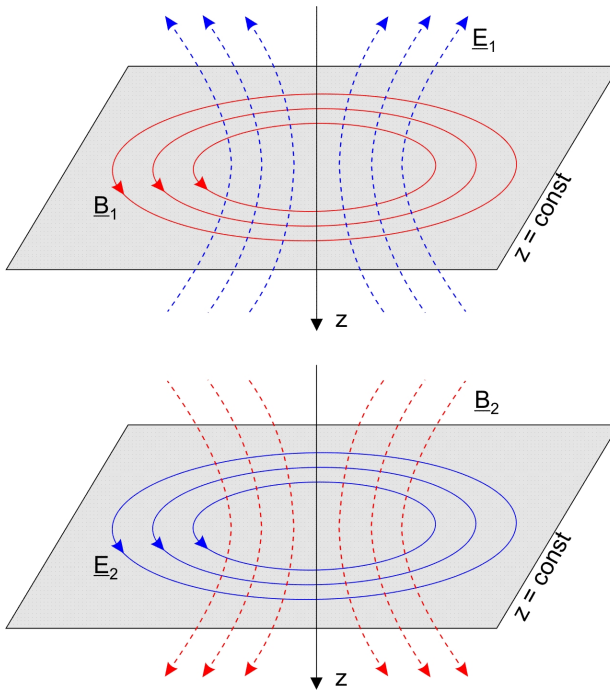
$$\underline{E} = \frac{1}{\mu_0\sigma} \nabla \times \underline{B} = \underline{E}_1(\underline{r}) + \underline{E}_2(\underline{r}) \quad (+ \underline{E}_3(\underline{r}))$$

with

$$\underline{E}_1 = \frac{1}{\mu_0\sigma} \nabla \times \nabla \times (\phi \underline{r})$$

$$\underline{E}_2 = i\omega \nabla \times (\psi \underline{r}) \quad .$$

So we get two modes of the fields, which can be described by the potentials  $\phi$  and  $\psi$  (see Fig. 5.6):



*TM-mode (tangential-magnetic)*

$$\underline{B}_1(\underline{r}) = \nabla \times (\phi \underline{r}) \quad (5.9a)$$

$$\underline{E}_1 = \frac{1}{\mu_0\sigma} \nabla \times \nabla \times (\phi \underline{r}) \quad (5.9b)$$

$$\text{In particular } B_z = 0 ! \quad (5.9c)$$

*TE-mode (tangential-electric)*

$$\underline{B}_2(\underline{r}) = \nabla \times \nabla \times (\psi \underline{r}) \quad (5.10a)$$

$$\underline{E}_2 = i\omega \nabla \times (\psi \underline{r}) \quad (5.10b)$$

$$\text{In particular } E_z = 0 ! \quad (5.10c)$$

Fig. 5.6: TM and TE mode of the source field.

The quantities  $\phi \underline{r}$  and  $\psi \underline{r}$  are known as magnetic and electric *Hertz's vectors*. The real field, coming from the earth's outer space and striking the earth's surface under an angle of

incidence  $\theta_i$ , will always contain both parts. We can anticipate that the TE mode is of great interest for passive long-period magnetotellurics, while the TM mode plays a major role in high frequency excitation (atmospherics and VLF-R) and especially in active CSAMT (where a current is injected into the earth via galvanic contacts)<sup>2</sup>.

First, the equation of induction for the TE-mode in  $z \geq 0$  is solved with an approach that is harmonic in both time and space – in (x-y, not z)-direction:

$$E_x = E_{x0} e^{i(v_x x + v_y y)} e^{-kz} e^{i\omega t}, \quad E_y = E_{y0} e^{i(v_x x + v_y y)} e^{-kz} e^{i\omega t}, \quad E_z = 0$$

$$\text{with } \gamma^2 = v_x^2 + v_y^2 + k_z^2 = v^2 + i\omega\mu_0\sigma = v^2 + k^2.$$

Due to  $\nabla \times \underline{E} = -i\omega \underline{B}$  follows for the magnetic field:

$$B_x = -\frac{1}{i\omega} \left( \frac{\partial E_z}{\partial y} - \frac{\partial E_y}{\partial z} \right) = \frac{1}{i\omega} \frac{\partial E_y}{\partial z} = -\frac{E_{y0}}{i\omega} k e^{-kz} e^{i(v_x x + v_y y)} = -\frac{1}{i\omega} k E_y$$

$$B_y = -\frac{1}{i\omega} \left( \frac{\partial E_x}{\partial z} - \frac{\partial E_z}{\partial x} \right) = -\frac{1}{i\omega} \frac{\partial E_x}{\partial z} = \frac{E_{x0}}{i\omega} k e^{-kz} e^{i(v_x x + v_y y)} = \frac{1}{i\omega} k E_x$$

$$B_z = -\frac{1}{i\omega} \left( \frac{\partial E_y}{\partial x} - \frac{\partial E_x}{\partial y} \right) = \frac{1}{\omega} (v_y E_x - v_x E_y)$$

At the earth's surface  $z = 0$  is:

$$E_x = E_{x0}, \quad E_y = E_{y0}, \quad E_z = 0$$

$$B_x = -\frac{\gamma}{i\omega} E_{y0}, \quad B_y = \frac{\gamma}{i\omega} E_{x0}, \quad B_z = \frac{v_y}{\omega} E_{x0} - \frac{v_x}{\omega} E_{y0}$$

Now we define the reciprocal wave number or *complex penetration depth*<sup>3</sup>:

$$C := \frac{1}{\gamma} = \frac{1}{\sqrt{i\omega\mu_0\sigma + v^2}} = \frac{1}{\sqrt{k^2 + v^2}} \quad (5.11)$$

consequently

$$E_x = i\omega C B_y, \quad E_y = -i\omega C B_x$$

$$B_z = C(iv_x B_x + iv_y B_y)$$

from which follows the known impedance:

$$Z = i\omega C = \frac{E_x}{B_y} = -\frac{E_y}{B_x}, \quad \rho = \frac{\mu_0}{\omega} |Z|^2 \quad \text{or} \quad (5.12a)$$

<sup>2</sup> In the theory of electromagnetic waves one often talks about transversal electromagnetic TEM waves. The direction of this polarization refers to the plane that is perpendicular to the direction of propagation, in which  $\underline{E}$  as well as  $\underline{B}$  oscillates. In our case the earth's surface is the important reference plane. A perpendicular incidence implies the assumption of a plain wave ( $v = 0$ ) and does not help here because this precondition is not satisfied in the near field e.g. of a CSAMT transmitter. The differentiation of the modes is irrelevant, as long as the quasi-homogeneity of the exciting field is guaranteed.

<sup>3</sup>  $C$  is also called Schmucker's response function and is often used as an alternative to the impedance in literature.

$$Z = i\omega C = i\omega \frac{B_z}{iv_x B_x + iv_y B_y} = \frac{\omega B_z}{v_x B_x + v_y B_y}, \quad \rho = \frac{\omega \mu_0}{v^2} \left| \frac{B_z}{B_h} \right| \quad (5.12b)$$

With (5.12b) we found another method to determine the resistivity of the half space from the proportion of the vertical and horizontal magnetic fields. For  $v \rightarrow 0$  (quasi-homogeneous field), however, the impedance  $Z$  can not be solved from (5.12b).

Now it is time to analyse when the far field condition is met. This obviously applies if:

$$|k| \gg v \quad \text{oder} \quad |C|v \ll 1, \quad (5.13a)$$

or if the lateral wave length is much larger than the wave length or the penetration depth in the subsurface, respectively:

$$|\ell| \gg \Lambda = 2\pi\delta \quad (5.13b)$$

Here the terminology of Chap. 2 is used. Unfortunately the structure of wave numbers of the exciting field is unknown in most cases because in practice there is always an overlay of waves from different sources. For some excitation types, however, the structure can be specified. So wave numbers can be assumed

$$v_n = n/r_e = n \cdot 1.57 \times 10^{-4} \text{ km}^{-1}, \quad n = 1, 2, 3, \dots$$

for the Schumann resonances (guided waves in the wave guide earth/ionosphere). A maximum estimate with  $\sigma = 10^{-4} \text{ S/m}$  for a homogeneous subsoil and  $f \approx 8 \text{ Hz}$  for  $n = 1$  results in  $|C| \approx 4 \text{ km}$ , so (5.12a) is satisfied. A similar estimation can be done for daily (Sq) and Dst variations. In the vicinity of the polar and equatorial electrojets this condition is surely not met. Violation of this condition, which is also called *frequency sounding condition*, is immediately visible in the curves of  $\rho_a$  and phases. It usually causes – in interaction with other sources – a dispersion of data or a behavior of the curves as it is shown in Fig. 5.7. This applies particularly for noise fields that are injected near a measuring station<sup>4</sup>.

Eq. (5.12a) now contains implicitly the horizontal wave numbers  $v$  due to  $C = 1/\gamma$  in eq. (5.11). For  $v \rightarrow 0$  it applies

$$C = \frac{1}{k} \quad \text{and} \quad \rho = \rho_a = \mu_0 \omega |C|^2 = \frac{\mu_0}{\omega} |Z|^2 \quad (5.14)$$

However, for an inhomogeneous source ( $v$  is finite) there is

$$\rho_a = \mu_0 \omega |C|^2 = \frac{2\pi\mu_0}{T} \left| \frac{1}{\sqrt{k^2 + v^2}} \right|^2.$$

If under a constant  $v$  the period is increased further, i.e.  $\omega \rightarrow 0$  and consequently  $k \ll v$ ,  $\rho_a$  is only a function of  $T$ , in a  $\log \rho_a$  ( $\log T$ )-plot it would be a straight line (see Fig. 5.7):

<sup>4</sup> In the chapter about the induced fields we'll have a closer look at the question, how *far* away from, e.g., a dipole or line source we have to be in order to satisfy the far field condition.

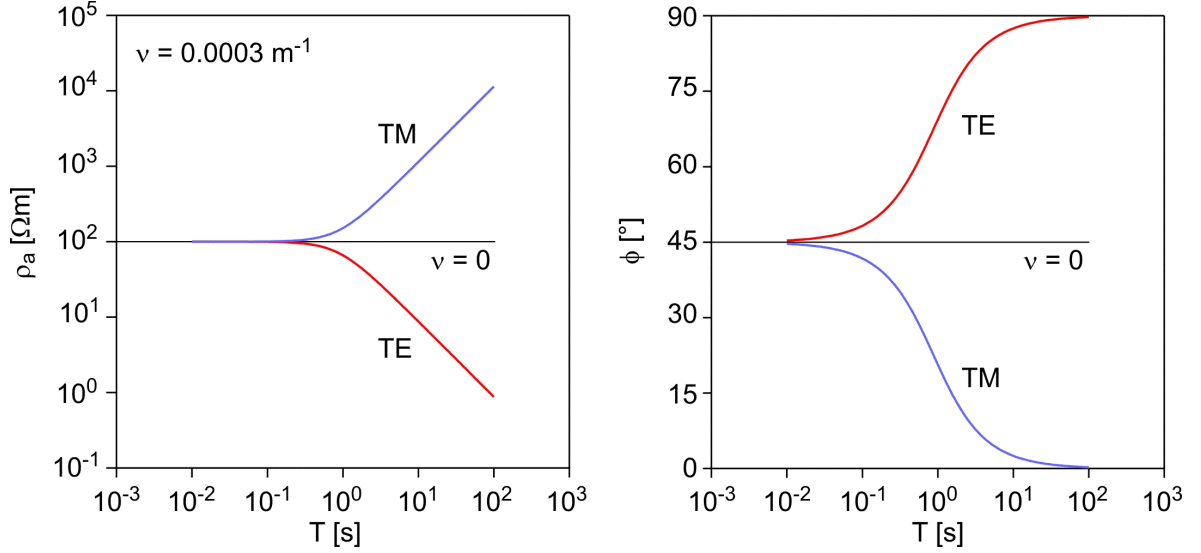


Fig. 5.7: Splitting of  $\rho_a(T)$ - and  $\phi(T)$ -curves for TE and TM mode under inhomogeneous excitation. The underground is a homogeneous half space with  $\rho = 100 \Omega m$ , as wave number we assume  $\nu = 0.0003 m^{-1}$ . The rise of the  $\rho_a(T)$ -curve is  $\pm 1$ .

$$\rho_a = \frac{2\pi\mu_0}{T} \frac{1}{\nu^2}$$

$$\log \rho_a(T) = \log\left(\frac{\text{const}}{T}\right) = \log(\text{const}) - \log T \quad . \quad (5.15)$$

Consequently, the  $\rho_a(T)$ -curve does not contain any information about the underground for large lateral wave numbers!

The solution for TM sources according to eq. (5.8a,b) is analogue to TE mode:

$$B_x = A_x e^{-\gamma z}, \quad B_y = A_y e^{-\gamma z}, \quad B_z = 0.$$

Due to  $\nabla \times \underline{B} = \mu_0 \sigma \underline{E}$  follows for the electric field:

$$E_x = -\frac{1}{\mu_0 \sigma} \frac{\partial B_y}{\partial z}, \quad E_y = \frac{1}{\mu_0 \sigma} \frac{\partial B_x}{\partial z}, \quad E_z = \frac{1}{\mu_0 \sigma} |i\nu_y B_x - i\nu_x B_y|$$

Then the solution in  $z \geq 0$  with  $C = 1/\gamma$  is:

$$E_x = \frac{A_y}{\mu_0 \sigma} \gamma e^{-\gamma z} \rightarrow Z = \frac{E_x}{B_y} = \frac{\gamma}{\mu_0 \sigma} = \frac{1}{\mu_0 \sigma C} \quad .$$

$$B_x = \mu_0 \sigma C E_y, \quad B_y = \mu_0 \sigma C E_x$$

$$E_z = C(i\nu_x E_y + i\nu_y E_x) \quad .$$

From this follows:

$$C = \frac{1}{\gamma} = \frac{1}{\mu_0 \sigma} \frac{B_y}{E_x} \quad .$$

The term  $B_y/E_x$  is called magnetotelluric *admittance*. It has the dimension [s/m] or [S] if it is defined with the field strength H. For very small lateral wave numbers ( $k^2 \gg \nu^2$ ) there is

$$C = \frac{1}{k} = \frac{1}{\sqrt{i\mu_0\omega\sigma}}$$

and so the same transfer function as in the TE case is obtained:

$$Z = \frac{1}{\mu_0\sigma C} = \frac{k}{\mu_0\sigma} = \sqrt{\frac{i\omega}{\mu_0\sigma}}.$$

$$\rho = \frac{\mu_0}{\omega} |Z|^2.$$

At a given, finite wave number  $v$  and  $\omega \rightarrow 0$  ( $k^2 \ll v^2$ )  $\rho_a$  becomes only a function of  $T$ , like in the TE case but with a positive rise now.

$$\rho_a = \frac{\mu_0}{\omega} \left| \frac{v}{\mu_0\sigma} \right|^2 = \text{const} \cdot T$$

$$\log \rho_a(T) = \log(\text{const}) + \log T \quad (5.16)$$

### 5.3 The magnetotelluric impedance for the layered half space

We observe a layered half space of  $M-1$  layers with conductivity  $\sigma_m$  and thickness  $d_m$  above a homogeneous substratum of conductivity  $\sigma_M$  in the depth  $z_M$  (Fig. 5.8). First, we consider the case of the TE mode.

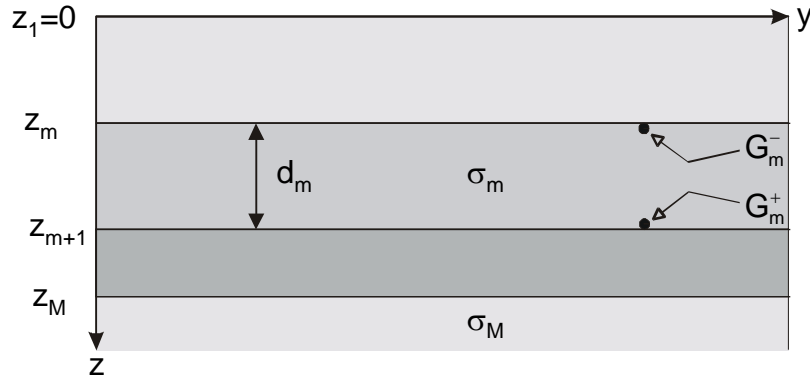


Fig. 5.8: Derivation of the impedance for a layered half space.

In the  $m$ -th layer  $E_x$  is:

$$E_x(z) = A_m e^{-\gamma_m z} + B_m e^{+\gamma_m z}, \quad \gamma_m^2 = i\omega\mu_0\sigma_m + v^2$$

for downwards ( $A_m$ ) and upwards ( $B_m$ ) diffusing parts of the field (now  $B_m$  is not = 0 any more) in the depth range  $z_m + 0, z_{m+1} - 0$ . In contrast to this, in the concluding half space there is  $B_M = 0$  again. From this results:

$$E_x(z) = A_M e^{-\gamma_M z}, \quad B_y(z) = \frac{k_M}{i\omega} A_M e^{-\gamma_M z}, \quad z \geq z_M.$$

The continuity of the tangential component also implies the continuity of the ratio (impedance)

$$\frac{E_x(z)}{B_y(z)} = \frac{i\omega}{\gamma_m G(z)} = i\omega C(z) \quad (5.17)$$

$$\text{with } G(z) = \frac{A_m e^{-\gamma_m z} - B_m e^{+\gamma_m z}}{A_m e^{-\gamma_m z} + B_m e^{+\gamma_m z}} \quad \text{in } z_m \leq z \leq z_{m+1} \quad .$$

$G(z)$  at the surface  $z = z_m + 0$  of the  $m$ -th layer we denote with  $G_m^-$ ,  $G(z)$  at the underside of the layer  $z = z_m - 0$  with  $G_m^+$ . At the boundary of the layers  $G(z)$  jumps in accordance with the wave numbers  $k$ :

$$\gamma_m G_m^+ = \gamma_{m+1} G_{m+1}^- \quad , \quad m = 1, 2 \dots M-1 \quad (5.18)$$

In a next step we have to connect  $G_m^+$  to  $G_m^-$ , that means the underside to the surface of the  $m$ -th layer:

$$G_m^- = \frac{A_m e^{-\gamma_m z_m} - B_m e^{\gamma_m z_m}}{A_m e^{-\gamma_m z_m} + B_m e^{\gamma_m z_m}} = G(z_m + 0) \quad \left[ = \frac{A_m e^{-\alpha} - B_m e^{\alpha}}{A_m e^{-\alpha} + B_m e^{\alpha}} \right]$$

$$G_m^+ = \frac{A_m e^{-\gamma_m z_{m+1}} - B_m e^{\gamma_m z_{m+1}}}{A_m e^{-\gamma_m z_{m+1}} + B_m e^{\gamma_m z_{m+1}}} = G(z_{m+1} - 0)$$

$$z_{m+1} = z_m + d_m, \text{ separating: } \gamma_m z_{m+1} = \gamma_m z_m + \gamma_m d_m = \alpha + \beta$$

with  $d_m$  as thickness of the  $m$ -th layer, that means  $e^{\gamma_m z_{m+1}} = e^{\gamma_m z_m} e^{\gamma_m d_m} = e^{\alpha} e^{\beta}$ ;  $e^{-\gamma_m z_{m+1}} = e^{-\alpha} e^{-\beta}$ .  $e^{\pm\beta}$  is described by hyperbolic functions:

$$e^{\beta} = \cosh \beta + \sinh \beta, \quad e^{-\beta} = \cosh \beta - \sinh \beta \quad ;$$

$e^{\beta}$  contains the variation of  $z_{m+1}$  to  $z_m$ <sup>5</sup>.

From this results:

$$\begin{aligned} G_m^+ &= \frac{A_m e^{-\alpha} e^{-\beta} - B_m e^{\alpha} e^{\beta}}{A_m e^{-\alpha} e^{-\beta} + B_m e^{\alpha} e^{\beta}} \\ &= \frac{A_m e^{-\alpha} (\cosh \beta - \sinh \beta) - B_m e^{\alpha} (\cosh \beta + \sinh \beta)}{A_m e^{-\alpha} (\cosh \beta - \sinh \beta) + B_m e^{\alpha} (\cosh \beta + \sinh \beta)} \\ &= \frac{(A_m e^{-\alpha} - B_m e^{\alpha}) \cosh \beta - (A_m e^{-\alpha} + B_m e^{\alpha}) \sinh \beta}{(A_m e^{-\alpha} + B_m e^{\alpha}) \cosh \beta - (A_m e^{-\alpha} - B_m e^{\alpha}) \sinh \beta} \quad . \end{aligned}$$

<sup>5</sup> Insertion for reminder (the illustration of the trigonometric functions is also shown for comparison):

hyperbol. functions	trigon. functions
$\sinh \beta = \frac{e^{\beta} - e^{-\beta}}{2}$	$\sin \beta = \frac{e^{i\beta} - e^{-i\beta}}{2i}$
$\cosh \beta = \frac{e^{\beta} + e^{-\beta}}{2}$	$\cos \beta = \frac{e^{i\beta} + e^{-i\beta}}{2}$
$\tanh \beta = \frac{e^{\beta} - e^{-\beta}}{e^{\beta} + e^{-\beta}}$	$\tan \beta = -i \frac{e^{i\beta} - e^{-i\beta}}{e^{i\beta} + e^{-i\beta}}$

We divide numerator and denominator each by  $A_m e^{-\alpha} + B_m e^{\alpha}$  :

$$\begin{aligned} G_m^+ &= \frac{\frac{A_m e^{-\alpha} - B_m e^{\alpha}}{A_m e^{\alpha} + B_m e^{\alpha}} \cosh \beta - \sinh \beta}{\cosh \beta - \frac{A_m e^{-\alpha} - B_m e^{\alpha}}{A_m e^{-\alpha} + B_m e^{\alpha}} \sinh \beta} \\ &= \frac{G_m^- \cosh \beta - \sinh \beta}{\cosh \beta - G_m^- \sinh \beta} \end{aligned}$$

and divide numerator and denominator again by  $\cosh \beta$  :

$$G_m^+ = \frac{G_m^- - \tanh \beta}{1 - G_m^- \tanh \beta}$$

or, what we really want:

$$\begin{aligned} G_m^+ - G_m^+ G_m^- \tanh \beta + \tanh \beta &= G_m^- \\ G_m^+ + \tanh \beta &= G_m^- + G_m^- G_m^+ \tanh \beta = G_m^- (1 + G_m^+ \tanh \beta) \\ G_m^- &= \frac{G_m^+ - \tanh \beta}{1 + G_m^+ \tanh \beta} = \frac{G_m^+ + \tanh(\gamma_m d_m)}{1 + G_m^+ \tanh(\gamma_m d_m)}. \end{aligned}$$

Now we substitute  $G_m^+$  and  $G_{m+1}^-$  with the aid of the jump condition (5.17):

$$\begin{aligned} G_m^+ &= \frac{\gamma_{m+1}}{\gamma_m} G_{m+1}^- \\ G_m^- &= \frac{\frac{\gamma_{m+1}}{\gamma_m} G_{m+1}^- + \tanh(\gamma_m d_m)}{1 + \frac{\gamma_{m+1}}{\gamma_m} G_{m+1}^- \tanh(\gamma_m d_m)} \quad \Big| \text{ Expand with } \gamma_m \\ &= \frac{\gamma_{m+1} G_{m+1}^- + \gamma_m \tanh(\gamma_m d_m)}{\gamma_m + \gamma_{m+1} G_{m+1}^- \tanh(\gamma_m d_m)}. \end{aligned} \tag{5.19}$$

For the concluding half space there is  $G_M^- = 1$ . Now a recursion formula is found to continue the function  $G(z)$  for a given conductivity model at the surface  $z_M + 0$  of the concluding homogeneous half space until  $G_1^-$  at the earth's surface  $z_1 = +0$ !

Then applies  $C_m = \frac{1}{\gamma_m G_m^-}$  and  $C_{m+1} = \frac{1}{\gamma_{m+1} G_{m+1}^-}$

As a consequence we obtain:

$$\gamma_m G_m^- = \frac{1}{C_m} = \frac{\frac{\gamma_m}{C_{m+1}} + \gamma_m^2 \tanh \beta}{\gamma_m + \frac{1}{C_{m+1}} \tanh \beta}$$

and therefore:

$$C_m = \frac{\gamma_m + \frac{1}{C_{m+1}} \tanh \beta}{\frac{\gamma_m}{C_{m+1}} + \gamma_m^2 \tanh \beta} \quad \left| \text{Expand with } C_{m+1} \right.$$

$$C_m = \frac{\gamma_m C_{m+1} + \tanh(\gamma_m d_m)}{\gamma_m (1 + \gamma_m C_{m+1} \tanh(\gamma_m d_m))} \quad (5.20)$$

This is the *recursion formula by Wait (1953) and Lipskaya (1954)*. It is of enormous importance and appears, e.g., implicitly in each inversion algorithm for solving 1D-problems! In this version it applies to finite wave numbers  $\nu$  with

$$\gamma_m = \sqrt{i\omega\mu_0\sigma_m + \nu^2} \quad .$$

For „plain waves“ ( $\nu \rightarrow 0$ ) the usual impedance  $Z = i\omega C$  is obtained again from (5.20). However, for great values of the argument  $\gamma_m d_m$  there are numerical problems arising from the calculation of the tanh-function and one better programs

$$C_m = \frac{1 - r_m \exp(-2\gamma_m d_m)}{\gamma_m (1 + r_m \exp(-2\gamma_m d_m))} \quad (5.20a)$$

with

$$r_m = \frac{1 - \gamma_m C_{m+1}}{1 + \gamma_m C_{m+1}} \quad \text{and due to} \quad \tanh \beta = \frac{e^\beta - e^{-\beta}}{e^\beta + e^{-\beta}} = \frac{1 - e^{-2\beta}}{1 + e^{-2\beta}} \quad .$$

In practice,  $C_M = 1/\gamma_M$  is determined first and then we proceed from layer to layer up to the surface<sup>6</sup>. In the case of a homogeneous half space the complex penetration depth  $C_m = 1/\gamma_m G_m^-$  becomes  $C = 1/\gamma$  again.

If one determines a resistivity at the surface  $z = +0$ , then:

$$\rho_a(T) = \frac{\mu_0}{\omega} |Z|^2 = 0.2 T |Z|^2$$

is an *apparent* resistivity<sup>7</sup>. It is usually plotted double logarithmically as function of period:  $\log_{10} \rho_a(\log_{10} T)$ . Note that in Russian literature the version  $\log_{10} \rho_a(\log_{10} \sqrt{T})$  is often found.

For the 2-layer case eq. (5.20) with  $C_1 = C$ ,  $C_2 = 1/\gamma_2$  and  $h$  as the depth of the layer results in:

$$C = \frac{1}{\gamma_1} \frac{\frac{\gamma_1}{\gamma_2} + \tanh(\gamma_1 h)}{1 + \frac{\gamma_1}{\gamma_2} + \tanh(\gamma_1 h)} \quad (5.21a)$$

For plain waves the transfer function  $C$  is determined by the ratio

<sup>6</sup> The function  $C$  (or  $Z$ ) at the *surface*  $z_m$  of a layer is determined only by the conductivity distribution *underneath* depth  $z \geq z_m$ . From this results particularly the possible application of MT on the sea bottom!

<sup>7</sup> The algorithm of DC-geoelectrics contains an analogue recursion formula for the resistivity transform, which is transferred by a Hankel transformation in apparent resistivities. This is similar for transient electromagnetics.



$$\frac{k_1}{k_2} = \sqrt{\frac{\sigma_1}{\sigma_2}} \quad .$$

In the very similar recursion formula of geoelectrics (see later chapters) there is a direct dependency of the conductivity contrast  $\sigma_1/\sigma_2$ . From this follows, that MT  $\rho_a$ -curves are always very “smooth“ and shows a weaker sensitivity for conductivity contrasts. This disadvantage of the MT-method is compensated by the information obtained from the phase.

If the identity is used for further evaluation of (5.21a):

$$\tanh(x + y) = \frac{\tanh x + \tanh y}{1 + \tanh x \tanh y} \quad ,$$

with  $x = \tanh^{-1}(\gamma_1/\gamma_2)$  the formulation, that is often found in textbooks, is obtained:

$$C = \frac{1}{\gamma_1} R = \frac{1}{\gamma_1} \tanh(x + \gamma_1 h) = \frac{1}{\gamma_1} \tanh\left[\gamma_1 h + \tanh^{-1}\left(\frac{\gamma_1}{\gamma_2}\right)\right] \quad ; \quad (5.21b)$$

for multi-layer cases this has to be completed accordingly. R is a correction term for the difference to a homogeneous half space.

For the TM mode the solution is analogue to the TE case, but now with the following approach:

$$\frac{B_x}{E_y} = \frac{\mu_0 \sigma_m}{\gamma_m G(z)} \quad .$$

The continuity condition has to be expanded:

$$\gamma_m G_m^+ \rho_m = \gamma_{m+1} G_{m+1}^- \rho_m \quad .$$

The same calculation as before leads to the recursion formula for the TM-mode:

$$C_m = \frac{C_{m+1} \gamma_m + \frac{\sigma_m}{\sigma_{m+1}} \tanh(\gamma_m d_m)}{\gamma_m \left( \frac{\sigma_m}{\sigma_{m+1}} + C_{m+1} \gamma_m \tanh(\gamma_m d_m) \right)} \quad . \quad (5.22)$$

The verification of the TM-mode can only occur by measuring  $E_+ = E_z (+0)$  and  $E_- = E_z (-0)$  which causes great problems in practice.

Due to the continuity of the current density  $\sigma_+ E_+ = \sigma_- E_-$  the ratio of the fields is:

$$\frac{E_-}{E_+} = \frac{\sigma_+}{\sigma_-} > 10^{-10} \quad ,$$

i.e. the currents are also in the dimension of the displacement currents and therefore they can be ignored. This does not apply any more for a direct connection of current (CSAMT).

The recursion formulae for both modes can easily be combined to:

$$C_m = \frac{C_{m+1} \gamma_m + \Gamma_m \tanh(\gamma_m d_m)}{\gamma_m (\Gamma_m + C_{m+1} \gamma_m \tanh(\gamma_m d_m))} \quad . \quad (5.23)$$

with  $\Gamma_m = \frac{\sigma_m}{\sigma_{m+1}}$  for TM- and  $\Gamma_m = 1$  for TE-mode.

For the simple 2-layer case concise master curves for  $\rho_a(T)$  and  $\phi(T)$  can be drawn (see Fig. 5.9a). The model response of 3-layer cases is shown in Fig. (5.9b) for a period range that corresponds to the instruments used at FUB. It becomes obvious that magnetotellurics is

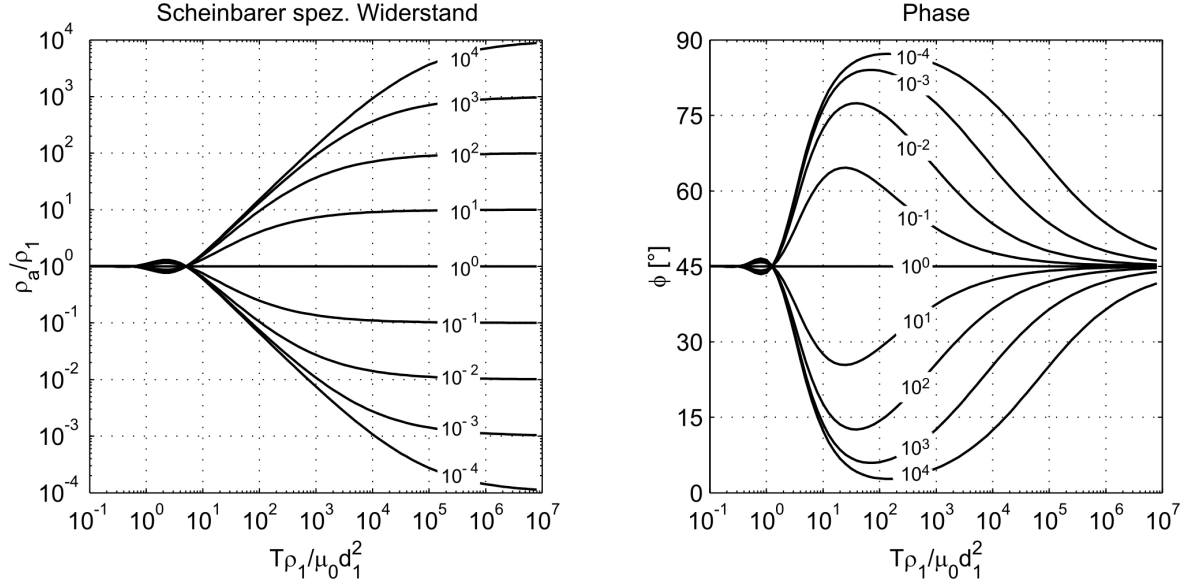


Fig. 5.9a: 2-layer master curves in magnetotellurics:  $\rho_a/\rho_1$  as a function of the ratio of skin depth and thickness of the 1st layer (without a  $\pi$  factor).

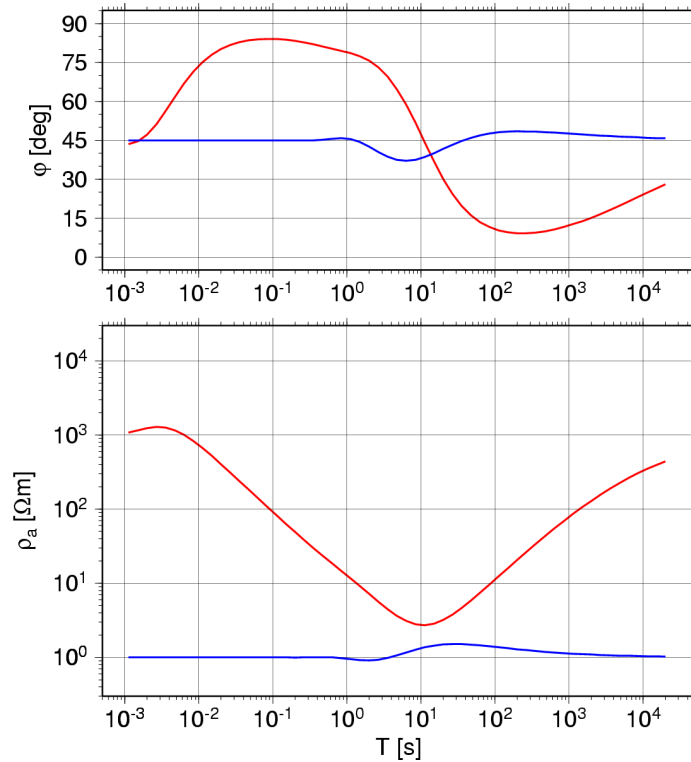


Fig. 5.9b: Response of 2 three-layer models. Red:  $\rho = (1000, 1, 1000) \Omega m$ , blue:  $\rho = (1, 1000, 1) \Omega m$ ; thickness of each layer is 1000 m. See also the Java script at: <http://userpage.fu-berlin.de/~mtag/mt1d/MT-Java.html>

primarily suitable to resolve good conductors<sup>8</sup>. Poor conductors are nearly transparent for electromagnetic waves.

#### 5.4 The magnetic field at the surface of a half space

The continuity of the horizontal fields has a very interesting consequence concerning the magnitude of the magnetic field at the boundary of the conductive (and layered) half space. The general solution of Helmholtz's equation

$$\nabla^2 \underline{B} - \gamma^2 \underline{B} = 0$$

is without loss of generality for one component:

$$B_{my} = a_m e^{-\gamma_m z} + b_m e^{+\gamma_m z} \quad (5.24)$$

with  $m = 0, 1$  in the air or in the earth, and with the propagation constant  $\gamma$  from chap. 2 of the field that was assumed to be quasi-homogeneous

$$\gamma = (k^2 - \kappa^2)^{1/2} = (i\omega\mu\sigma - \omega^2\mu\epsilon)^{1/2}.$$

Consequently, the wave numbers  $\gamma_m$  in the air/earth are:

$$\begin{aligned} \gamma_0 &= \omega(-\mu_0 \epsilon_0)^{1/2} \\ \gamma_1 &= (i\omega\mu_0\sigma_1 - \omega^2\mu_0\epsilon_1)^{1/2}, \end{aligned}$$

with  $\mu_1 = \mu_0$ , as usual. Now from Ampère's law  $\nabla \times \underline{B} = \mu(\sigma + i\omega\epsilon)\underline{E}$  follows:

$$E_{mx} = -\frac{1}{\mu(\sigma_m + i\omega\epsilon_m)} \frac{\partial B_{my}}{\partial z}$$

and the boundary conditions:

$$\begin{aligned} \frac{1}{i\omega\epsilon_0} \frac{\partial B_{0y}}{\partial z} &= \frac{1}{\sigma_1 + i\omega\epsilon_1} \frac{\partial B_{1y}}{\partial z} \quad \text{and} \\ B_{0y} &= B_{1y}. \end{aligned}$$

result from the continuity of the horizontal fields in  $z = 0$ .

If the fields from eq. (5.24) are calculated explicitly for air space and earth:

$$\begin{aligned} B_{0y} &= a_0 e^{-\gamma_0 z} + b_0 e^{\gamma_0 z} \\ B_{1y} &= a_1 e^{-\gamma_1 z}, \end{aligned}$$

we obtain for  $z = 0$ :

$$a_0 + b_0 = a_1 \quad \text{and} \quad (5.25a)$$

---

<sup>8</sup> The oscillations before the final rise/drop of the curves are due to destructive/constructive interference of the downgoing and the reflected wave from the interface. Spies & Eggers (1986) introduce another definition for the apparent resistivity, in which especially the oscillations do not appear. Also note that the resolution capability concerning highly resistive layers is different for controlled source methods.

$$\frac{\gamma_0}{i\omega\epsilon_0}(-a_0 + b_0) = \frac{-\gamma_1 a_1}{\sigma_1 + i\omega\epsilon_1} . \quad (5.25b)$$

The reflection coefficient  $b_0/a_0$  can be calculated as:

$$\frac{b_0}{a_0} = \frac{Z_0 - Z_1}{Z_0 + Z_1} .$$

Here  $Z_{1,2}$  denote the impedances with:

$$Z_0 = \frac{\mu_0}{i\omega\epsilon_0} \quad \text{and} \quad Z_1 = \frac{\mu_0}{\sigma_1 + i\omega\epsilon_1}$$

Considering the boundary condition (5.25a) and  $b_0/a_0 \approx 1$ , because  $Z_0 \gg Z_1$  we obtain for the field in the subsoil:

$$B_{1y}(z) = a_1 e^{-\gamma_1 z} = a_0 \left(1 + \frac{b_0}{a_0}\right) e^{-\gamma_1 z} \approx 2a_0 e^{-\gamma_1 z} .$$

and consequently in  $z = +0$

$$B_{1y}(+0) = 2a_0 . \quad (5.26a)$$

The magnetic field at the earth's surface is twice as large as the primary field. Therefore it does not contain any information about the conductivity of the subsoil! At first glance, this result is astonishing but it is in accordance with the boundary conditions because for  $z = -0$  we have:

$$B_{0y}(-0) = a_0 + b_0$$

and, since  $b_0 \approx a_0$  because of  $Z_0 \gg Z_1$ :

$$B_{0y}(-0) = 2a_0 . \quad (5.26b)$$

Consequently, the electrical field contains all information about the subsurface. However, if there are lateral conductivity anomalies, this does not hold anymore (see next chapter).

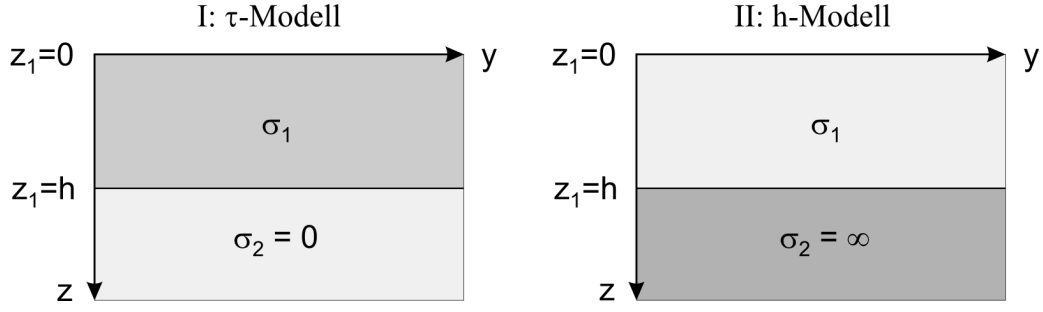
### 5.5 Extremal models for the 2-layer case

For a further understanding of  $\rho_a$ - and phase curves we confine ourselves to 2 extremal models for the 2-layer case (Fig. 5.10). In model I an isolator with  $\sigma_2 = 0$  is located underneath a well conducting cover of conductivity  $\sigma_1$  and thickness  $h$ . In model II the isolator is replaced by a perfect conductor of  $\sigma_2 = \infty$ .

As before for the 2 layer case Wait's formula for plain waves results in:

$$C(z=0) = C = C_1 = \frac{k_1 C_2 + \tanh(k_1 h)}{k_1 (1 + k_1 C_2 \tanh(k_1 h))} \quad \text{and with } C_2 = \frac{1}{k_2} :$$

$$C = \frac{\frac{k_1}{k_2} + \tanh(k_1 h)}{k_1 + \frac{k_1^2}{k_2} + \tanh(k_1 h)}$$

Fig. 5.10: Definition of  $\tau$ - and  $h$ -models.

With  $\sigma_2 \rightarrow 0$  goes  $k_2 \rightarrow 0$  (model I) and with  $\sigma_2 \rightarrow \infty$  goes  $k_2 \rightarrow \infty$  (model II):

$$C_I = \frac{1}{k_1} \coth(k_1 h) \quad \text{and} \quad C_{II} = \frac{1}{k_1} \tanh(k_1 h)$$

Now we analyze the response function for  $\omega \rightarrow 0$  or  $T \rightarrow \infty$ , respectively. A series expansion of  $\tanh x$  and  $\coth x$  yields to:

$$\coth x = \frac{1}{x} + \frac{x}{3} - \frac{x^3}{45} + \dots \quad \text{and} \quad \tanh x = x - \frac{x^3}{3} + \frac{2x^5}{15} - \dots$$

With respect to the first elements follows:

$$C_I = \frac{1}{k_1^2 h} = \frac{1}{i\omega\mu_0\sigma_1 h} = \frac{1}{i\omega\mu_0\tau_1} \quad \text{and} \quad C_{II} = \frac{1}{k_1} k_1 h = h \quad ,$$

consequently:

$$Z_I = \frac{1}{\mu_0\tau_1} \quad \text{and} \quad Z_{II} = i\omega h \quad (5.27)$$

In the first case the integrated conductivity of the covering is obtained directly from the impedance, while in the second case its thickness is obtained. This also explains the naming of the models.

For apparent resistivity and phase then applies:

$$\rho_{aI} = \frac{\mu_0}{\omega} \left| \frac{1}{\mu_0\tau_1} \right|^2 = T \cdot \text{const} \quad \text{and} \quad \phi_I = 0^\circ \quad , \quad (5.28a)$$

$$\rho_{aII} = \omega\mu_0 h^2 \quad \text{and} \quad \phi_{II} = 90^\circ \quad . \quad (5.28b)$$

At a double logarithmic notation of  $\rho_a(T)$  the following linear equations arise:

$$\log \rho_{aI} = \log T + \text{const} \quad (5.29a)$$

$$\log \rho_{aII} = \log \omega + \log(\mu_0 h^2) = \log\left(\frac{1}{T}\right) + \text{const} = -\log T + \text{const} \quad (5.29b)$$

In the  $\tau$ -model, the gradient of the straight line is 1, while it is  $-1$  in the  $h$ -model. *Therefore the increase of the  $\rho_a$ -curve will not exceed  $\pm 45^\circ$  even at an infinite resistivity contrast, and the phase is limited to the 1st quadrant.* As we will see later, this applies not only for the 1D-case, but also for the 2D-case (always in B-polarization and except for some exotic cases also

in E-polarization) and in most cases also for 3D-structures. Only for special structures (e.g. concentration of current flow in strongly bended conductors near the surface or in ocean bottom soundings near the continental slope) these limits for the sounding curves do not apply necessarily (see e.g. Egbert 1990, Weidelt 1996).

From the  $\rho_a$ -curves found in that way some parameters of the underground can be determined directly. In the  $\tau$ -model the conductance or integrated conductivity  $\tau_1$  of the covering(s) can be resolved over an isolating basement:

$$\tau_1 = \sqrt{\frac{T_p}{2\pi\mu_0\rho_a(T_p)}} \quad (5.30)$$

Here P is a point on the sounding curve with an increase of  $45^\circ$ . A case like that is, e.g., often given – of course only approximately – in sediment basins. If the real value of the conductivity  $\rho_B$  of the basement is known or assumed a correction term of  $(1/2\omega\mu_0\rho_B)^{1/2}$  to  $\tau_1$  from eq. (5.30) can be added (see Berdichevsky & Dimitriev 2002, p. 107).

In contrast to this, in the h-model, the thickness of the perfect conductor can directly be determined from the  $\rho_a$ -curve decreasing by  $-45^\circ$ :

$$h = \sqrt{\frac{T_p\rho_a(T_p)}{2\pi\mu_0}} \quad (5.31)$$

Here  $C_{II} = h \in \Re$  means that there is nearly no induction in the covering. A realization of this extremal model can be found, e.g., when studying aquifers under highly-resistive, dry sands of deserts or good conductors in the middle crust, which are often found in the region of Palaeozoic or Precambrian basements.

## 5.6 Thin sheets

If one layer (not necessarily the first one) has such a low thickness that a) for a given frequency the skin depth is much bigger than  $h$  (exactly  $h^2 \ll \delta^2$ ) and b) the inductive scale length  $C(h)$  of the subjacent layers is also much bigger than  $h$ , then there is  $E(z=h) \approx E(z=0)$ . This means that e.g. the electrical field remains constant, while the magnetic field jumps by a value that is proportional to the conductance of this layer:  $B(h) \approx B(0) - \mu\tau E(0)$ . To derivate this relation  $dE/dz$  is expanded into a Taylor series (see e.g. J.T. Weaver, Numerical in Modelling in EM Induction, in: Roy, Verma, Mallick (eds.): Deep Electromagnetic Exploration, Springer, 1999, pp. 331).

Mathematically such a “*thin sheet*” is idealized by a transition  $h \rightarrow 0$  with constant  $\tau$ . The thin sheet concept provides the basis for very effective modeling algorithms in 2 and 3 dimensions.

## 5.7 Resistivity-depth-transformations

So far we have seen how to get from the parameterization of the underground by forward- or modelling calculation a reply or response function  $C$  (or  $Z$ ). The determination of the underground parameters (conductivity and thickness of layers) that are obtained from the transfer functions  $C$  or  $Z$  are called inverse calculation or simply inversion. This will be

discussed in detail later. Here two methods of a heuristic inversion that describes a direct transformation of the measured  $\rho_a$  and phases as a function of the period to a resistivity-depth-model shall be derived first.

First we stick to the 2-layer case and permit a finite conductivity of the substratum in the  $h$ -model of the former chapter.  $\sigma_2$  is not  $= \infty$  any more, but considerably bigger than  $\sigma_1$ :  $\sigma_2 \gg \sigma_1$ . Then  $\phi \geq 45^\circ$  does always apply and:

$$k_1 \ll k_2, \quad \tanh(k_1 h) \approx k_1 h, \quad \delta_1 \gg \delta_2 \quad \text{due to} \quad \frac{1}{k} = \frac{\delta}{1+i} = \frac{\delta_2}{2}(1-i)$$

and consequently

$$C = \frac{\frac{k_1}{k_2} + k_1 h}{k_1 + \frac{k_1^2}{k_2} k_1 h} = \frac{k_1 \left( \frac{1}{k_2} + h \right)}{k_1 \left( 1 + \frac{k_1^2}{k_2} h \right)} = \frac{1}{k_2} + h = h + \frac{\delta_2}{2}(1-i)$$

$$C = \left( h + \frac{\delta_2}{2} \right) - \frac{\delta_2}{2} i = \text{Re } C + i \text{Im } C$$

By definition there is

$$z^* = \text{Re } C = h + \frac{\delta_2}{2} \quad ; \quad (5.32)$$

from the imaginary part follows:

$$\delta_2 = -2 \text{Im } C = \sqrt{\frac{2\rho_2}{\omega\mu_0}}, \quad \text{so} \quad \rho_2 = 2\omega\mu_0 |\text{Im } C|^2 \quad \text{and with} \quad \rho_a = \omega\mu_0 |C|^2$$

$$\rho_2 = 2\rho_a \frac{|\text{Im } C|^2}{|C|^2} = 2\rho_a \sin^2 \theta$$

or, if the common MT-phase  $\phi = \arg(Z)$  is used:

$$C = \frac{Z}{i\omega} = -\frac{i}{\omega} Z = e^r e^{-\pi/2} e^\phi, \quad \text{thus} \quad \theta = \phi - \frac{\pi}{2}.$$

Now a  $\rho^*$  is defined as:

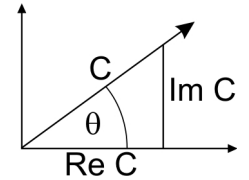
$$\rho^* := \rho_2 = 2\rho_a \cos^2 \phi \quad . \quad (5.33)$$

If we now determine  $z^*$  from  $\rho_a$ , from (5.32) results:

$$\frac{z^*}{C} = \frac{\text{Re } C}{C} = \cos \theta = \sin \phi \quad \text{and with} \quad C = \sqrt{\frac{\rho_a}{\omega\mu_0}}$$

$$z^* = \sqrt{\frac{\rho_a}{\omega\mu_0}} \sin \phi \quad (5.34)$$

$\sigma_2 \ll \sigma_1$  shall also apply in the  $\tau$ -model and consequently there will be  $\tau_1 = h \sigma_1$ ,  $h/\delta_1 \ll 1$  and  $\delta_1 \ll \delta_2$ , so always  $\phi \leq 45^\circ$ . From this follows:



$$C = \frac{\frac{k_1}{k_2} + k_1 h}{k_1 \left(1 + \frac{k_1^2}{k_2} h\right)} = \frac{\frac{1}{k_2}}{1 + \frac{k_1^2}{k_2} h} = \frac{\frac{\delta_2}{1+i}}{1 + i\omega\mu_0\sigma_1 h \frac{\delta_2}{1+i}} = \frac{\frac{\delta_2}{1+i}}{1 + i\omega\mu_0\tau_1 \frac{\delta_2}{1+i}} .$$

The admittance  $Y = 1/Z$  can be written in the following form:

$$Y = \frac{1}{i\omega C} = \frac{1}{i\omega} \frac{1 + i\omega\mu_0\tau_1 \frac{\delta_2}{1+i}}{\frac{\delta_2}{1+i}} = \frac{1-i}{\omega\delta_2} + \mu_0\tau_1 = \left(\mu_0\tau_1 + \frac{1}{\omega\delta_2}\right) - i\frac{1}{\omega\delta_2} = \text{Re } Y + i \text{Im } Y$$

$$\rightarrow \mu_0\tau_1 = \text{Re } Y + \text{Im } Y$$

$$\rightarrow \delta_2 = -\frac{1}{\omega \text{Im } Y} = \sqrt{\frac{2}{\omega\mu_0} \frac{\rho_2}{|\text{Im } Y|^2}} \rightarrow \rho_2 = \frac{\mu_0}{2} \frac{1}{\omega |\text{Im } Y|^2} .$$

With  $\arg(Y) = -\phi = \theta$  and  $\rho_a = \mu_0\omega C^2 = \frac{\mu_0}{\omega} Z^2 = \frac{\mu_0}{\omega} \frac{1}{Y^2}$  follows:

$$\rho_2 = \frac{1}{2} \frac{\mu_0}{\omega} \frac{1}{|\text{Im } Y|^2} = \frac{1}{2} \rho_a \frac{|Y|^2}{|\text{Im } Y|^2} = \frac{1}{2} \rho_a \frac{1}{\sin^2 \phi} \quad \text{and}$$

$$\rho^* := \rho_2 = \frac{1}{2} \rho_a \frac{1}{\sin^2 \phi} \quad (5.35)$$

Consequently, the  $\rho^*$ - $z^*$ -transformation can be summarized as:

$$z^* = \sqrt{\frac{\rho_a}{\omega\mu_0}} \sin \phi$$

$$\rho^* = \begin{cases} 2\rho_a \cos^2 \phi & \phi \geq 45^\circ \\ \frac{\rho_a}{2 \sin^2 \phi} & \phi \leq 45^\circ \end{cases} . \quad (5.36)$$

In this form it is only derived for 2-layer cases, but it is also commonly used for multi-layer cases. Fig. 5.11 shows two examples for 3-layer cases, the upper figure shows an intermediate layer of high conductivity, the lower figure one of poor conductivity. The figure reveals once more the better resolution of good conductors. For a homogeneous half space  $z^*$  is equal to the half of the skin depth (because  $\rho = \rho_a$ ,  $\phi = 45^\circ$  and  $\sin \phi = 2^{-1/2}$ ):

$$z^* = \sqrt{\frac{\rho_a}{\omega\mu_0}} \sqrt{\frac{1}{2}} = \sqrt{\frac{2\rho_a}{4\omega\mu_0}} = \frac{1}{2} \delta \quad (5.37)$$

Another resistivity-depth-transformation that is often used is the one named after *Niblett and Bostick*. Here the parameters of the underground are determined from the  $\rho_a$ - and phase curves in a variant, that is similar to  $\rho^*$ - $z^*$ . In another variant the increase of the  $\log \rho_a(\log T)$ -curve is used:



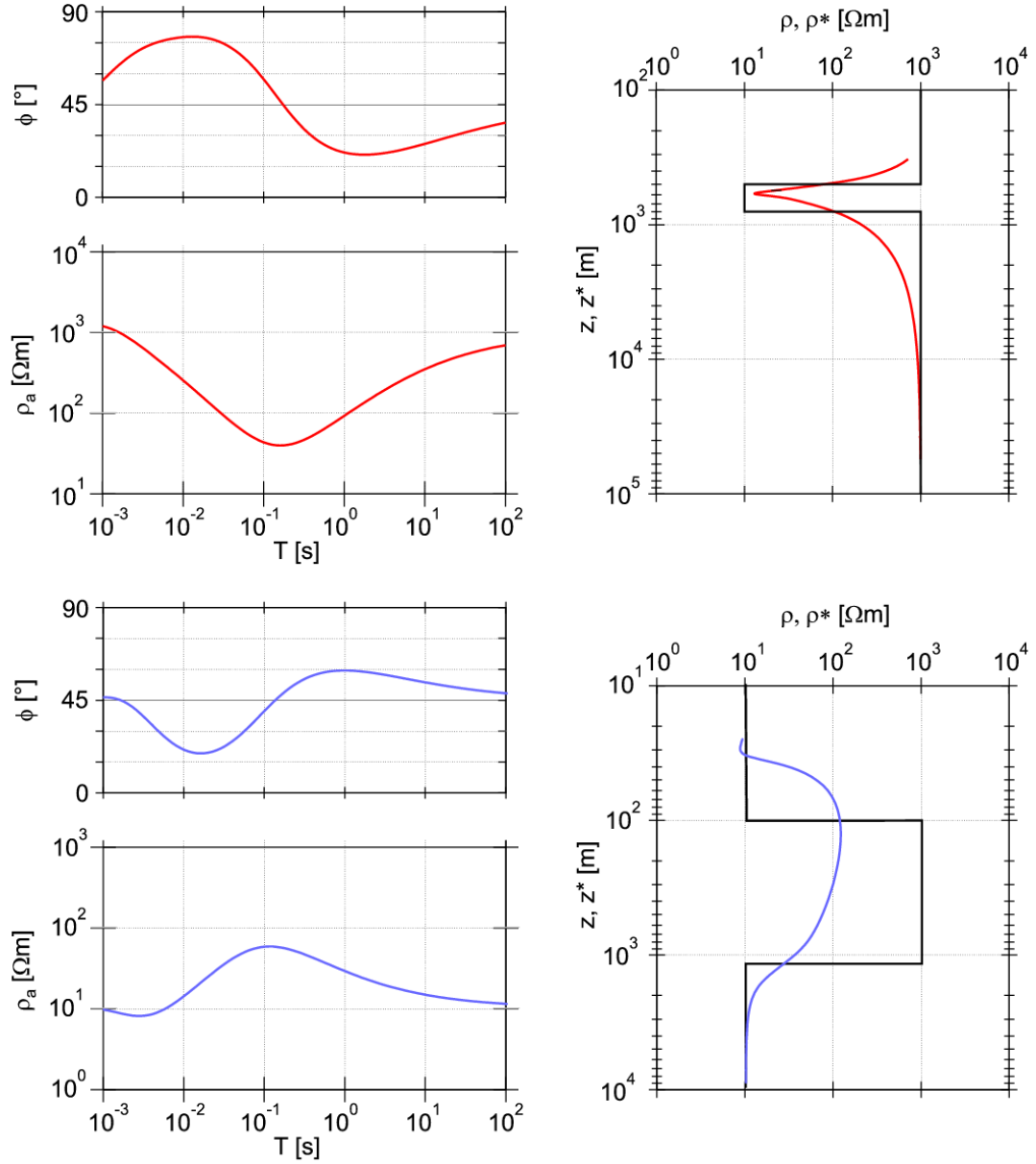


Fig. 5.11: Two examples for the  $\rho^*$ - $z^*$ -transformation. In both cases left:  $\rho_a(T)$  and  $\phi(T)$ , right: model and  $\rho^*(z^*)$ .

$$m := \frac{d \log \rho_a(T)}{\log T} \quad \text{with } |m| \leq 1.$$

As before, we look at the two h- and  $\tau$ -limiting models. In the h-model there is

$$\rho_a(T) = \frac{2\pi\mu_0 h^2}{T} \quad (\text{which follows from } \rho_a = \mu_0 \omega C^2 \text{ and } C = h)$$

with an increase  $m = -1$ ; in the  $\tau$ -model there is

$$\rho_a(T) = \frac{T}{2\pi\mu_0 \tau^2} \quad (\text{which follows from } C = \frac{1}{i\omega\mu_0 \tau})$$

with an increase of  $m = 1$ . Each pair of values  $(\rho_a, T)$  can be assigned to a pair of values  $(\tau, h)$ .

If  $\tilde{\rho}(z)$  is, as  $\rho^*(z)$  before, an approximation to the real resistivity distribution  $\rho(z)$ , we obtain:

$$\tilde{\tau} = \int_0^h \frac{dz}{\tilde{\rho}(z)},$$

or, what is equivalent:

$$\begin{aligned} \tilde{\rho}(h) &= \frac{dh}{d\tilde{\tau}} = \frac{h}{\tilde{\tau}} \frac{2dh/h}{2d\tilde{\tau}/\tilde{\tau}} = \rho_a \frac{d \log h^2}{d \log \tilde{\tau}^2} = \rho_a \frac{d \log T + d \log \rho_a}{d \log T - d \log \rho_a} \\ \tilde{\rho}(h) &= \rho_a \frac{1+m}{1-m} \end{aligned} \quad (5.38a)$$

and

$$\tilde{h} = \sqrt{\frac{\rho_a T}{2\pi\mu_0}} \quad (5.38b)$$

for the Niblett-Bostick-transformation.

Apparent resistivity and phase are connected by a *Kramers-Kronig dispersion relation* now:

$$\phi(\omega_0) = \frac{\pi}{4} - \frac{\omega}{\pi} \text{P} \int_0^\infty \frac{1}{\omega^2 - \omega_0^2} \log \frac{\rho_a(\omega)}{\rho_0} d\omega$$

with

$$\text{P} \int \dots$$

as Cauchy's principal value integral<sup>9</sup>. From this follows the relation

$$\phi \approx \frac{\pi}{4} (1+m)$$

and we obtain a derivation, that comprises the phase of the impedance:

$$\tilde{\rho}(\tilde{h}) = \rho_a \left( \frac{\pi}{2\phi} - 1 \right) \quad (5.38c)$$

Even though it was defined for a 2-layer extremal model the Niblett-Bostick-transformation as well as the  $\rho^*$ - $z^*$ -transformation is also used for n-layer cases in general.

## 5.8 Conductivity distribution from spatial gradients of the magnetic field

If there are small (and measurable) spatial variations of the source field, but in a way, that  $v|C| \ll 1$  is still valid, the conductivity distribution can also be derived from the gradient of the horizontal fields. If one differentiates  $E_y = -ZB_x$  with respect to  $\partial y$  and  $E_x = -ZB_y$  with respect to  $\partial x$  and takes the difference

<sup>9</sup> A derivation of this ratio of the relationship between real and imaginary part of  $C$  can be found in the appendix or, e.g., in Weaver (1994).

$$\frac{\partial E_y}{\partial x} - \frac{\partial E_x}{\partial y} = -Z \left[ \frac{\partial B_x}{\partial x} + \frac{\partial B_y}{\partial y} \right] ,$$

and inserts the 2nd Maxwell equation  $\nabla \times \underline{E} = -i\omega \underline{B}$  :

$$\frac{\partial E_y}{\partial x} - \frac{\partial E_x}{\partial y} = -i\omega B_z ,$$

the result is:

$$Z = Z(\omega) = \frac{i\omega B_z}{\frac{\partial B_x}{\partial x} + \frac{\partial B_y}{\partial y}} . \quad (5.39)$$

With (5.39) we can obtain the conductivity contribution from the ratio of the vertical component to the horizontal gradients of the magnetic field. This method is usually called "*horizontal gradient method*" or sometimes "*magneto-variational sounding or profiling (MVS or MVP)*" and requires the (preferably) simultaneous registration of field variations at (preferably) many stations on a profile or grid. In practice, the horizontal variations of fields for lateral inhomogeneous  $\sigma(x,y,z)$  are more important. Here the fields at moving stations are correlated with normal fields (above a one-dimensional underground) or with fields of reference stations. This is also called MVP.

In the "*vertical gradient method*" the skin effect can directly be observed – for example via simultaneous registration at the earth's surface and in a drill hole or in a mine. However, this requires the knowledge of the conductivity  $\sigma_0$  between the measuring points in the depth and at the surface. This has to be extracted by other methods. From Ampère's law follows directly:

$$\frac{\partial B_x}{\partial z} = \mu_0 \sigma_0 E_y = -\mu_0 \sigma_0 Z B_x \quad \text{and} \quad -\frac{\partial B_y}{\partial z} = \mu_0 \sigma_0 E_x = \mu_0 \sigma_0 Z B_y ,$$

consequently

$$Z = Z(\omega) = -\frac{\partial B_x / \partial z}{\mu_0 \sigma_0 B_x} \quad \text{and} \quad Z = Z(\omega) = -\frac{\partial B_y / \partial z}{\mu_0 \sigma_0 B_y} . \quad (5.40)$$

## 6 Two- and three-dimensional conductivity distribution in MT

### 6.1 General notes

Now we look at lateral variations of conductivity,  $\sigma = \sigma(x, z)$  shall be a function of  $x$  and  $z$  only and not variable in  $y$ -direction (fig. 6.1). Consequently the fields  $F$  in chapter 2 are also just a function of  $x$  and  $z$  (and of the frequency  $\omega$  as well, of course) and in Maxwell's equations the derivatives with respect to  $y$  vanish:  $\partial F / \partial y = 0$ .

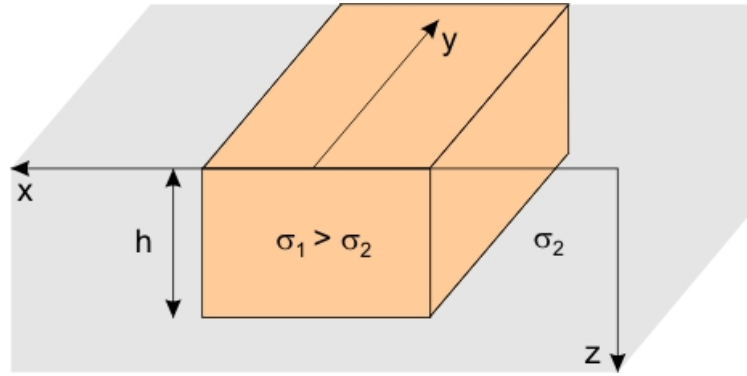


Fig. 6.1: Structure of a rift spread infinitely in  $y$ -direction as an idealized 2-dimensional anomaly.

As a result from Maxwell's equations two decoupled system of equations are obtained:

E-polarization (TE mode)

$$\frac{\partial B_x}{\partial z} - \frac{\partial B_z}{\partial x} = \mu_0 \sigma E_y \quad (6.1a)$$

$$\frac{\partial E_y}{\partial x} = -\frac{\partial B_z}{\partial t} \quad (6.1b)$$

$$\frac{\partial E_y}{\partial z} = \frac{\partial B_x}{\partial t} \quad (6.1c)$$

B-polarization (TM mode)

$$\frac{\partial B_y}{\partial x} = \mu_0 \sigma E_z \quad (6.1d)$$

$$\frac{\partial B_y}{\partial z} = -\mu_0 \sigma E_x \quad (6.1e)$$

$$\frac{\partial E_x}{\partial z} - \frac{\partial E_z}{\partial x} = -\frac{\partial B_y}{\partial t} \quad (6.1f)$$

The equations on the left contain only one horizontal E-field component that is parallel to the conductivity contrast ( $E_y$ ), also known as *E-polarization*. The horizontal magnetic field  $B_x$  is vertical to the boundary *and in this mode there does exist a vertical magnetic field  $B_z$* . On the right hand side the case of *B-polarization* is described: the horizontal magnetic field  $B_y$  oscillates parallel to the conductivity contrast,  $E_x$  is perpendicular to the boundary and *in this mode a vertical electrical field  $E_z$  does exist*.<sup>1</sup>

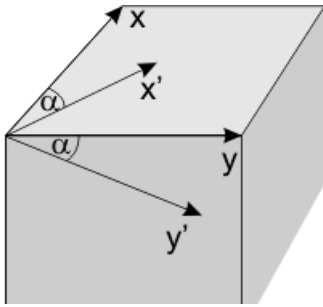
Up to now the relation between the horizontal magnetic and electrical components was a scalar quantity, the impedance  $Z$ . It now becomes a tensor  $\underline{Z}$  and the defining equation is extended to:

<sup>1</sup> In this manuscript the other common terms TE and TM mode (tangential electrical or magnetic) are mainly used for the polarization of the *source field*. In B-polarization there is no vertical current flowing through the boundary ground/air, the level in which the measurements are conducted, and  $\partial B_y / \partial x = 0$ . This is different in Offshore-MT at the bottom of the sea where there are also vertical currents and  $B_y$  varies with  $x$ .

$$\underline{E}_h = \underline{Z} \underline{B}_h \quad \text{or} \quad \begin{pmatrix} E_x \\ E_y \end{pmatrix} = \begin{pmatrix} Z_{xx} & Z_{xy} \\ Z_{yx} & Z_{yy} \end{pmatrix} \begin{pmatrix} B_x \\ B_y \end{pmatrix} . \quad (6.2a,b)$$

If the conductivity anomaly really strikes N/S or E/W, the elements  $Z_{xx}$  and  $Z_{yy}$  are 0 and from the minor diagonal two apparent resistivities  $\rho_{axy}$ ,  $\rho_{ayx}$  and phases  $\phi_{xy}$ ,  $\phi_{yx}$  are obtained. If  $\underline{Z}$  degenerates into a one-dimensional impedance then  $Z_{xy} = -Z_{yx}$  again. However, in the general two-dimensional case,  $|Z_{xy}| \neq |Z_{yx}|$  applies.

If the strike angle  $\alpha$  of the anomaly is not  $0^\circ$  or  $90^\circ$  the fields and with them the impedance tensor can be rotated so that the elements of the main diagonal vanish:



$$\underline{E}' = \underline{R} \underline{E} \quad , \quad \underline{B}' = \underline{R} \underline{B} \quad \text{and} \quad (6.3a)$$

$$\underline{Z}' = \underline{R} \underline{Z} \underline{R}^T \quad \text{with } \underline{R} = \text{matrix of rotation:} \quad (6.3b)$$

$$\underline{R} = \begin{pmatrix} \cos \alpha & \sin \alpha \\ -\sin \alpha & \cos \alpha \end{pmatrix} \quad \text{with } \det \underline{R} = 1 . \quad (6.3c)$$

Here the superscript T indicates the transpose. Determining this strike angle is one of the most difficult problems in current magnetotelluric research as will be shown later.

In practice a "Tensor MT measurement" is always conducted in which all the horizontal components of  $\underline{E}$  and  $\underline{B}$  are measured to take account of lateral conductivity contrasts. A scalar MT measurement, that comprises only the measurement of one horizontal magnetic field and one perpendicular telluric field component, is inadequate in nearly every case! However, in the VLF or RMT methods this condition leads to practical difficulties, which will be shown later.

The sensitivity described in the equations (6.2, 6.3) regarding lateral structures is one of the main advantages of the magnetotelluric method, at least in theory. By measuring the horizontal components of  $\underline{E}$  and  $\underline{B}$  *at only one point* the strike direction of an anomaly can be determined.

In practice, however,  $Z_{xx}'$ ,  $Z_{yy}'$  will never vanish exactly; for this reason minimization of the elements of the main diagonal or the maximization of the elements of the minor diagonal is often regarded as sufficient:

$$|Z_{xx}'|^2 + |Z_{yy}'|^2 = \text{Min!} \Leftrightarrow |Z_{xy}'|^2 + |Z_{yx}'|^2 = \text{Max!} . \quad (6.4)$$

Now there are several methods to determine the "optimum" strike angle. For the moment, only the method according to Swift (1967) shall be mentioned here<sup>2</sup>.

$$\frac{\partial}{\partial \alpha} \left( |Z_{xx}(\alpha)|^2 + |Z_{yy}(\alpha)|^2 \right) = \text{Min} \rightarrow \alpha_s = \frac{1}{4} \arctan \left\{ \frac{2 \operatorname{Re} \left( (Z_{xx} - Z_{yy})^* (Z_{xy} - Z_{yx}) \right)}{|Z_{xx} - Z_{yy}|^2 - |Z_{xy} + Z_{yx}|^2} \right\} . \quad (6.5)$$

<sup>2</sup> The measurements are always carried out in a coordinate system that is set up to magnetic north. If the strike angle is transferred into a geographic map the declination has to be considered, if necessary.

As we'll see later, this *Swift angle* often reflects only the influence of inhomogeneities near the surface and is thus of limited use.

There are several invariants against transformation of coordinates:

$$\begin{aligned} I_1 &= Z_{xx}Z_{yy} - Z_{xy}Z_{yx} = Z_{\text{eff}}^2 = Z_{\text{det}}^2 \\ I_2 &= Z_{xx} + Z_{yy} \\ I_3 &= Z_{xy} - Z_{yx} = 2Z_{\text{ave}} \end{aligned} \quad (6.6)$$

Sometimes average  $\rho_a$ - or  $\phi$ -curves are calculated from the invariants  $Z_{\text{det}}$  and  $Z_{\text{ave}}$  (the latter is also known as *Berdichevsky invariant*). It has to be pointed out already here that the information obtained with these invariants might be misleading.

The *skew* or *skewness* is introduced as a measure for two-dimensionality:

$$S = \frac{|I_2|}{|I_3|} = \frac{|Z_{xx} + Z_{yy}|}{|Z_{xy} - Z_{yx}|} . \quad (6.7)$$

It vanishes exactly for 1-dimensional or 2-dimensional relations (numerator = 0). It is disputed and it largely depends on the individual case up to which value  $S$  the subsoil can be graded as two-dimensional. Often  $S = 0.3$  is assumed to be the threshold value, but note that this means that 30% of the data cannot be explained by a two-dimensional approach!

The relation obtained from the minor diagonal impedances is often called *anisotropy coefficient*, a term that is a bit ambiguous:

$$A = \left| \frac{Z'_{xy}}{Z'_{yx}} \right| \quad (6.7).$$

An anomaly is defined as electromagnetically effective, i.e., it influences the transfer function at a certain measuring point on the surface of the earth, if it is - for a given frequency - within the induction space or -volume that is formed by a semicircle<sup>3</sup> around the station with radius  $r = |C|$  (fig. 6.2). Of course, there is certain arbitrariness in this. One could also choose, e.g.,  $r = \delta$  as radius of influence (see later).

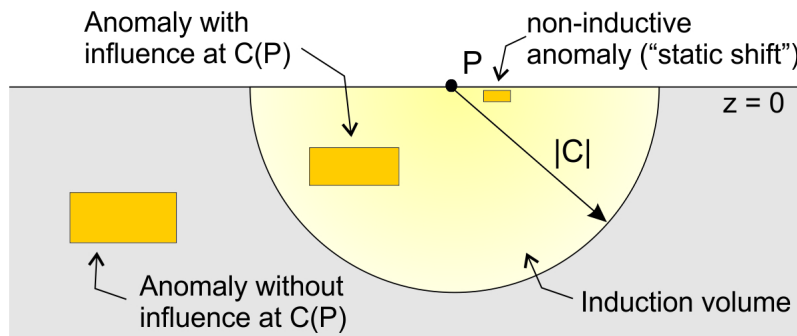


Fig. 6.2: Definition of the induction space at a given frequency.

<sup>3</sup> Of course, a semi-sphere applies only if the host medium is homogenous. In the case of a layered structure this volume becomes more complicated, correspondingly.

## 6.2 Further examination of the B- and E-polarization

To understand the behavior of fields and transfer functions at conductivity boundaries we refer back to our considerations concerning boundary conditions in chapter 2. At the boundary every magnetic field, the transversal current density and the longitudinal E-field are continuous while the longitudinal current density and the transversal E-field are discontinuous. Consequently, the transfer functions and with them  $\rho_a$  and phase will show a continuous transient behavior in E-polarization, but a discontinuous one in B-polarization.

For B-polarization we first look at two quarter spaces with conductivities  $\sigma_1$  and  $\sigma_2$  (Fig. 6.3). For the *normal fields* far away from the conductivity boundary ( $x \gg \delta_1, \delta_2$ ) applies:

$$J_{1x}(z) = \sigma_1 E_{1x}(z) \quad \text{or} \quad J_{2x}(z) = \sigma_2 E_{2x}(z)$$

On the surface of the earth we normalize each magnetic field  $H_{1y}(0)$  and  $H_{2y}(0)$ :

$$\begin{aligned} \frac{J_{1x}(z)}{H_{1y}(0)} &= \frac{\sigma_1 E_{1x}(z)}{H_{1y}(0)} & \frac{J_{2x}(z)}{H_{2y}(0)} &= \frac{\sigma_2 E_{2x}(z)}{H_{2y}(0)} \\ &= \sigma_1 \left( \frac{i\omega\mu_0}{\sigma_1} \right)^{1/2} e^{-ik_1 z} & &= \sigma_2 \left( \frac{i\omega\mu_0}{\sigma_2} \right)^{1/2} e^{-ik_2 z} \\ &= (1+i) \frac{1}{\delta_1} e^{-z/\delta_1} e^{-iz/\delta_1} & &= (1+i) \frac{1}{\delta_2} e^{-z/\delta_2} e^{-iz/\delta_2} \end{aligned}$$

Here

$$\zeta = \frac{E_x(0)}{H_y(0)} = \frac{\mu_0 \omega}{k}$$

was used.

Continuity or better preservation of the total current requires:

$$\int_0^\infty J_{1x}(z) dz = \int_0^\infty J_{2x}(z) dz \quad (\text{with } J \text{ as modified current density for } y = 1) \quad ,$$

consequently with Ampère's law it follows:

$$\oint_C H_{1y} d\ell = I_1 = \int_0^\infty J_{1x}(z) dz \quad \text{or} \quad \oint_C H_{2y} d\ell = I_2 = I_1 = \int_0^\infty J_{2x}(z) dz \quad .$$

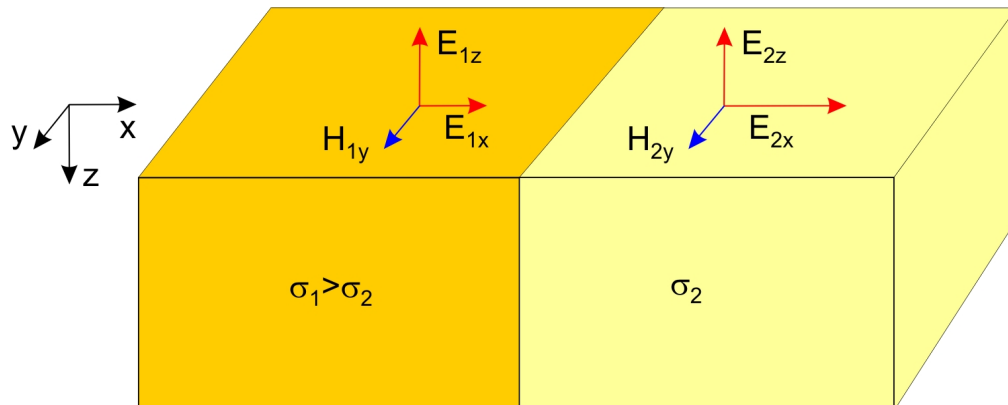


Fig. 6.3: Field quantities in B-polarization for 2 quarter spaces.

The consequence is  $H_{1y} = H_{2y}$ . As in the one-dimensional case, the magnetic field does not contain any information about the subsurface. This is different for the telluric field: Due to

$$E_{1x} = \zeta_1 H_{1y} \quad , \quad E_{2x} = \zeta_2 H_{2y} \quad ,$$

at the boundary layer, it jumps by the value of the resistivity ratio, which also results from the continuity of current density:

$$J_x = \sigma_1 E_{1x} = \sigma_1 E_{2x} \quad , \quad \text{thus}$$

$$\frac{E_{1x}}{E_{2x}} = \frac{\sigma_2}{\sigma_1} = \frac{\rho_1}{\rho_2} \quad .$$

In analogy to a parallel-plate capacitor, in B-polarization there are charges induced on the boundary layers which influence the local E-field in a way that the current density remains continuous (fig. 6.4).

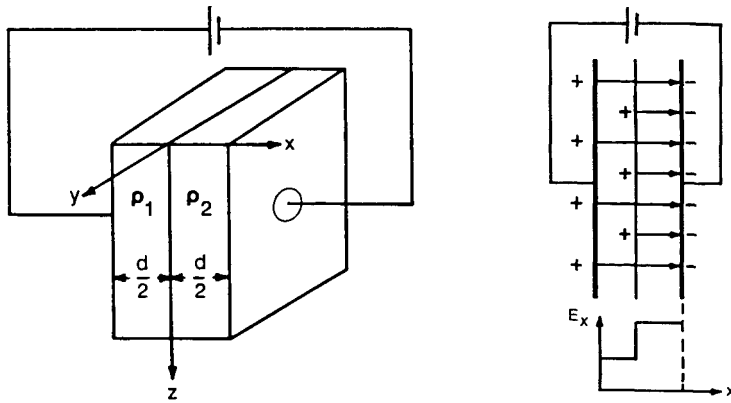


Fig. 6.4: Left: Analogy of B-polarization to a parallel-plate capacitor, right: charges and lines of field strength.

B-polarization is particularly important for small anomalies near the surface which are too small to have an inductive influence (i.e., on the phase). However, here the charging effect at the boundary layers leads to an upward or downward scaling of the electrical field and consequently of the apparent resistivities. The scaling is proportional to the resistivity contrast. This very important effect usually remains hidden because the perturbing elements causing this effect are unknown if detailed, e.g., a DC geoelectric or TEM, surface mapping around the measuring point is not carried out. The effect is called *static shift or static distortion*. From a very small period in which the anomaly is still inductively effective, it results in a parallel shift of the  $\rho_a$ -curves up to period  $T \rightarrow \infty$  (i.e. DC) while the phase remains unaffected<sup>4</sup>.

This effect is scale-invariant as it does not disappear even if the sounding frequency is raised into the AMT-domain. The dimension of an anomalous body always has to be considered with regard to sounding frequency and therefore the induction volume: what shows up as a real induction anomaly at high frequencies causes a static shift at longer periods.

<sup>4</sup> Consequently, the only solution to modeling conductivity anomalies is: The larger weight has to be laid on the fit of model response to the measured phases; for the  $\rho_a$ -values it might be sufficient to reproduce the *shape* of the curves.



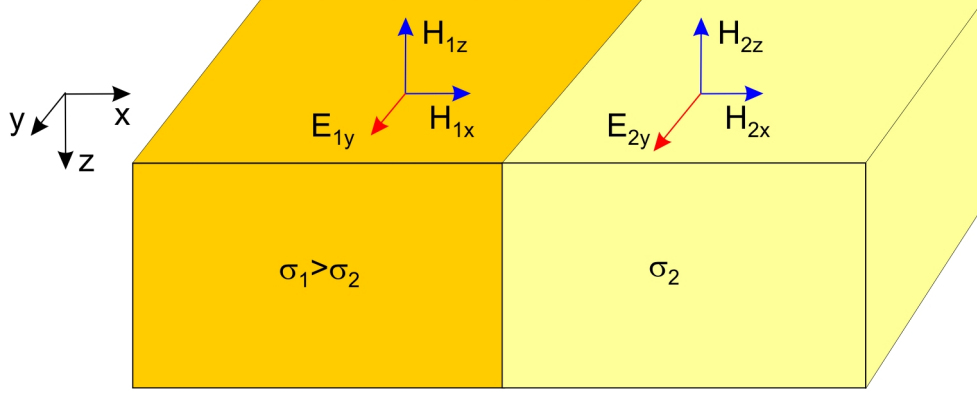


Fig. 6.5: Field quantities in the E-polarization for 2 quarter spaces.

In E-polarization (fig. 6.5) applies:  $E_y$ ,  $H_x$  are continuous,  $J_y$  is discontinuous and for  $x \gg d$ , i.e., far away from the conductivity boundary:

$$\begin{aligned} |E_{1y}| &= H_{1x} (\mu_0 \omega \rho_1)^{1/2} e^{z/\delta_1} = H_{0x} (\mu_0 \omega \rho_1)^{1/2} e^{z/\delta_1} \\ |E_{2y}| &= H_{0x} (\mu_0 \omega \rho_2)^{1/2} e^{z/\delta_2} \end{aligned}$$

with  $H_{0x}$  as surface field. For the current densities then applies:

$$\begin{aligned} |J_{1y}| &= \sigma_1 E_{1y} = H_{0x} (\mu_0 \omega \sigma_1)^{1/2} e^{z/\delta_1} \\ |J_{2y}| &= \sigma_2 E_{2y} = H_{0x} (\mu_0 \omega \sigma_2)^{1/2} e^{z/\delta_2} . \end{aligned}$$

At the boundary the current density jumps (see. Fig. 6.6, above) and shows a characteristic overshoot while the E-field is continuous (Fig. 6.6, middle)<sup>5</sup>.

The vertical and horizontal magnetic fields are applied to fig. 6.6 (below), finally, in fig. 6.7 the behavior of the real and imaginary parts are marked.

In practice there is often no unique strike of regional anomalies. For this reason the transfer functions in B- and E-polarization cannot be separated easily because of the static effects shown above. The distortion is described by a real-valued matrix  $\underline{\underline{D}}$  that gives the measured impedance  $\underline{\underline{Z}}$  when multiplied with the (ideal) regional impedance  $\underline{\underline{Z}}_r$ :

$$\underline{\underline{Z}} = \underline{\underline{D}} \underline{\underline{Z}}_r \quad \text{or} \quad \begin{pmatrix} Z_{xx} & Z_{xy} \\ Z_{yx} & Z_{yy} \end{pmatrix} = \begin{pmatrix} D_{11} & D_{12} \\ D_{21} & D_{22} \end{pmatrix} \begin{pmatrix} 0 & Z_{r1} \\ Z_{r2} & 0 \end{pmatrix} , \quad (6.9)$$

and an additional multiplication with a rotation matrix  $\underline{\underline{R}}$ , if necessary. For further information on distortion analysis, see later.

<sup>5</sup> This overshoot can be observed in the E-field of the B-polarization. For this reason the  $\rho_a$ - and phase curves also show this overshoot in a continuous B-field. These figures are taken from McNeill & Labson (1991).

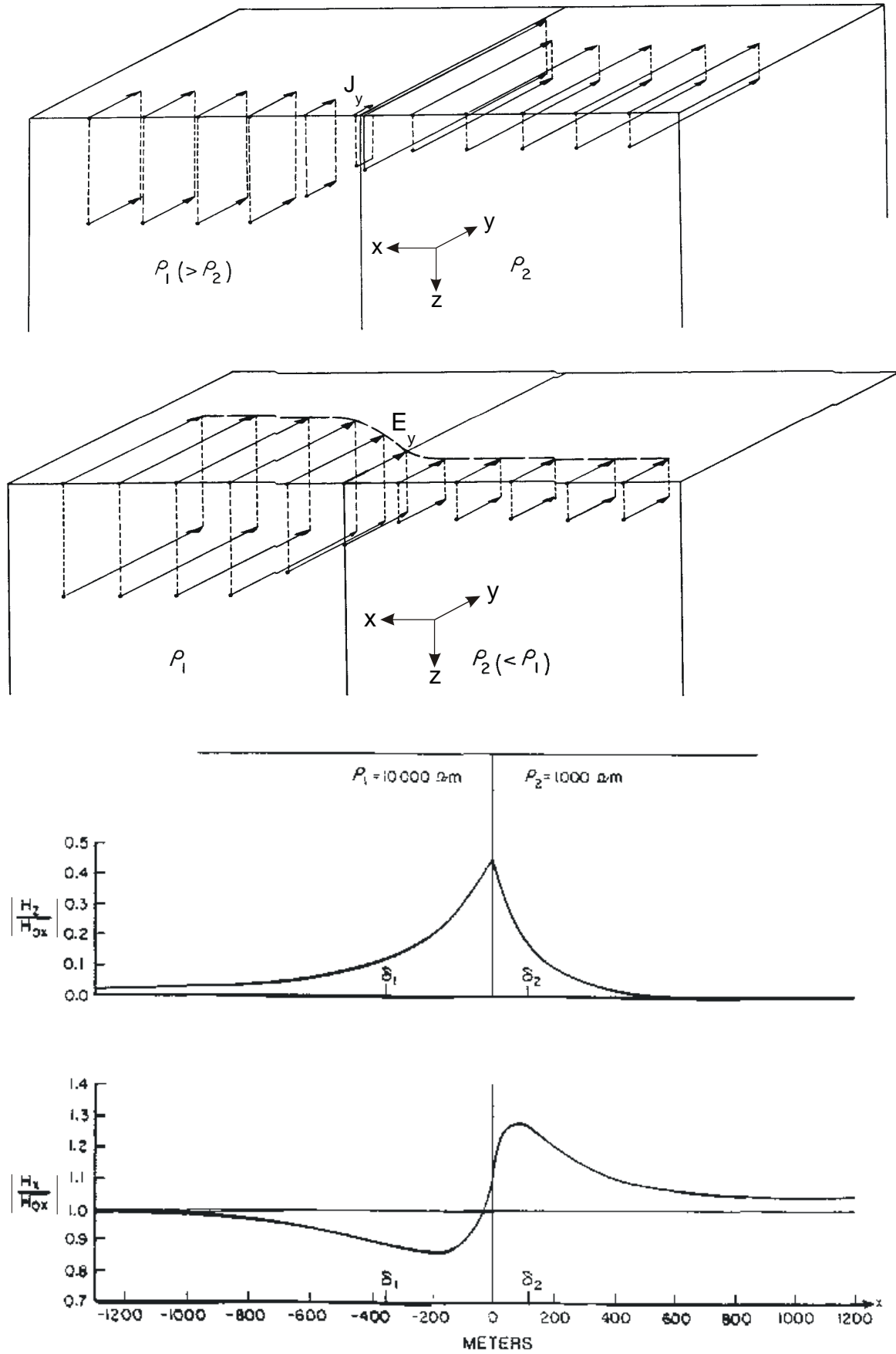


Fig. 6.6: Above: Jump of the current density in E-polarization. Middle: Continuity of the telluric field in E-polarization. Below:  $H_z$  and  $H_x$  normalized to  $H_{x0}$  at the boundary.

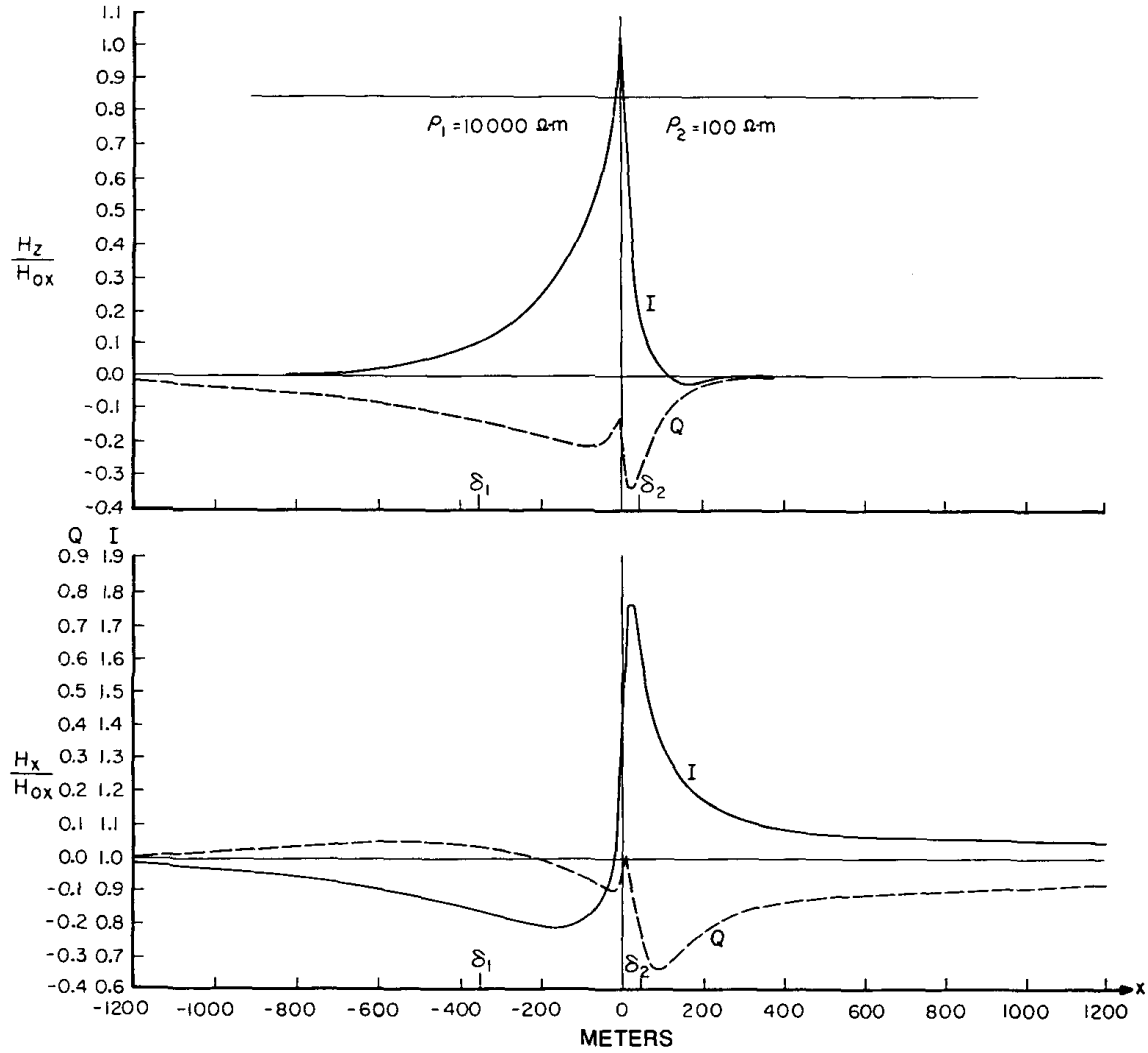


Fig. 6.7:  $H_z$  and  $H_x$  normalized to  $H_{x0}$  at the boundary, for the parts of the in-phase as well as the quadrature. For reasons of clarity the conductivity contrast is higher than in Fig. 6.6.

### 6.3 Geomagnetic depth sounding, induction arrows

Due to the occurrence of a vertical magnetic field in E-polarization, a corresponding purely magnetic transfer function can be calculated:

$$\underline{B}_z = \underline{T}_x \underline{B}_x + \underline{T}_y \underline{B}_y \quad . \quad (6.10)$$

$\underline{T} = (\underline{T}_x, \underline{T}_y)$  is often called *tipper* (from "to tip", the magnetic field vector "tips" out of the horizontal). It is a complex function of the frequency like the impedance  $Z$  or the penetration depth  $C$ . From the in-phase- and out-of-phase parts the following equations are derived:

$$\begin{aligned} \underline{P} &= \text{Re } \underline{T}_x \underline{e}_x + \text{Re } \underline{T}_y \underline{e}_y \\ \underline{Q} &= \text{Im } \underline{T}_x \underline{e}_x + \text{Im } \underline{T}_y \underline{e}_y \end{aligned} \quad (6.11)$$

with  $\underline{e}_x, \underline{e}_y$  as unit vectors.  $\underline{P}$  and  $\underline{Q}$  are usually plotted on a map as *induction arrows* or *vectors*.

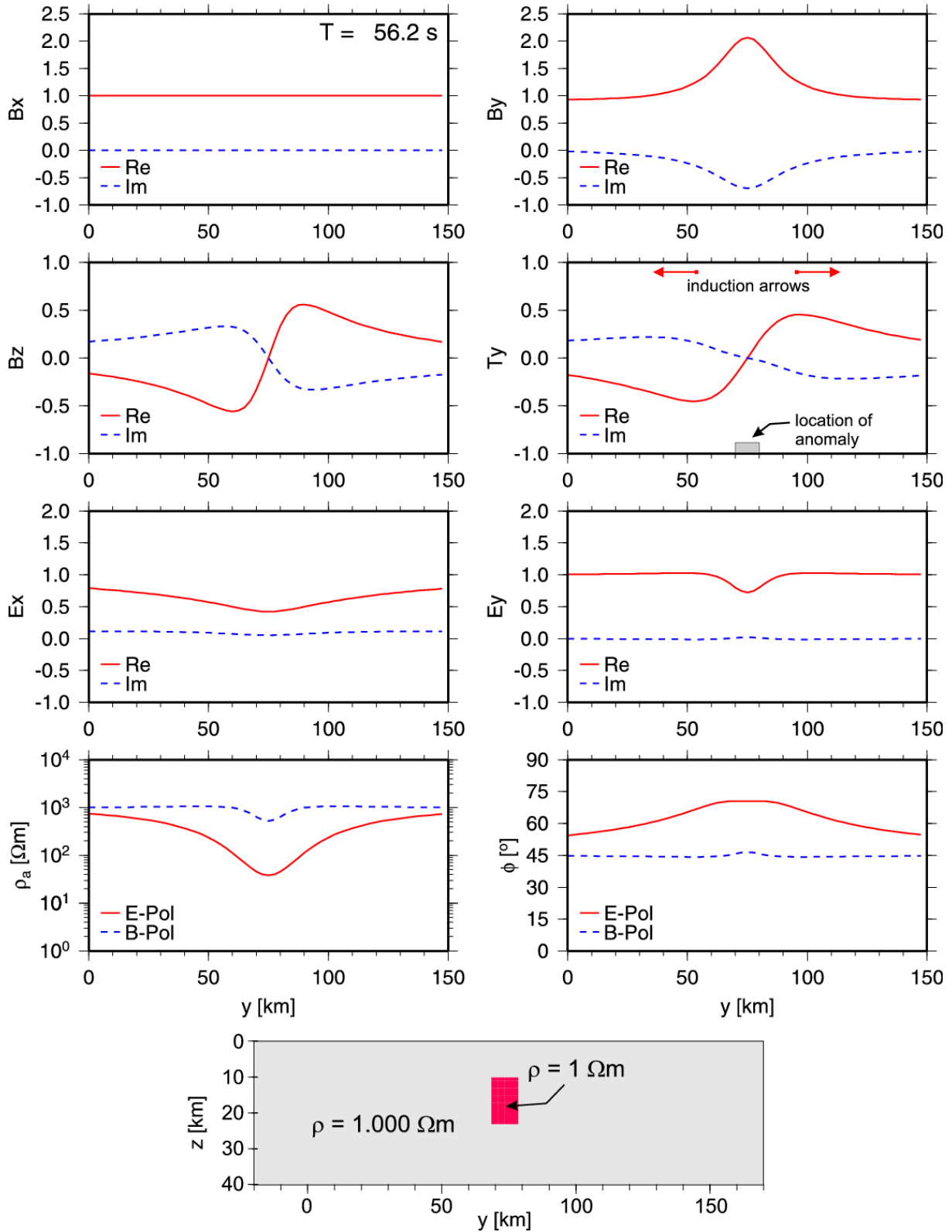


Fig. 6.8a: Response of a 2-dimensional model with a deep good conductor, embedded in a homogeneous half space, for a period of 56s. Here the local field quantities or transfer functions are described. The strike direction of the anomaly is N-S. Consequently  $E_x$ ,  $B_y$  and  $B_z$  correspond to the fields of E-polarization,  $B_x$ ,  $E_y$  and  $E_z$  (the latter is not shown here) correspond to B-polarization. The direction of the induction arrows with  $\underline{e}_y$  positive in eastern direction follows immediately from  $T_y$  that changes sign above the anomaly.

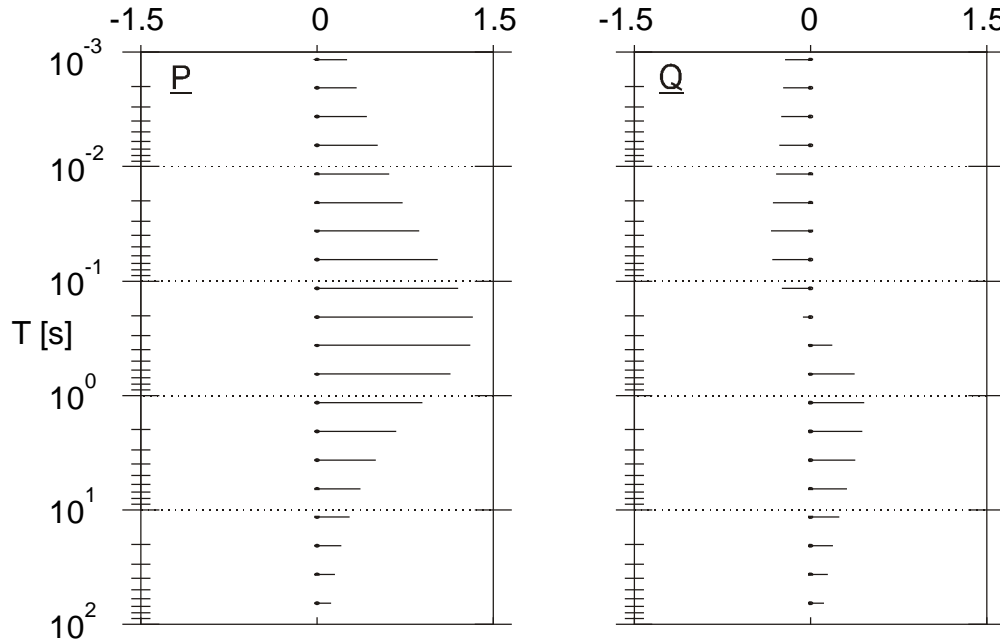


Fig. 6.8b: Example showing real and imaginary arrows as function of period for a station at the right boundary of a highly-conductive anomaly.

Even though the quantities  $\underline{P}$  and  $\underline{Q}$  are written as vectors they cannot necessarily be added or subtracted like normal vectors; this is only possible if there is a weak electromagnetic coupling among two (or more) anomalies.

Electromagnetic coupling of two anomalies means that the secondary field induced in an abnormal area does also induce a field in an adjacent anomaly. This effect can be ignored and the induction arrows can be treated as normal vectors only if the distance between both anomalous bodies is "large enough". This becomes relevant for example in the case of an anomaly near a coast. The *coast effect* results from the large conductivity contrast sea-continent; it cannot simply be subtracted to evaluate an additional anomaly on land. Instead it has to be included in the model, requiring a much larger grid.

The real arrows always point away from the good conductor for all frequencies while the im-

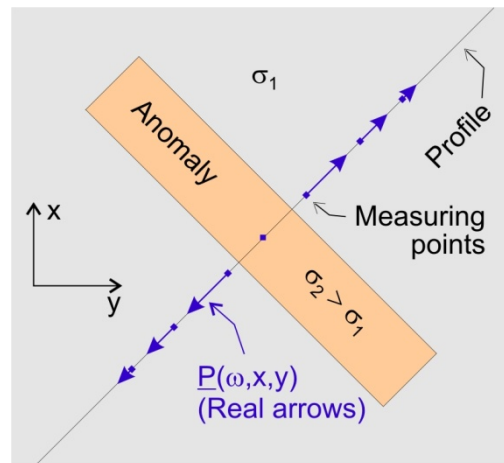


Fig. 6.9: Schematic depiction of real arrows for a fixed frequency  $\omega$  along the profile over a 2-dimensional anomaly that is highly conductive compared to its surroundings.

imaginary arrows change their signs, namely at the frequency with the largest inductive effect where the real arrow reaches its maximum. This is shown in fig. 6.8 and 6.9. For high frequencies the imaginary arrow and the real arrow point into opposite directions, for low frequencies they point into the same direction<sup>6</sup>. The definition given above goes back to *Schmucker*, but other conventions exist: for the Parkinson arrow  $\underline{P}_{\text{Parkinson}} = -\underline{P}$ , while the imaginary arrows remain the same; in the convention according to Wiese  $\underline{Q}_{\text{Wiese}} = -\underline{Q}$  while the in-phase arrows have the same direction as above<sup>7</sup>.

If the anomaly does not extend infinitely any more, i.e., in a 3-dimensional case, the real arrows on a surrounding station array still point away from the well-conductive structure (see Fig. 6.10). However, this does not hold for the imaginary arrows any more. For a number of anomalies with overlapping fields the distribution of real arrows can show a difficult pattern which does not indicate the conductivity distribution intuitively any more. This is the case particularly for anisotropic structures.

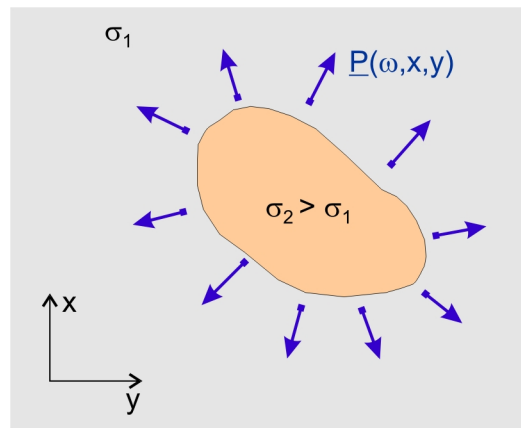


Fig. 6.10: In the 3-dimensional case the real arrows always point away from a good conductor. However, if there is a number of adjacent bodies this does not hold any more.

#### 6.4 Some remarks on the VLF method

In the VLF method as well as in geomagnetic depth sounding we make use of the occurrence of the vertical magnetic field component  $B_z$  in E-polarization by measuring  $B_z$  and dividing it by the horizontal field (depending on strike direction of the anomaly either  $B_x$  or  $B_y$ ). This shall be shown for the case of a vertical, well-conductive dike (fig. 6.11).

In the anomaly eddy currents  $J_x$  are induced which concentrate in the upper part of the plate because of the skin effect. Their magnetic field  $B_2$  overlays the "normal field"  $B_{1y}$  that is composed of the primary source field and the induced secondary field in the homogeneous or

<sup>6</sup>The reason is the different behavior of decay in the in-phase and out-of-phase-fields with depth described in chapter 2 (see also fig. 6.7).

<sup>7</sup>We use the terms Wiese or Parkinson convention, respectively, when real arrows point away or towards the anomaly. For reasons of clarity it is recommended not to stick dogmatically to one convention but choose the one that shows the effect most clearly.

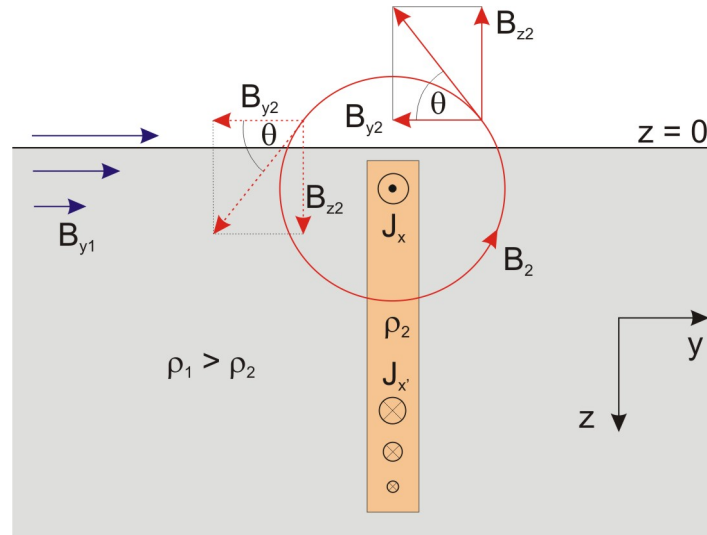


Fig. 6.11: The magnetic fields of a well-conductive plate in homogeneous subsoil.  $B_{y1}$  is the normal field,  $B_{y2}$  and  $B_{z2}$  are the components of the secondary field  $B_z$  caused by the anomalous body on the left and right side. The plate is extended in  $x$ -direction which corresponds to  $E$ -polarization as well as to the direction of the transmitter here.  $\theta$  is the corresponding tilt angle.

layered half space<sup>8</sup>. Then the components  $B_{y2}$  and  $B_{z2}$  are measured at the surface. The relation  $B_z/B_y$  changes the sign over the anomaly (correspondingly, the derived induction arrows change their direction).

The strike direction of the conductive anomalous body should be in the direction to the transmitter to achieve a maximum coupling of the magnetic source field to this body. This becomes evident in Figs. 6.11 and 6.12. In this case the magnetic field of the transmitter is in horizontal direction to the striking of the anomalous body ( $E$ -polarization), there is a maximum induction effect and the measured vertical field only reflects the influence of the conductor. In every other direction  $E$ - and  $B$ -polarizations will be mixed; if the direction to the transmitter is perpendicular to the strike of the anomaly there will be pure  $B$ -polarization and the secondary magnetic field is 0. In practice it will be very difficult to measure the ideal case of  $E$ -polarization because profile direction should always be perpendicular to the (assumed)

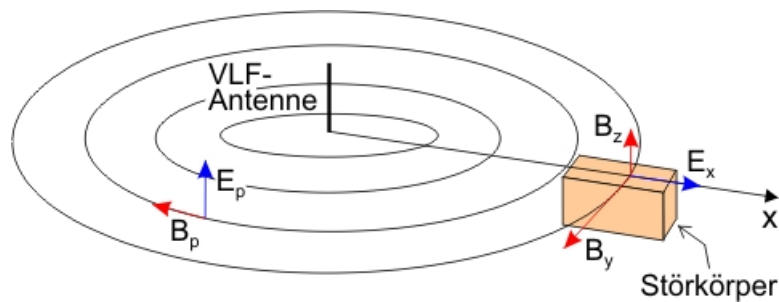


Fig. 6.12: Connection between the strike direction of the anomaly and the optimum transmission direction in VLF-method ( $E$ -polarization). Although first the radiated field is  $TM$ -polarized it becomes more and more  $TE$ -parts due to reflections at the ionosphere and the surface of the earth which become inductively effective then. Of course, at the location of the receiver the field does not have a spherical symmetry any more, this case is based on the assumption of plane waves.

<sup>8</sup> For the layered half space the total magnetic field at the surface is  $H_{\text{tot}} = 2 H_{\text{primry}}$ . For explanation see chapter 5.

strike of the anomaly and because there is only a limited number of transmitters. Consequently, the induction anomaly will usually be determined as too small. Usually the tilt angle  $\theta$  (see fig. 6.13) or the relation  $B_z/B_{\text{hor}}$  (separated into real and imaginary part, in %) <sup>9</sup> are measured, each as function of location.

Unfortunately VLF-transmitters for the communication with submarines and which radiate between 15-30 kHz are located very irregularly on the globe (Fig. 6.14, a table with their frequencies is shown on e.g. [www.abem.se](http://www.abem.se), but the different tables often contradict each other!).

As in magnetotellurics, in the VFL-R-variant <sup>10</sup> (with additional measuring of the electrical field) the signals radiated by the transmitters for submarine communication are used to calculate apparent resistivities and phases. Often, for a layered half space only a 2-layer case can be

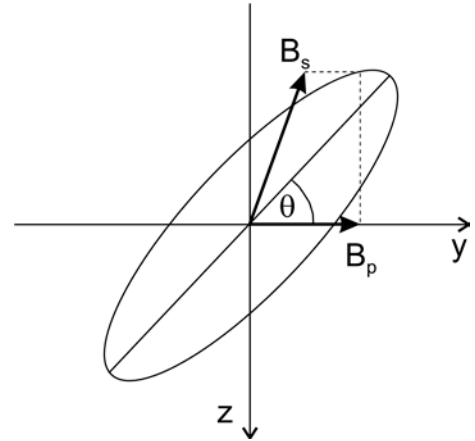


Fig. 6.13: Polarization ellipse of the magnetic field. Both the primary and the secondary field oscillate with the period  $T$ , the resultant forms an ellipse (mod. according to Kearey et al. 2002).

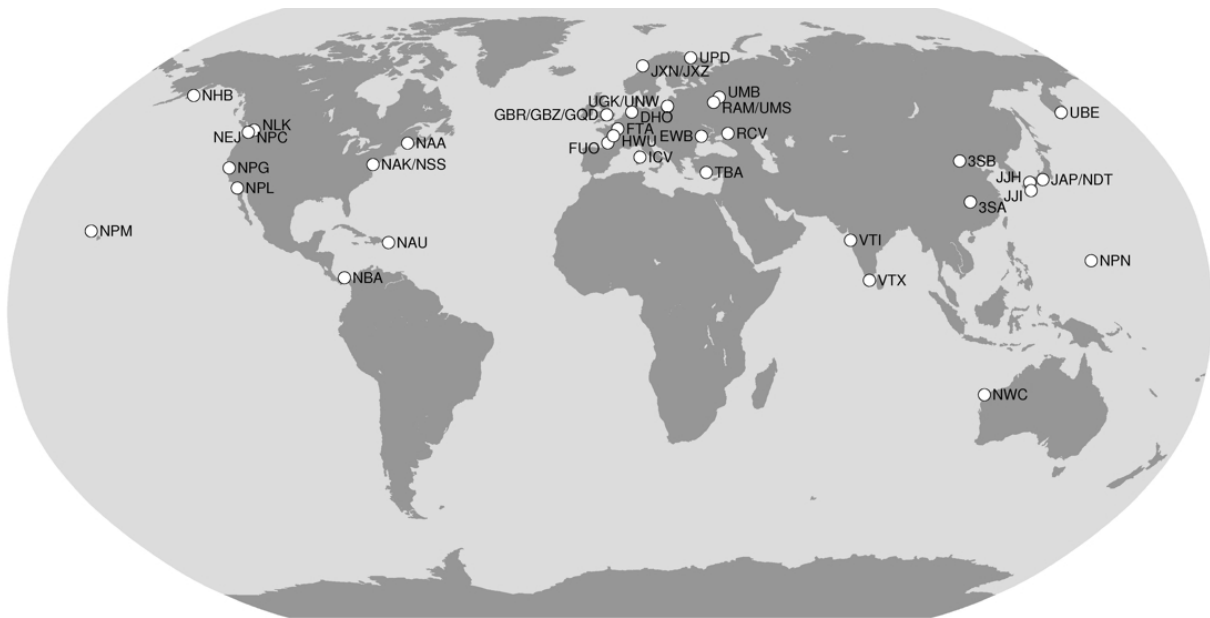


Fig. 6.14: Distribution of VLF-transmitters. Note the bad coverage in Africa, South America and the Antarctic.

<sup>9</sup> If the relation vertical/horizontal component or the tilt angle are applied over a vertical dike a crossover (zero-crossing) of these response functions is obtained. Therefore the data are sometimes transformed over adjacent measured values with a "Fraser-filter" (Fraser 1969):  $X_i = (X_{i+1} + X_{i+2}) - (X_{i-1} + X_{i-2})$ . Consequently, the zero-crossings over the centre of the anomaly become maxima. Using a "Karous-Hjelt-Filter" it is possible to show equivalent current densities from the vertical magnetic fields standardized on the horizontal field. For the coefficients see Karous & Hjelt (1983).

<sup>10</sup> The radiomagnetotelluric RMT method is an extension of the VLF-R method toward more and higher frequencies. Here the frequency domain reaches from approximately 10 kHz up to several 100 kHz. If there are still higher frequencies the part of the displacement current becomes important so that the influence of the dielectric constant  $\epsilon_r$  cannot be ignored any more.



resolved because of the limited frequency range. The criterion is the measured value of the phase: if  $\phi$  is larger than  $45^\circ$  the second layer is a better conductor, and the other way round for  $\phi < 45^\circ$ .

Transmitter	Freq. (kHz)	Location	Country	Direction	Position	
<b>DHO</b>	23.4	Rhauderfehn	D	$322^\circ$	$53^\circ 08' \text{ N}$	$007^\circ 31' \text{ E}$
<b>FUO</b>	18.3	Bordeaux	F	$245^\circ$	$44^\circ 65' \text{ N}$	$000^\circ 48' \text{ E}$
<b>GBR</b>	16.0	Rugby	GB	$292^\circ$	$52^\circ 22' \text{ N}$	$001^\circ 11' \text{ E}$
<b>GBZ</b>	19.6	Criggion	GB	$291^\circ$	$52^\circ 43' \text{ N}$	$003^\circ 03' \text{ E}$
<b>NAA</b>	24.0	Cutler	USA	$297^\circ$	$44^\circ 39' \text{ N}$	$067^\circ 17' \text{ E}$
<b>JXZ</b>	16.4	Hegeland	N	$1^\circ$	$66^\circ 25' \text{ N}$	$013^\circ 01' \text{ E}$
<b>NWC</b>	22.3	Exmouth	AUS	$96^\circ$	$21^\circ 49' \text{ S}$	$114^\circ 09' \text{ E}$
<b>UMS</b>	17.1	Moskau	RUS	$59^\circ$	$55^\circ 49' \text{ N}$	$037^\circ 01' \text{ E}$

Tab. 6.1: List of available transmitters during a measurement in the Upper Palatinate (Bavaria, Germany). The directions have been determined from the local magnetic field components by an Omni-plus instrument.

For mappings there are the limitations regarding E- and B-polarization like in the VLF-method. In B-polarization an even stronger mapping effect can be obtained because the apparent resistivity jumps due to the discontinuity of the E-field that is vertical to the anomalous body. In contrast, in E-polarization the  $\rho_a(y)$ -curve is continuous.

Table 6.1 shows an example of a list of transmitters that could be received during measurements at the Franconian Line (FL) in the Upper Palatinate (Bavaria, Germany) and the accompanying directions (Fig. 6.15). The FL indicates the conductivity contrast that was to be mapped. It's obvious that transmitter DHO<sup>11</sup> has the best position for E-polarization, UMS for B-polarization. Finally Fig. 6.16 shows some measuring results.

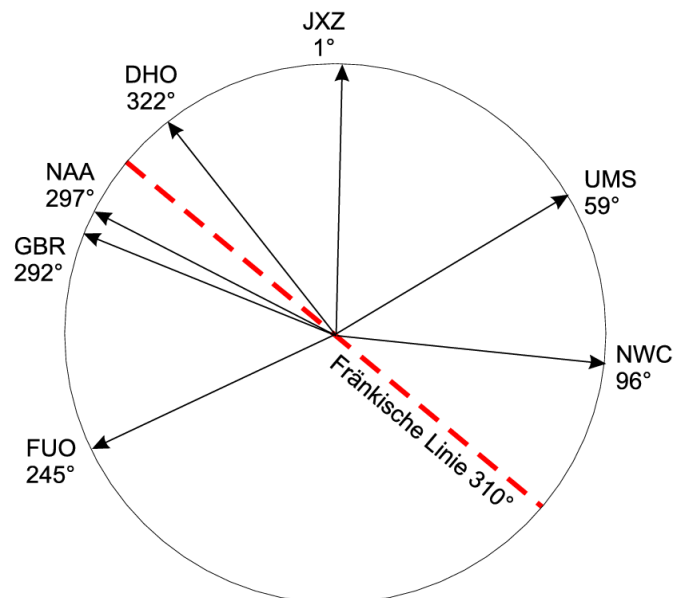


Fig. 6.15: Directions of the transmitters and their relation to the Franconian Line (modified according to a report of a study conducted by the FUB 2000).

<sup>11</sup>The transmitter Rhauderfehn (or Burlage) in East Friesland (North Germany) does apparently transmit on the same frequency as Lualualei (NPM, Hawaii). In each measuring campaign the transmitters must be scanned frequently because VLF-transmitters are sometimes turned off or their frequency is changed.

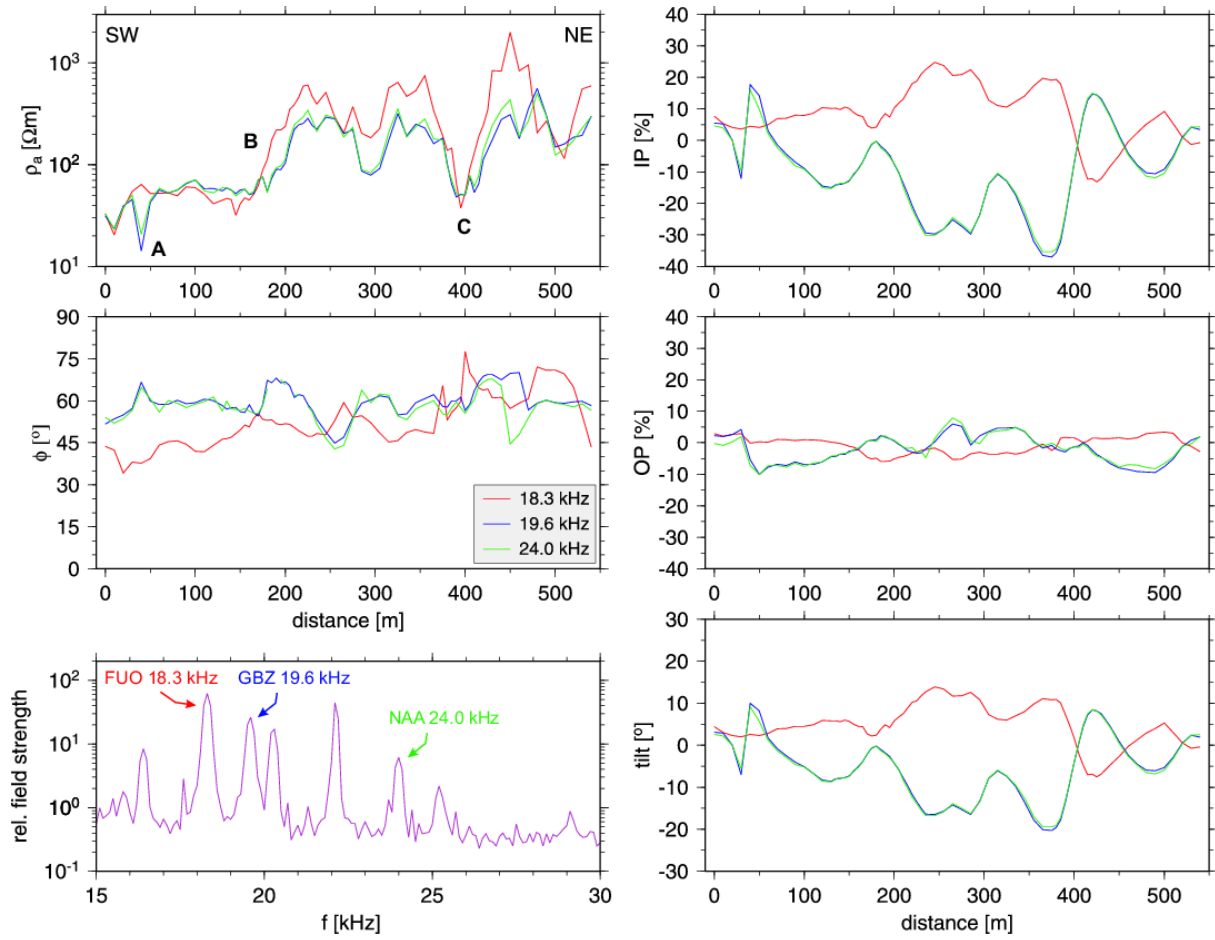


Fig. 6.16: Example of a VLF sounding at the Franconian Line. Anomaly A can probably be attributed to a pipe, B shows the increase of resistivity of the sedimentary foreland to the crystalline of the area Erbendorf-Vohenstrauß and C is located at the same position at which a strong SP- and geoelectric anomaly were encountered (see later chapters). The transmitters NAA and GBZ are approximately located in strike direction (E-polarization) and have nearly identical values. FVO is in nearly vertical direction to them (B-polarization). From the in-phase component and the tilt angle it becomes clear that these modes are not exactly matched and that it comes to a mixing of modes. The other strong transmitters (see spectrum lower left) are located even worse. During the measuring time in the beginning of May 2003 Rhauderfehn transmitted only unreliably, UMS could also not be used. Data were recorded for the diploma thesis of T. Martin.

### 6.5 Anomalous magnetic fields – Magnetovariational Profiling (MVP)

In Figs. 6.6 and 6.7 local magnetic fields have already been connected with fields at observation points that are far away from the conductivity anomaly. Here the magnetic fields over a 1-dimensional structure are called the *normal field*  $B_0$ . The anomalous fields  $B_a$  in the range of influence of a lateral anomaly can be connected with these fields. As a result we obtain linear relations again<sup>12</sup>:

<sup>12</sup> According to definition the normal vertical field is 0 and therefore it does not appear in the equation. In practice it is difficult or impossible to find a one-dimensional reference site. In that case there will also be a  $B_{z0}$  at the reference station and another column has to be added to the matrix of the transfer functions. The descriptions  $h_H$ , etc. go back to Schmucker (1970).

$$\begin{pmatrix} B_{xa} \\ B_{ya} \\ B_{za} \end{pmatrix} = \begin{pmatrix} W_{xx} & W_{xy} \\ W_{yx} & W_{yy} \\ W_{zx} & W_{zy} \end{pmatrix} \begin{pmatrix} B_{x0} \\ B_{y0} \end{pmatrix} = \begin{pmatrix} h_H & h_D \\ d_H & d_D \\ z_H & z_D \end{pmatrix} \begin{pmatrix} B_{x0} \\ B_{y0} \end{pmatrix} \quad (6.12)$$

In analogy to induction arrows "*perturbation arrows*" are defined from the anomalous horizontal fields. This applies for both real as well as imaginary parts:

$$\begin{aligned} \underline{p} &= h_H \underline{e}_x + d_H \underline{e}_y \\ \underline{q} &= h_D \underline{e}_x + d_D \underline{e}_y \end{aligned} \quad ; \quad (6.13).$$

If they are rotated by 90° counter-clockwise they show the direction of the anomalous current system (see Fig. 6.17). From the transfer functions  $z_H$  and  $z_D$  "anomalous" induction arrows  $\underline{P}_a = \text{Re } z_H \underline{e}_x + \text{Re } z_D \underline{e}_y$  and  $\underline{Q}_a = \text{Im } z_H \underline{e}_x + \text{Im } z_D \underline{e}_y$  can also be derived.

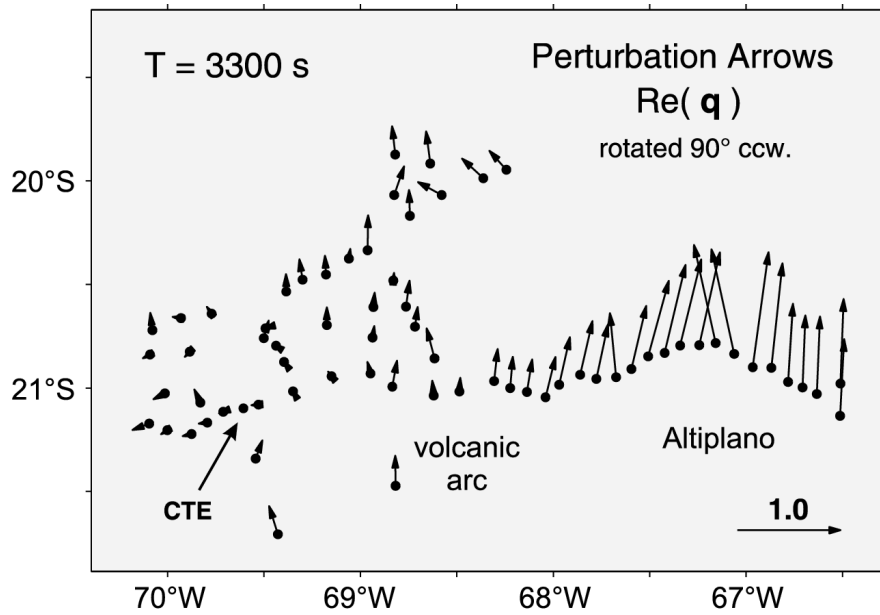


Fig. 6.17: Real perturbation arrows rotated by 90° counter-clockwise in the Central Andes. The large arrows on the right half of the picture that systematically point to the North form a current system under the Bolivian Altiplano, a location with a large conductivity anomaly that has also been discovered with magnetotelluric methods. CTE is the reference site. An inducing field in EW-direction causes a strong, anomalous current in NS-direction which again causes an anomalous field in EW-direction  $B_{ya}$  (large  $d_D$ ). By rotation the direction of the anomalous current is obtained.

## 6.6 Distortion of magnetotelluric data

Up to now magnetotelluric soundings are mostly conducted on profiles which are perpendicular to the assumed strike of the structures that have to be studied. Real 3-dimensional studies with stations placed on a grid, whose mesh has a reasonable distance to the skin- or target depth, are still an exception. The reasons are on the one hand the immense measuring efforts and on the other hand the 3-dimensional models which require a lot of resources (calculation time and memory demands). Therefore we can only hope that the structures in the subsoil are

actually (at least approximately) 2-dimensional and that a common coordinate system can be found in which every transfer function can be rotated in. However, often this is wishful thinking and determining the strike direction for a specific set of data is more difficult than it was supposed to be. One should never leave it at a simple analysis according to Swift (equation 6.5) because the influence of inhomogeneities near the surface is particularly strong and destructive in these parameters.

The horizontal components of the observed electrical field are connected with the observed horizontal magnetic field via the impedance:

$$\underline{\underline{E}}_h = \underline{\underline{Z}} \underline{\underline{B}}_h \quad . \quad (6.14)$$

As said already above, the electrical field is diverted or rather intensified or reduced at anomalies near the surface. These local anomalies do not have an inductive effect if they are small-scaled in relation to penetrating depth. Mathematically this is described as a real-valued  $2 \times 2$ -matrix  $\underline{\underline{D}}$ . The regional electrical field  $\underline{\underline{E}}_h^0$  that is assumed to be ideally two-dimensional must be multiplied with this matrix to obtain the observed field  $\underline{\underline{E}}_h$ :

$$\underline{\underline{E}}_h = \underline{\underline{D}} \underline{\underline{E}}_h^0 \quad . \quad (6.15)$$

The regional impedance that consists only of elements  $\neq 0$  on the minor diagonal:

$$\underline{\underline{E}}_h^0 = \underline{\underline{Z}}^0 \underline{\underline{B}}_h^0 \quad , \quad (6.16)$$

is also distorted now:

$$\underline{\underline{E}}_h = \underline{\underline{D}} \underline{\underline{E}}_h^0 = \underline{\underline{D}} \underline{\underline{Z}}^0 \underline{\underline{B}}_h^0 \quad . \quad (6.17)$$

Here the measured magnetic field  $\underline{\underline{B}}_h$  is equated with the regional magnetic field  $\underline{\underline{B}}_h^0$ . The phase shift between E- and B-field does not change because the distortion matrix  $\underline{\underline{D}}$  is real. This does not apply for the static shift, however. According to Groom & Bailey (1989)  $\underline{\underline{D}}$  can be factorized further as:

$$\underline{\underline{D}} = \underline{\underline{g}} \cdot \underline{\underline{A}} \cdot \underline{\underline{T}} \cdot \underline{\underline{S}} \quad . \quad (6.18)$$

with S indicating Shear, T Twist, A Anisotropy and g Gain, but I will not go into this in more detail here.

In first approximation it can be assumed that the magnetic field is not or only little affected by the distortions near the surface so that they can be ignored. If magnetic distortions shall be taken into consideration nevertheless the measured magnetic field is not equal to the regional field any more. Instead, according to Chave & Smith (1994) e.g., the resulting magnetic field  $\underline{\underline{B}}_h$  is described as the sum of the regional field  $\underline{\underline{B}}_h^0$  and a part caused by the distorted E-field:

$$\underline{\underline{B}}_h = \underline{\underline{B}}_h^0 + \underline{\underline{C}} \underline{\underline{E}}_h^0 \quad . \quad (6.19)$$

Here the elements of the matrix  $\underline{\underline{C}}$  have the unit of admittance. With (6.16)

$$\underline{\underline{B}}_h = \underline{\underline{B}}_h^0 + \underline{\underline{C}} \underline{\underline{Z}}^0 \underline{\underline{B}}_h^0 = \left( \underline{\underline{I}} + \underline{\underline{C}} \underline{\underline{Z}}^0 \right) \underline{\underline{B}}_h^0 \quad \rightarrow \quad \underline{\underline{B}}_h^0 = \left( \underline{\underline{I}} + \underline{\underline{C}} \underline{\underline{Z}}^0 \right)^{-1} \underline{\underline{B}}_h \quad .$$

is obtained.

Consequently, from (6.7) results:

$$\underline{\underline{E}}_h = \underline{\underline{D}} \underline{\underline{Z}}^0 \left( \underline{\underline{I}} + \underline{\underline{C}} \underline{\underline{Z}}^0 \right)^{-1} \underline{\underline{B}}_h = \underline{\underline{Z}} \underline{\underline{B}}_h \quad . \quad (6.20)$$

Now the impedance derived from observation is put down to the regional 2-dimensional impedance via two distortion matrices. These matrices are determined by "decomposition".

The distortion also influences the observed vertical magnetic field

$$\underline{\underline{B}}_z = \underline{\underline{T}} \underline{\underline{B}}_h \quad . \quad (6.21)$$

We formulate correspondingly (6.19):

$$\underline{\underline{B}}_z = \underline{\underline{B}}_z^0 + \underline{\underline{Q}} \underline{\underline{E}}_h^0 \quad . \quad (6.22)$$

From this it results analogously to (6.20):

$$\underline{\underline{B}}_z = \underline{\underline{T}} \underline{\underline{B}}_h = \left( \underline{\underline{T}}^0 + \underline{\underline{Q}} \underline{\underline{Z}}^0 \right) \left( \underline{\underline{I}} + \underline{\underline{C}} \underline{\underline{Z}}^0 \right)^{-1} \underline{\underline{B}}_h \quad . \quad (6.23)$$

Here  $\underline{\underline{T}}^0$  is the regional 2-dimensional transfer function.

→ Phase tensor to be implemented soon...

## 6.7 The influence of topography on magnetotelluric transfer functions

If MT soundings are conducted in the mountains it might be necessary to take into consideration the influence of topography which is particularly concise in the B-polarization (see Fig. 6.18). In a valley there is a concentration of current lines, while on a mountain the current lines are dispersed. The vertical equipotential surfaces are bent correspondingly on a mountain and in a valley. If there is a fixed distance of the probes (which shall be small compared to the topographic dimensions), a smaller voltage is measured on the surface of the mountain (the equipotential surfaces are dispersed) than at the bottom of the valley (the equipotential surfaces are concentrated). In contrast, the magnetic field of the B-polarization is constant (the total current under each observation point remains the same, see also fig. 6.8a). Contrary to our intuition, it becomes apparent that mountains are good conductors while valleys are poor

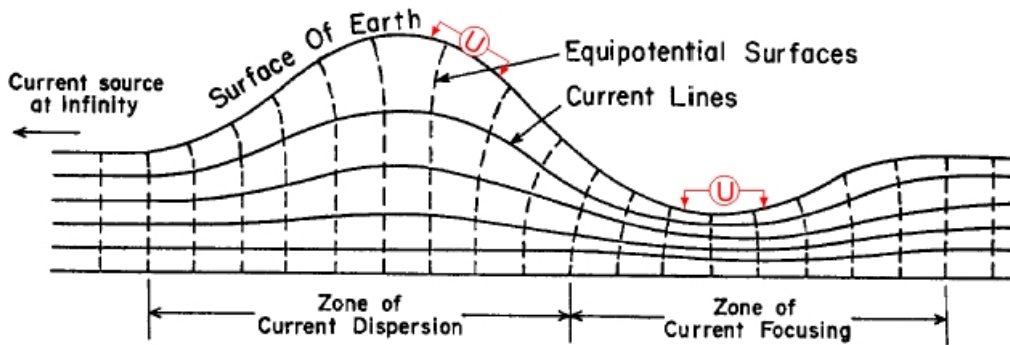


Fig. 6.18: Illustration of current lines and equipotential surfaces in B-polarization with topography (modified from Fox et al. 1980). Originally this picture has been drawn for a geoelectric sounding with sources that are far away but it is also adequate to describe the relations in magnetotellurics. The topography shall be 2-dimensional; otherwise the subsoil is homogeneous. In B-polarization the currents flow in the plane of projection.

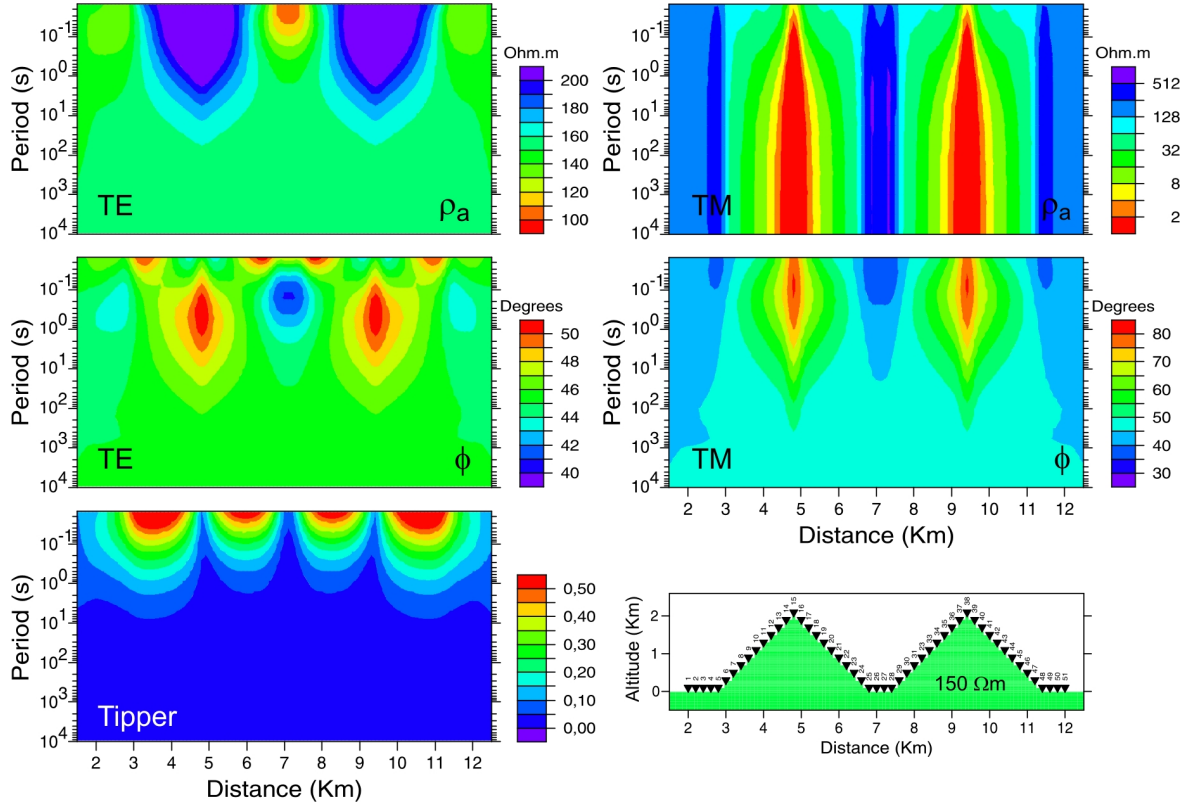


Fig. 6.19: Response of a 2-dimensional model with topography (below right); it consists of a homogeneous half space and two mountains with an inclination of the slope of  $45^\circ$ . TE mode (above left), TM mode (above right), norm of the tipper (below left). For reasons of clarity the sections of  $\rho_a$  and  $\phi$  are scaled differently. For long periods the topographic effect is reduced to a static shift in TM-mode. From the diploma thesis by D. Eydam.

conductors. If the spatial dimension of topography is small compared with penetration depth at a given frequency its influence is just analogous to a static shift. In E-polarization the topographic effects are the other way round, but they are smaller and they are relevant only for short periods. As it could be expected the tipper also shows significant effects only at short periods, in particular at the slopes. Here real induction arrows point away from the slope (in the valley between the mountains the influences are compensated, see fig. 6.19). The current focussing can be increased by valley fillings which are often well-conductive. For further information on topography see also Wannamaker et al. (1986) and Fischer (1986).

## 7 Basics concerning inversion of electromagnetic data

The process of finding a solution to a given model (i.e., calculate the responses like apparent resistivities and phases) is termed *forward modeling*. The backward procedure, i.e., estimate the model parameters (e.g., layer resistivities and thicknesses) is called *inversion*. Here we give only a brief introduction into inversion theory and we refer to several excellent textbooks on the subject<sup>1</sup>.

For a moment we think of the geoelectric problem as a linear problem (which it's certainly not). The forward problem is then written as:

$$\underline{d} = G\underline{m} \quad \text{oder} \quad d_i = \sum G_{ij} m_j \quad i = 1, \dots, n, j = 1, \dots, p \quad . \quad (7.1)$$

The model parameters are contained in the model vector  $\underline{m}$ , the data in the data vector  $\underline{d}$ . The operator  $G$ , also called data kernel, delineates how to transform the parameter  $m_j$  to the data  $d_i$ . Equation (7.1) describes a *linear problem*, the data  $d_i$  are proportional to the parameters  $m_j$ . For instance,

$$y_i = a x_j + b$$

is of course a linear problem – a straight line. A linear geophysical problem is, e.g., the gravity of a body with density  $\rho(\underline{r}_0)$ :

$$g(\underline{r}) = \int_s \frac{\rho(\underline{r}_0)}{(\underline{r} - \underline{r}_0)^3} d\underline{r}^2 \quad .$$

When we approximate the integral by a sum, we obtain an equation of type (7.9). On the other hand, the travel time  $t$  of a seismic signal along a path  $L$  isn't linearly dependent on wave velocity:

$$t = \int_L \frac{1}{v(x, z)} dl \quad ,$$

but on it's reciprocal, the slowness  $s = 1/v$ . In discrete form we obtain

$$t_i = \sum L_{ij} c_j \quad ;$$

the non-linear problem has thus been linearized by transformation of the variables. Often the parameters are available in the form  $\exp(m_j)$  (as in MT and VES!), we then achieve a linearization by taking the logarithm:

$$x_j = \log m_j \quad \text{and} \quad y_j = \log d_j \quad .$$

Often, however – also in our case – such a simple new parameterization is not sufficient; a linear problem is then achieved by approximation with a Taylor series. The inversion is now carried out iteratively.

The system of equations (7.1) has an unique solution only if  $N = M$  and matrix  $G$  is not singular:

<sup>1</sup> See, e.g., Hjelt, S.-E. (1992): *Pragmatic Inversion of Geophysical Data*, Springer-Verlag, Berlin, or Meju, M.A. (1994): *Geophysical Data Analysis: Understanding Inverse Problem Theory and Practice*, Society of Exploration Geophysicists, Tulsa, Oklahoma, or Asters, R.C., Borchers, B., and Thurber, C.H. (2005): *Parameter Estimation and Inverse Problems*, International Geophysics Series, 90, Elsevier.

$$\underline{\mathbf{m}} = \mathbf{G}^{-1} \underline{\mathbf{d}} = \mathbf{H} \underline{\mathbf{d}} \quad (7.2)$$

If there are more observations than model parameters the system of equations (7.1) is overdetermined<sup>2</sup>, in the reverse case it is underdetermined. An overdetermined system can get underdetermined if  $\mathbf{G}$  is singular.

An overdetermined system may be solved, e.g., by the method of *least squares*. Instead of (7.1) we now search a solution of

$$\underline{\mathbf{d}} = \mathbf{G} \underline{\mathbf{m}} + \underline{\mathbf{e}} \quad ; \quad (7.3)$$

$\underline{\mathbf{e}}$  is the vector of vector residuals. We solve by minimization of the squared errors:

$$S = \underline{\mathbf{e}}^T \underline{\mathbf{e}} = (\underline{\mathbf{d}} - \mathbf{G} \underline{\mathbf{m}})^T (\underline{\mathbf{d}} - \mathbf{G} \underline{\mathbf{m}}) = \sum_{i=1}^n \left( d_i - \sum_{j=1}^p G_{ij} m_j \right)^2 \stackrel{!}{=} \text{Min} . \quad (7.4)$$

This means that the derivative of  $S$  to the model parameters = 0:

$$\frac{\partial S}{\partial m_j} = \frac{\partial \left[ \underline{\mathbf{d}}^T \underline{\mathbf{d}} - \underline{\mathbf{d}}^T \mathbf{G} \underline{\mathbf{m}} - \underline{\mathbf{m}}^T \mathbf{G}^T \underline{\mathbf{d}} + \underline{\mathbf{m}}^T \mathbf{G}^T \mathbf{G} \underline{\mathbf{m}} \right]}{\partial m_j} = 0 . \quad (7.5)$$

From there it follows:

$$-\underline{\mathbf{d}}^T \mathbf{G} - \mathbf{G}^T \underline{\mathbf{d}} + \mathbf{G}^T \mathbf{G} \underline{\mathbf{m}} + \underline{\mathbf{m}}^T \mathbf{G}^T \mathbf{G} = 0 \quad (7.6a)$$

$$2\mathbf{G}^T \mathbf{G} \underline{\mathbf{m}} = 2\mathbf{G}^T \underline{\mathbf{d}} . \quad (7.6b)$$

For the transition from 7.5  $\rightarrow$  7.6a we applied the product rule. Equations (7.6b) are called the normal equations. It follows as solution

$$\hat{\underline{\mathbf{m}}} = \left( \mathbf{G}^T \mathbf{G} \right)^{-1} \mathbf{G}^T \underline{\mathbf{d}} . \quad (7.7)$$

The matrix  $\mathbf{H} = [\mathbf{G}^T \mathbf{G}]^{-1} \mathbf{G}^T$  is termed *generalized inverse* in least square sense. Numerical calculation of this matrix may be obtained, e.g., with the Gauss-Jordan- or the LU-methods.

A measure of quality of the solution is the *resolution matrix*

$$\mathbf{R} = \mathbf{H} \mathbf{G} \quad (7.8)$$

which becomes equal to the identity matrix in the case of a unique solution. Minor diagonals deviating from 0 mark the connection of parameters, e.g., in the product  $\rho_i h_i$  (see equivalence principle).

The quality of data fit is often expressed via the *RMS error (root mean square)*

$$\text{RMS} = \sqrt{\frac{(\underline{\mathbf{d}} - \mathbf{F}(\underline{\mathbf{m}}))^T \mathbf{R}_{dd}^{-1} (\underline{\mathbf{d}} - \mathbf{F}(\underline{\mathbf{m}}))}{n}} \quad (7.9a)$$

or

<sup>2</sup> An example: For 24  $\rho_a$ -values (8 per decade at periods between 10...10,000s) the system is overdetermined for a 5-layer case (5  $\rho$ -values and 4 thicknesses).



$$\text{RMS} = \sqrt{\frac{1}{n} \sum_{i=1}^n \left( \frac{d_i - F_i(\underline{\mathbf{m}})}{\Delta d_i} \right)^2} . \quad (7.9b)$$

Here  $n$  is the number of data points ( $\rho_{a,i}$ ) and  $\mathbf{R}_{dd}^{-1}$  is the error covariance matrix and  $\Delta d_i$  the data error. Don't we have such an error available (which happens in some geoelectric methods), the error is arbitrarily set equal to a constant (for instance = 1), alternatively we may also set a minimal error (*error floor*). The RMS error describes the global fit of the model response to the data. For an "ideal" fit, i.e., the deviation of model response from the data is in the range of data errors ( $d_i - F_i(\underline{\mathbf{m}}) \approx \Delta d_i$ ) the RMS would be  $\approx 1$ ; this is a value which is difficult to achieve in practice<sup>3</sup>. Often the fitting errors are normalized by the data and one gets a relative RMS, mostly expressed in percent:

$$\text{RRMS} = \sqrt{\frac{1}{n} \sum_{i=1}^n \left( \frac{d_i - F_i(\underline{\mathbf{m}})}{d_i} \right)^2} \quad \text{PRRMS} = \text{RRMS} \times 100 \quad (7.9c,d)$$

It's clear that our EM or geoelectric problem is *non-linear* and that it can't be linearized by simple re-parameterization (e.g.,  $\rho \rightarrow \log \rho$ ). How can we solve such non-linear problems (which are even *ill-posed*, which means that large parameter variations may have a small impact on the response, e.g., in the case of equivalent models or suppression of layers)?

A non-linear problem has the general form:

$$\underline{\mathbf{d}}_i = f_i(m_1, \dots, m_m) = f_i(\underline{\mathbf{m}}) \quad \text{oder} \quad \underline{\mathbf{d}} = F(\underline{\mathbf{m}}) , \quad (7.10)$$

with  $F$  as a functional which transforms the model parameters into the model response (like the Wait-Lipskaya algorithm to calculate  $\rho_{a,i}$  from  $\rho_j, h_j$ ). Many inversion algorithms expect a starting or initial model  $\underline{\mathbf{m}}^0$ , which is somehow created (a homogeneous half space or structures from *a-priori information*, for example if one knows a layer boundary from other methods, etc.). The theoretical model response is then:

$$\underline{\mathbf{d}}_i^0 = f_i(m_1^0, \dots, m_p^0) \quad \text{oder} \quad \underline{\mathbf{d}}^0 = F(\underline{\mathbf{m}}^0) . \quad (7.11)$$

Let  $F$  now be linear around  $\underline{\mathbf{m}}^0$ , so that we may express the response of a small change around  $\underline{\mathbf{m}}^0$  as a Taylor series:

$$\begin{aligned} F(\underline{\mathbf{m}}) &= f_i(m_1^0 + \delta m_1, m_2^0 + \delta m_2, \dots, m_p^0 + \delta m_p) \\ &= f_i(\underline{\mathbf{m}}^0) + \frac{\partial f_i}{\partial m_1} \delta m_1 + \frac{\partial f_i}{\partial m_2} \delta m_2 + \dots + \frac{\partial f_i}{\partial m_p} \delta m_p + \text{terms of higher order} \quad (7.12) \\ &= F(\underline{\mathbf{m}}^0) + \left\{ \sum_{j=1}^p \frac{\partial f_i(\underline{\mathbf{m}}^0)}{\partial m_j} \delta m_j \right\} + O(\|\delta \underline{\mathbf{m}}\|) \end{aligned}$$

The observations  $\underline{\mathbf{d}}$  always contain errors, (7.10) has thus to be amended:

$$\underline{\mathbf{d}} = F(\underline{\mathbf{m}}) + \underline{\mathbf{e}} . \quad (7.13)$$

<sup>3</sup> The amount of the data error thus enters directly into the RMS; if one underestimates the measuring errors one obtains a too large RMS and vice versa. A somehow arbitrarily chosen error floor may thus decrease the fitting error. The value of the RMS has always to be regarded with respect to the specific problem. It should never be used as a sole measure for successful modeling; of similar importance is the reproduction of the curve shape.

To obtain a solution, we have to minimize this error  $\underline{e} = \underline{d} - F(\underline{m})$ . It follows:

$$\underline{d} - F(\underline{m}) = \underline{d} - F(\underline{m}^0) - \left\{ \sum_{j=1}^p \frac{\partial f_i(\underline{m})}{\partial m_j} \Big|_{\underline{m}^0} \delta m_j \right\} = \underline{y} - A \underline{x} \quad (7.14)$$

and

$$\underline{e} = \underline{y} - A \underline{x} \quad . \quad (7.15)$$

$A$  is the matrix of partial derivatives (*Frechet derivatives*), also called *Jacobi* or *sensitivity matrix*; they describe the response of an – infinitesimal – model variation. The  $x_j = \delta m_j$  contain the unknown corrections to  $\underline{m}^0$ , to be determined in order to minimize  $\underline{e}$ .

We thus try to minimize the *objective function*

$$\begin{aligned} S = S(\underline{m}) &= \underline{e}^T \underline{e} = (\underline{d} - F(\underline{m}))^T (\underline{d} - F(\underline{m})) \\ &= (\underline{y} - A \underline{x})^T (\underline{y} - A \underline{x}) \end{aligned} \quad (7.16)$$

This may be done with, e.g., the Gauss-Newton method; in the framework of this lecture we cannot go into details here. The minimization is carried out iteratively, i.e., in a first step a modification  $\underline{x} = \delta \underline{m}$  is applied to the starting model  $\underline{m}^0$ , this leads to a – hopefully improved – model estimate  $\underline{m}^1$  and so on:

$$\underline{m}^{k+1} = \underline{m}^k + (A^T A)^{-1} A^T \underline{y} \quad . \quad (7.17)$$

The problems of such a least squares inversion are often found in the stability of the solution, i.e., calculating the inverse  $(A^T A)^{-1}$ . To stabilize the inversion, in the *Marquardt-Levenberg method* (also called *ridge regression*) weights are added to the main diagonal of  $A^T A$  and instead of  $S$  the new objective function

$$\phi = S_1 + \alpha S_2 = \underline{e}^T \underline{e} + \alpha (\underline{x}^T \underline{x} - L^T L) \quad (7.18)$$

is minimized.  $\alpha$  is a damping factor, describing the relative weight of  $S_1$  and  $S_2$ , respectively;  $L$  further bounds the parameter variation. One obtains the iterative solution

$$\underline{m}^{k+1} = \underline{m}^k + (A^T A + \alpha I)^{-1} A^T \underline{y} \quad . \quad (7.19)$$

An example of a resolution matrix is shown in table 7.1, which refers to a geoelectric data set (see the following chapter) from Saxony, Germany. A 4-layer model was calculated, resulting in 7 parameters (4 resistivities  $\rho_1 - \rho_4$ , 3 layer thicknesses  $d_1 - d_3$ ). The percent RMS for this inversion was 3.9%. Best resolved is the resistivity of the 2nd layer, also the conductance of the 2nd layer is well resolved (0.89), badly resolved is the resistivity of the 3rd layer (0.09); this reflects the principle of layer suppression so that one may perhaps ignore this layer. The inversion with a 3-layer model yields a slightly worse fit with an RMS of 4.4%. For further discussion see Fig. 7.8.

$\rho_1$	0.60						
$\rho_2$	-0.02	0.99					
$\rho_3$	-0.01	-0.01	0.09				
$\rho_4$	0.00	0.00	0.02	0.89			
$d_1$	0.14	0.01	0.01	0.00	0.94		
$d_2$	-0.03	-0.02	-0.20	-0.01	0.02	0.89	
$d_3$	0.02	0.01	-0.11	-0.09	-0.01	0.11	0.22
	$\rho_1$	$\rho_2$	$\rho_3$	$\rho_4$	$\rho_1$	$\rho_2$	$\rho_3$

Table 7.1: Resolution matrix for a geoelectric sounding in Saxony.

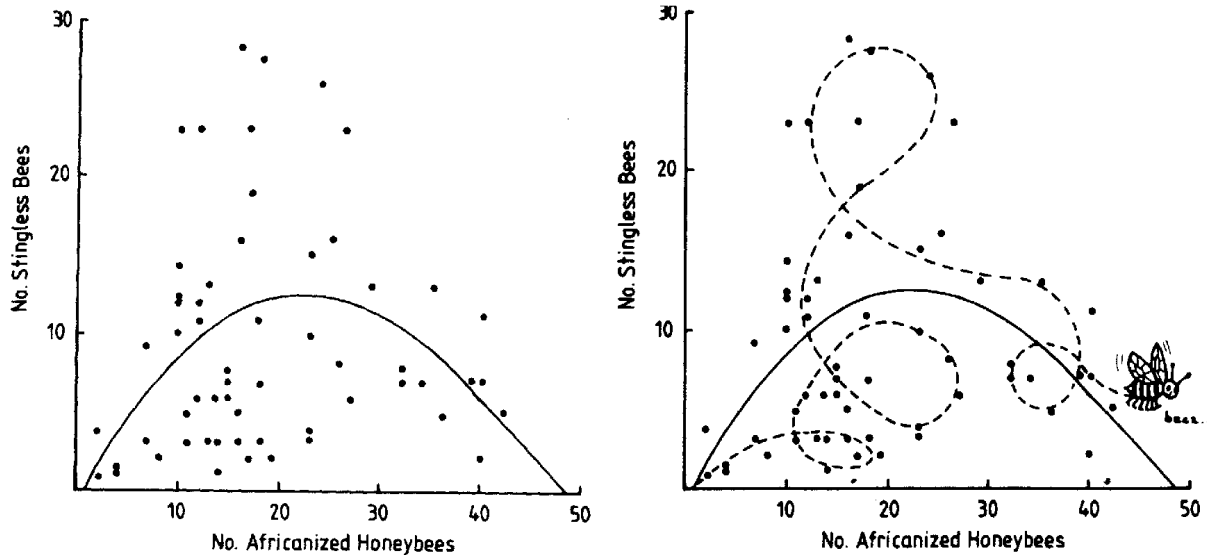


Abb. 7.8: Two examples for venturous modeling with under- and over-parameterization. Taken from the online manuscript "How to graph badly", J. Boyd, Univ. Michigan.

### Tikhonov Regularization

In earlier chapters it was already emphasized that geophysical problems are often “*ill-posed*”. Many methods exist to stabilize a solution particularly in the presence of noise, e.g., damped cutoff in singular value decomposition (SVD). For the time being, these methods are only treated in the German version of the lecture notes.

Here we extend this regularization by introducing constraints which have somehow something to do with the length of the model vector (the absolute value), i.e., its *flatness*, *smoothness* and *roughness*, respectively<sup>4</sup>. These methods are applicable for both linear data kernels  $G$  as well as non-linear functionals  $G(\underline{m})$ . Meaningful and stable solutions are often obtained only by this kind of regularization.

<sup>4</sup> An illustration: The Longitudinal Valley is flat, the Coastal Cordillera smooth, the Eastern Cordillera rough.

We first look at approaches which only incorporate the length  $\|\underline{m}\|$  of the model vector in the search for a stabilized solution. This may happen in various ways.

- 1) We look at solutions for which  $\|\underline{G}\underline{m} - \underline{d}\| \leq \delta$  is fulfilled and minimize  $\|\underline{m}\|$ :

$$\|\underline{m}\| = \text{Min!} \quad \text{für} \quad \|\underline{G}\underline{m} - \underline{d}\| \leq \delta \quad (7.20)$$

With growing  $\delta$  the number of suitable models increases, too and the value of  $\|\underline{m}\|$  decreases (see Fig. 7.9).

- 2) We look at solutions for which  $\|\underline{m}\| \leq \varepsilon$  is fulfilled and minimize  $\|\underline{G}\underline{m} - \underline{d}\|$ :

$$\|\underline{G}\underline{m} - \underline{d}\| = \text{Min!} \quad \text{für} \quad \|\underline{m}\| \leq \varepsilon \quad (7.21)$$

With growing  $\varepsilon$  the model increases and the number of suitable models increases, too.

- 3) Another option is the solution of the smoothed least squares problems

$$\|\underline{G}\underline{m} - \underline{d}\|^2 + \alpha^2 \|\underline{m}\|^2 = \text{Min!} \quad . \quad (7.22)$$

This is the original ansatz of *Tikhonov regularization* of zero order. The second term is a penalty function, it penalizes deviations from a given model idea, here thus the shortness of the model vector. One can show that by suitable choice of the constants  $\delta$ ,  $\varepsilon$  and  $\alpha$  all three approaches yield the same solution. If the values of  $\|\underline{m}\|$  and  $\|\underline{G}\underline{m} - \underline{d}\|$  are plotted in a diagram with  $\alpha$  as parameter, one often obtains an L-shaped curve, the so-called “*L-curve*”. An optimal model is obtained by choosing the regularization parameter  $\alpha$  such that the solution is close to the inflection point of the L-curve.

Until now we have only taken the length of the model vector as criterion for minimization. This is, however, inadequate in many cases because we don't want to find models which are close to zero but which are close to another value (e.g., a homogeneous half space of constant conductivity) or models which are simple in that they are particularly flat, i.e., the model parameters vary only slowly in model space.

We generalize eq. (7.22) by introducing a differentiate operator  $L$  and don't minimize now  $\|\underline{m}\|$  any more, but instead  $\|L\underline{m}\|$ :

$$\|\underline{G}\underline{m} - \underline{d}\|^2 + \alpha^2 \|L\underline{m}\|^2 = \text{Min!} \quad (7.23)$$

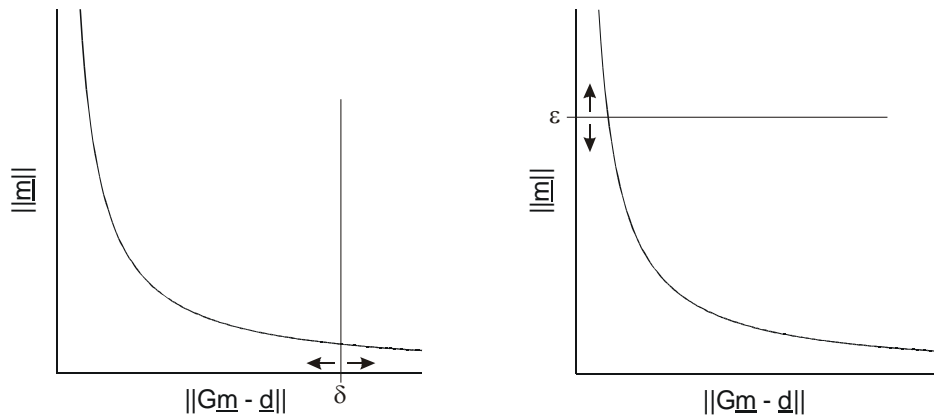


Fig. 7.9: Optimum values of  $\|\underline{m}\|$  and  $\|\underline{G}\underline{m} - \underline{d}\|$  at variation of  $\delta$  (left) and  $\varepsilon$  (right).

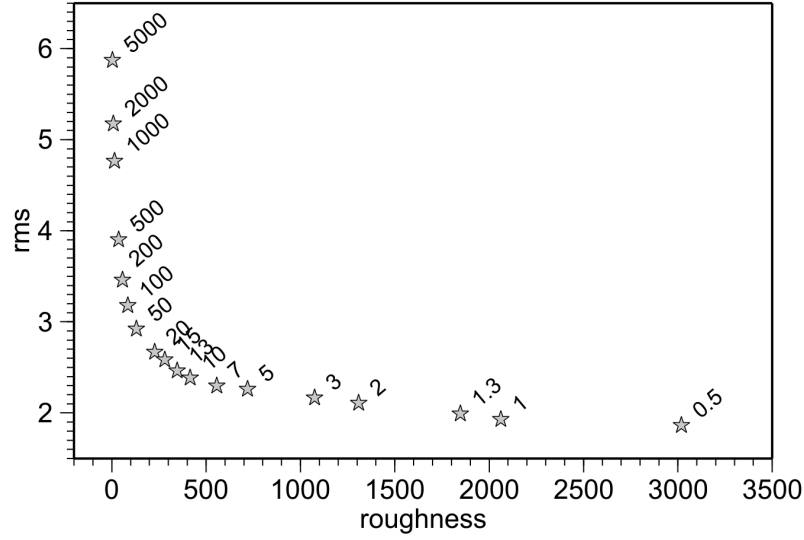


Fig 7.10: Example of an L-curve for a 2-D model of the Bolivian Altiplano (Brasse & Eydram 2008).

Another option consists in penalizing the deviation from a given model by replacing  $\underline{m}$  with the deviation  $(\underline{m} - \underline{m}_a)$  from an a-priori model  $\underline{m}_a$ :

$$\|\underline{G}\underline{m} - \underline{d}\|^2 + \alpha^2 \|\underline{L}(\underline{m} - \underline{m}_a)\|^2 = \text{Min!} \quad . \quad (\text{D.30})$$

The magnitude of the regularization parameter  $\alpha$  thus determines the smoothness of the model. Rougher models often lead to a smaller fit  $\delta$ ; however, they often contain structures which are not required by the data. The search of an “optimal” model – e.g., in the sense of the L-curve criterion – thus always means the sampling of model space by variation of  $\alpha$ .